SIGNAL-TO-NOISE RATIO ENHANCEMENT IN THE PRESENCE OF PULSE WIDTH MODULATION INTERFERENCE

by

Mark J. Muzal

ProQuest LLC.
789 East Eisenhower Parkway
P.O. Box 1346
Ann Arbor, MI 48106 – 1346

A thesis submitted to the Faculty and Board of Trustees of the Colorado School of Mines in partial fulfillment of the requirements for the degree of Master of Science (Engineering Systems).

Golden, Colorado

Date: 8/27/96

Signed: 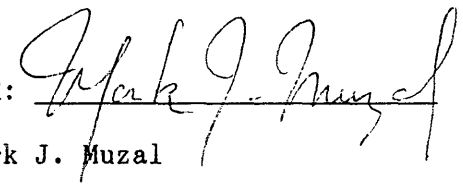

Mark J. Muzal

Approved: 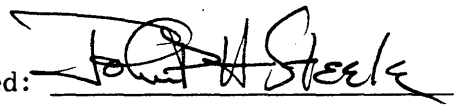

Dr. John Steele

Golden, Colorado

Date: 8/28/96

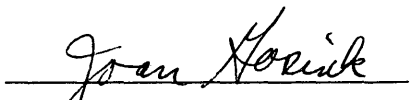

Dr. Joan Gosink

Professor and Head,

Division of Engineering

ABSTRACT

Pulse width modulation (PWM) is a technique which employs rapid voltage switching to effectively control motor speed. However, PWM produces electromagnetic interference (EMI) which may corrupt sensor output voltages. The interference is particularly troublesome where accurate sensing is required.

This problem was encountered during a recent system health monitoring research project funded by Idaho National Energy Laboratories, where temperature, fluid pressure, volume flow rate, and vibration acceleration were required to be monitored near a 29.8 kW (40 hp) PWM-controlled three-phase induction motor. Without implementing any noise reduction techniques, the EMI generated by the controller overwhelmed the detectors, making accurate sensing impossible.

This thesis describes the test equipment and its operation, reviews the mechanics of PWM motor control, investigates the nature and character of electrical interference generated by the motor controller, and describes techniques which were successfully applied to bring the PWM-generated EMI noise to acceptable levels. Through controller adjustments, grounding, shielding, and filtering, the signal-to-noise

ratios of the sensor signals were sufficiently enhanced to allow accurate system health monitoring in the presence of PWM-generated electromagnetic interference.

TABLE OF CONTENTS

LIST OF FIGURES

LIST OF TABLES

ACKNOWLEDGMENTS

Michelle Archueleta

Baldor Corporation

Dr. Chris Braun

Galen Braun

Jim Ditto

Tom Droulliard

Karl Fleischer

Dr. Tom Grover

Idaho National Energy Research Laboratory

John Jezek

Dr. Pat Kelecy

Dr. Nigel Middleton

Rex Rideout

Tim Seifert

Sensotech Corporation

Dr. John Steele

Harry Tran

Orlen Wolf

Chapter 1.

INTRODUCTION

In 1995 the Idaho National Energy Research Laboratory (INEL) commissioned the Colorado School of Mines Engineering Division to assist in its efforts in developing nuclear remediation technology. Specifically, INEL was interested in the feasibility of implementing a crane-mounted robotic arm to excavate, manipulate, and process radioactive waste material in-situ at a nuclear waste repository. The hydraulic-powered Schilling arm was selected as the appropriate robotic device to attach to a gantry crane, due to its reliability, durability, strength, and ability to carry out sensitive and delicate manipulations. Power to the Schilling arm's hydraulic actuators is supplied via a flexible hose attached to a floor-mounted hydraulic power unit (HPU). The HPU is a pump driven by a large, pulse-width modulated 3-phase induction motor. The crane/robot/HPU combination would have to operate under continuous exposure to potentially lethal nuclear radiation, and failure of any part of the above system would be costly, time consuming, and potentially hazardous. For example, if the HPU failed, all operations would cease until a person could enter the radioactive area to provide unscheduled service to the unit. INEL realized that by applying SHARP technology (System Health Assessment and Real-time

Prediction, Steele 1995), machine failure might be anticipated, and dangerous, costly breakdowns might be circumvented through pre-emptive maintenance.

With funding from INEL (contract # CSM 4-41532), CSM acquired an equivalent model HPU (the INEL Hydraulic Test Bench). The test bench was installed in the robotics laboratory at CSM, and was outfitted with an array of sensors which include thermocouples, pressure sensors, accelerometers, and other detectors. During operation of the HPU, the diagnostic output signals are conditioned, digitized, and routed to an Ethernet for remote observation in real time at multiple sites. Algorithms are now being developed which will allow remote observers to diagnose selected aspects of machine health based on the real-time information available on line (Archuleta, 1996, Brown, 1996, and Seifert, 1996).

However, during the early set-up phase of the project, it became clear that a serious problem had been overlooked. The sensors were being overwhelmed by electromagnetic interference (EMI) emanating from the pulse-width-modulated motor controller which drives the HPU. In addition, the electromagnetic perturbations were apparently interfering with the ability of a nearby computer to receive sensor data from the Ethernet. It was clear that real-time system health assessment would not be possible unless the noise problem could be corrected.

The objectives of this project were to investigate the noise problems associated with the motor controller, develop corrective actions, and implement a noise reduction program. Ultimately, the noise was reduced to acceptable levels by relocating system components, adjusting motor controller settings, grounding, shielding, and filtering.

In the strictest sense, the word *noise* describes a purely random process, and the word *interference* describes an intrusive, unwanted signal which is void of useful information although it may be band-limited and coherent. Noise phenomena (e.g. Johnson noise) are generally regarded as naturally-occurring, whereas *interference* can be man-made. In this thesis, the word *noise* is not meant to imply a random process, and is used synonymously with the word *interference.*

Chapter 2.

LITERATURE SEARCH AND BACKGROUND

A literature search for analogous case studies which address EMI avoidance was carried out. So far, the literature regarding EMI effects in high-power-high-speed switching converters, especially in high-power motor drive systems is still lacking (Zhong, 1995). The interested reader is referred to the references listed in Zhong's paper.

Nuclear detonations generate electromagnetic pulses (EMP) which have been studied intensely by the US government during the Cold War, however the limited unclassified information available on this subject is usually of a theoretical nature and not directly applicable to this specific problem; nuclear effects are generally treated as far-field (Thornton, 1991). As in the military, solutions to specific noise problems in industry are sometimes regarded as proprietary.

The paucity of published case studies addressing PWM-generated EMI issues may be because EMI avoidance, as a field of study, is widely regarded as an art rather than a science. Practical solutions to EMI problems generally require an ad-hoc, heuristic approach.

In Zhong's exceptional paper, cost-effective improvements in motor controller design (involving incorporation of LC filter elements in the controller itself) were proposed. Although it was not practical to modify existing Baldor motor controller internal circuitry in the system-health-monitoring project, the paper provided useful insight into the nature of PWM-generated EMI. Also of use was the sentinel work by Ott (1976), which helped guide grounding, shielding, and filtering efforts. Patient, direct experimentation rather than secondary research or computer modeling ultimately yielded an acceptable solution. For example, various grounding, shielding, and filtering configurations were implemented and tested in order to find the best configuration. Also, the equations which describe the interference patterns (equations 7.1.3 and 8.5.1) were derived from experimental data rather than by theoretical means.

Soft-switching converters (ones which use resonant snubber circuitry to switch at zero voltage or zero current) significantly reduce EMI and are a viable option in applications where EMI is a problem; however, in this project the existing converter could not be exchanged for a quieter model due to cost constraints.

The EMI analysis was conducted primarily in the time-domain rather than in the frequency domain for two reasons. Firstly, the interference consists of very sharp impulse patterns, which are flat and broad-band

in the frequency domain. The frequency domain does not yield useful information on the amplitude and spacing of the spikes, information which is critical to this analysis. Secondly, as will be demonstrated in Chapter 6, the observed frequency of the interference voltage depends on the impulse response of the receiving circuit and therefore is not a direct attribute of the EM field.

Chapter 3.

TEST BENCH OPERATION

This section describes the multifunctional Signal Conditioning/ Monitoring/Speed control unit (SCMS), which was necessarily designed and built for this thesis project to 1) facilitate test bench remote operation, 2) allow simultaneous multi-channel analog sensor signal observation, and 3) provide optional signal conditioning opportunities (and analog monitoring of conditioned analog signals) prior to A/D conversion. The SCMS features two modes of remote motor speed control and includes an LED display which indicates various motor operating conditions. The SCMS is located in Brown Hall along the west wall of Room 154 and is hard-wired to the test bench (located behind the west wall) via three sections of flexible conduit.

Grounding, shielding, and filtering are discussed in Chapter 8. Individual test bench component specifications are given in Appendix A. A description of each test bench variable and detailed operating procedures are given in Appendix B. See BALDOR Series 15 H Inverter Control Installation and Operating Manual for additional operating instructions (Baldor, 1994). SCMS circuit schematics are given in Appendix C. Figure 3.1 shows the location of test bench controls, and

Figures 3.2 through 3.4 diagram the SCMS control panel, physical layout, and external connections.

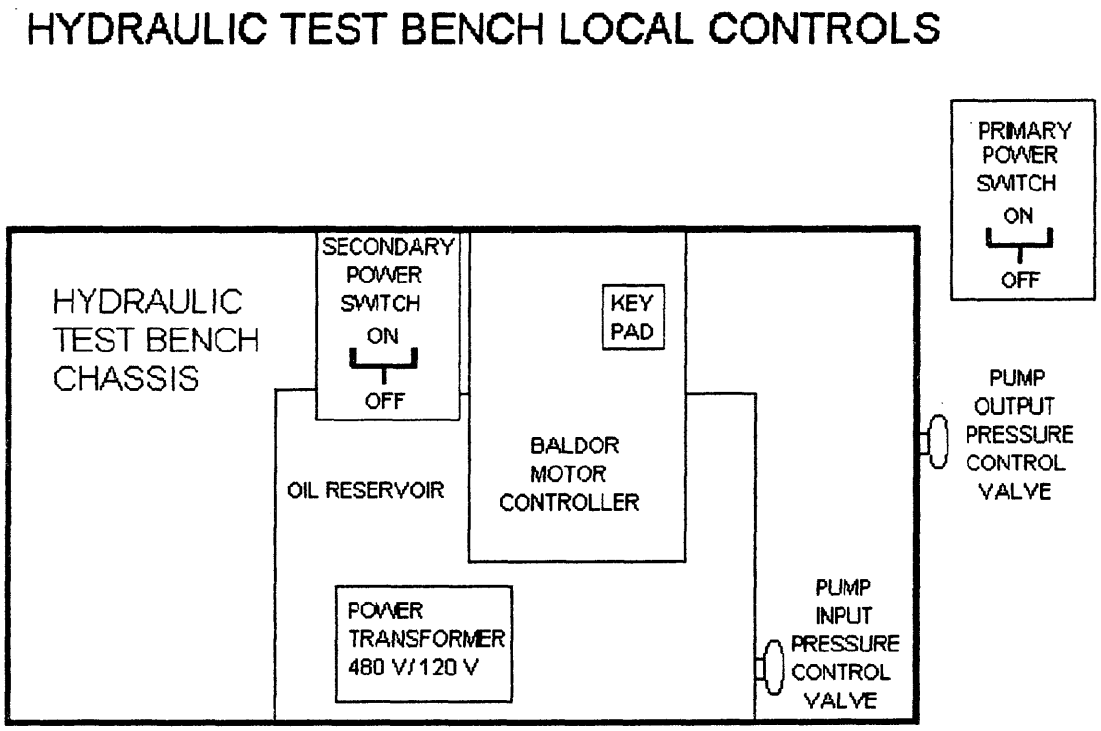

Figure 3.1. Hydraulic Test Bench Local Controls (Front View).

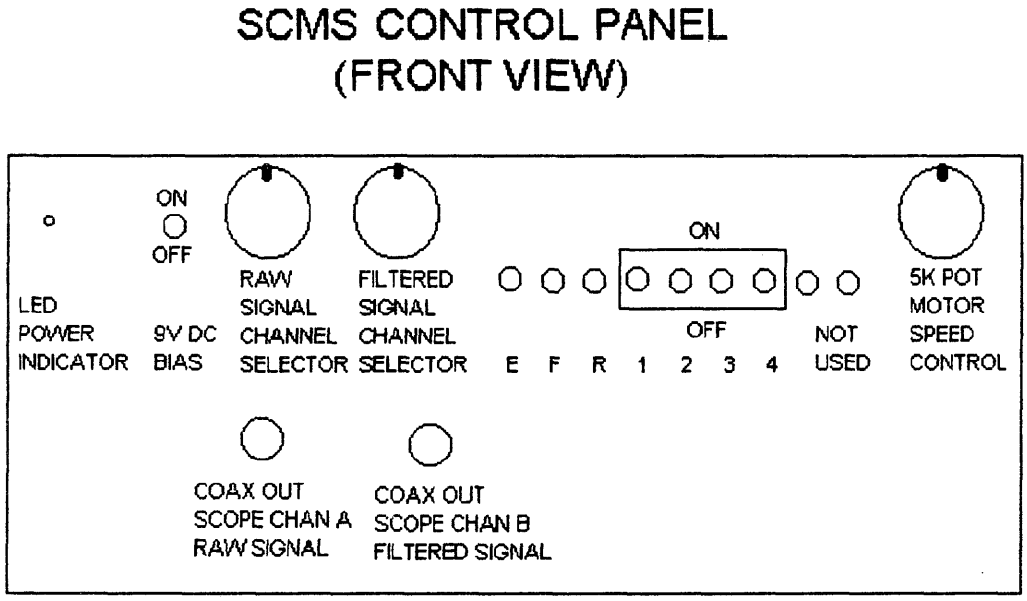

Figure 3.2. SCMS Control Panel (Front View).

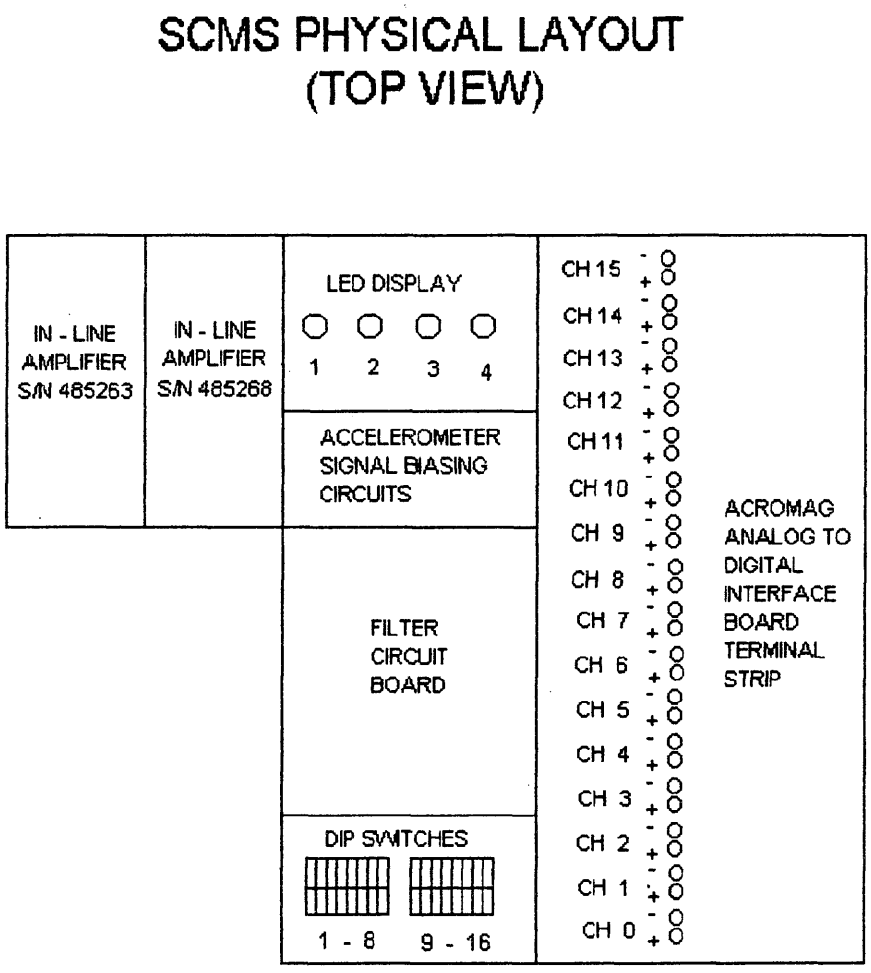

Figure 3.3. SCMS Physical Layout (Top View, with Cover Removed).

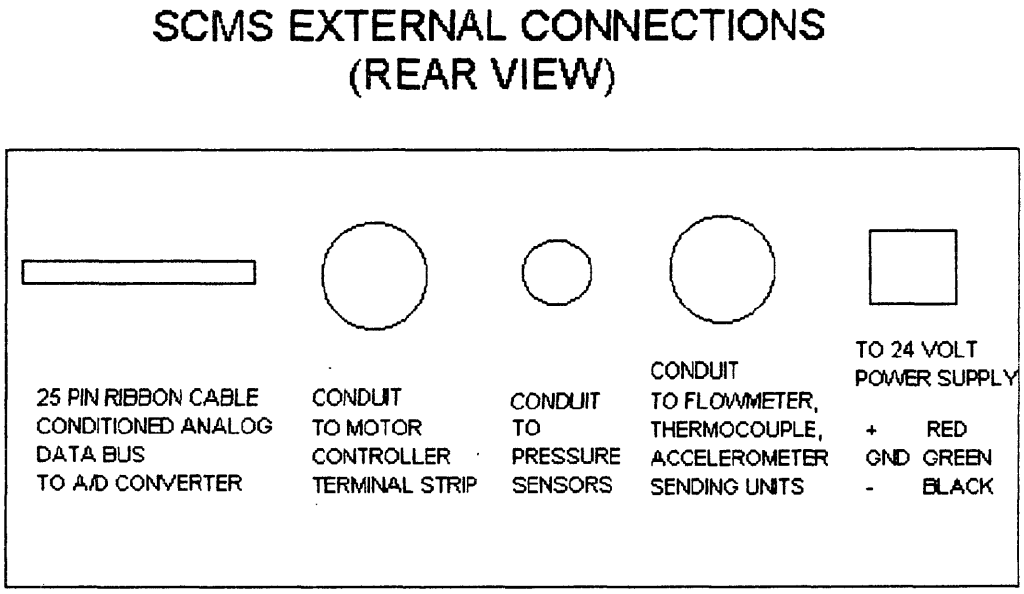

Figure 3.4. SCMS External Connections (Rear View).

Chapter 4.

MECHANICS OF THREE-PHASE PULSE WIDTH MODULATION

Speed control of DC motors can be accomplished by merely changing the DC input voltage to the motor. The speed of an AC induction motor, however, depends on the frequency of a sinusoidal input voltage (and also motor load). AC induction motors have historically been used as constant speed devices until a practical means of modulating the input frequency and voltage was conceived. This is now accomplished using Silicon Controlled Rectifiers (SCRs), Insulated Gate Bipolar Transistors (IGBTs), and other similar high-speed switching devices. Pulse Width Modulation (PWM) is a popular motor control technique which utilizes such devices. As in the case with the INEL hydraulic test bench, PWM can also be used to control three-phase induction motors.

Earlier types of adjustable speed drives have been rendered obsolete by PWM technology (Flett, 1994). Controllers which make use of high - speed switching are less expensive, more efficient, more reliable, have improved low-speed capabilities, and are now universally accepted to the exclusion of earlier types. As a result, PWM-generated EMI is becoming epidemic.

PWM controllers do not actually produce sinusoidal voltages; they produce short-duration voltage pulses which are modulated representations of the sinusoidal source voltage. Figure 4.1 shows a simple PWM output voltage ($V_{controller}$) together with the sinusoidal modulation voltage which it simulates ($V_{sinusoid}$). If Vcontroller is connected to the motor leads, it will operate almost as if it were receiving the corresponding sinusoidal voltage. Note that the duration d of the pulses corresponds to the amplitude of $V_{sinusoid}$; the longer

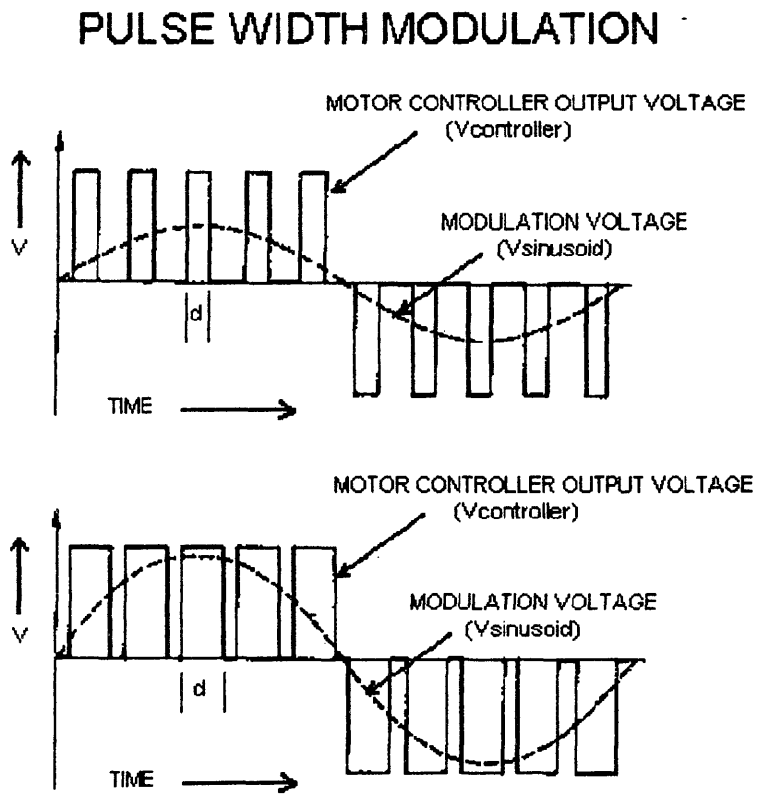

Figure 4.1. Pulse Width Modulation (Modified from Williams, 1992).

the ON pulse, the higher the amplitude. Changing the pulse width of $V_{controller}$ does not change the frequency of $V_{sinusoid}$.

Figure 4.2 shows the next level of complexity in the construction of a pulse-width modulated motor controller output signal. A triangular

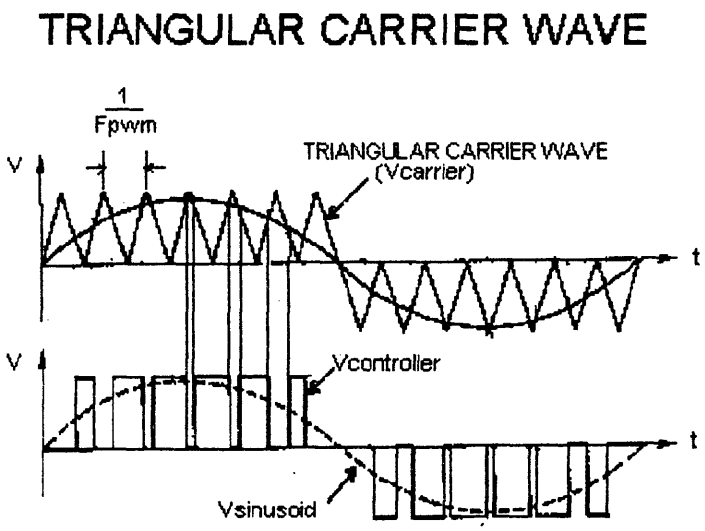

Figure 4.2. Triangular Carrier Wave (Modified from Williams, 1992).

carrier wave $V_{carrier}$ of high frequency F_{pwm} is first superimposed on $V_{sinusoid}$. The points where the two curves intersect determine the duration of the pulses in $V_{controller}$. Note that the time-integral of $V_{controller}$ and $V_{sinusoid}$ are approximately equal. This enhancement results in smoother, more efficient motor operation. Also note that the

motor windings behave as RL circuit elements which filter $V_{controller}$ to produce $V_{sinusoid}$.

Figure 4.3 illustrates an additional level of complexity involved in three-phase PWM modulation. The top graph shows the triangular

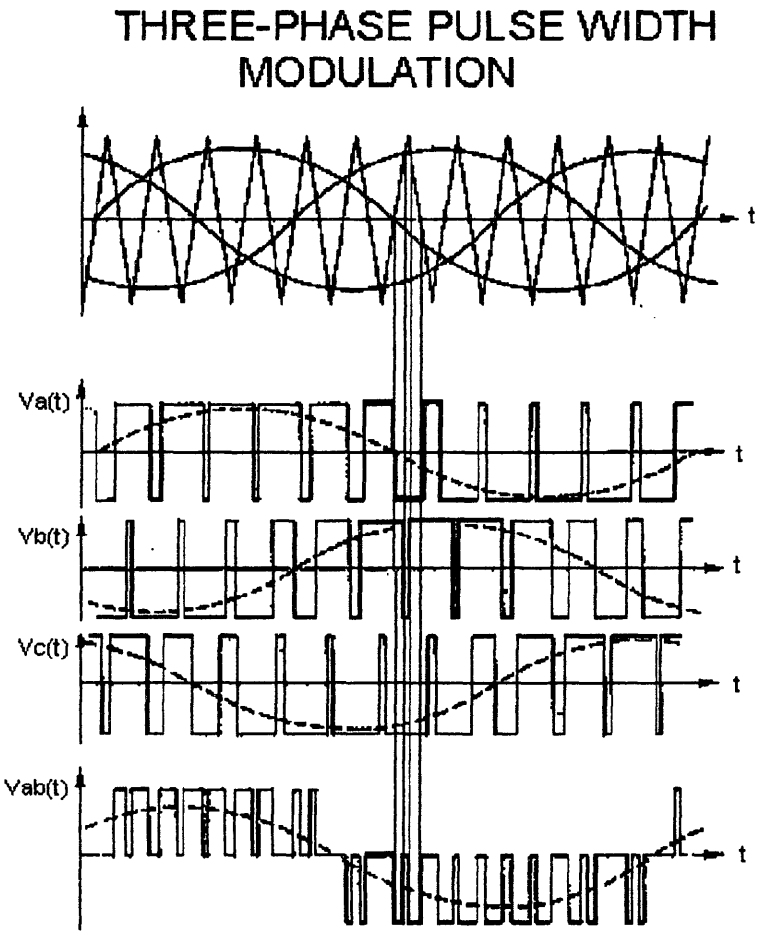

Figure 4.3. Three-Phase Pulse-Width Modulation (Modified from Williams, 1992).

carrier wave and each of the three phases of the sinusoidal motor input voltage which we wish to modulate. The middle three graphs show each of the three-phase line-to-neutral PWM controller outputs and the bottom graph shows one of the line-to-line PWM controller voltages. The line-to-line voltage $V_{ab}(t)$ is equal to the difference in the line-to-ground voltages $V_a(t)-V_b(t)$.

To maintain constant motor torque in AC induction motors, one must increase the amplitude of $V_{sinusoid}$ as speed increases due to frequency rise (Flett, 1994). In the Baldor motor controller, the amplitude of the sinusoidal input voltage (prior to modulation) can be changed in direct proportion to its frequency (linear V/Hz profile, Figure 4.4).

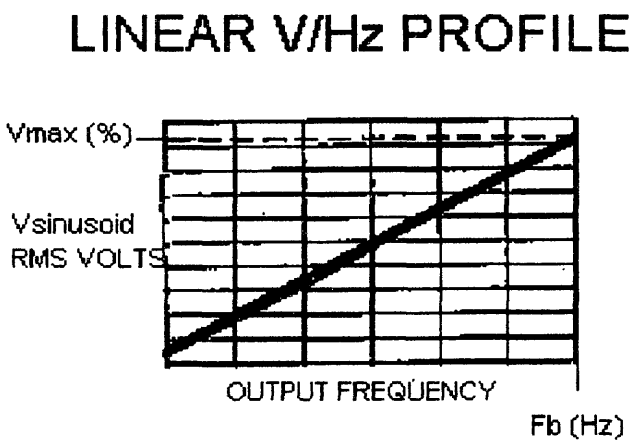

Figure 4.4. Linear V/Hz Profile (Modified from Baldor, Inc., 1994).

The constant of proportionality between amplitude and frequency is controlled by the operator from the keypad using the parameter CONTROL BASE FREQUENCY, or F_b.

To better understand the origin of the noise voltages observed on the test bench sensor circuits, the actual output waveforms of the Baldor motor controller were observed. Measurement of the PWM controller output voltages involves working with lethal electric currents (53 amperes maximum), so strict safety precautions were observed. As shown in Figure 4.5, attenuating differential voltage probes were used to obtain the line-to-line controller output voltages

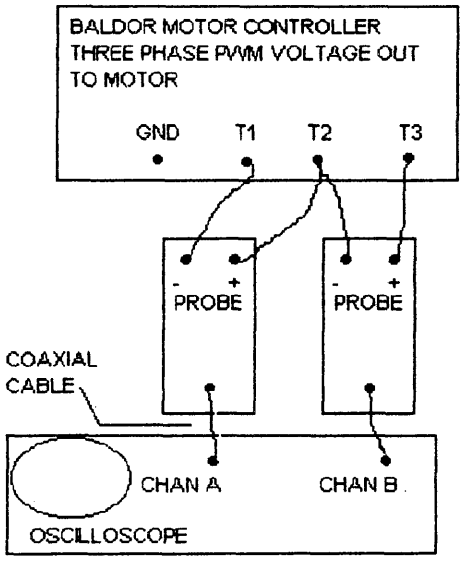

Figure 4.5. Oscilloscope Configuration for Measuring Controller Output.

on two of the three output phases for a range of operating conditions. Figure 4.6 shows a typical oscilloscope trace resulting from this configuration.

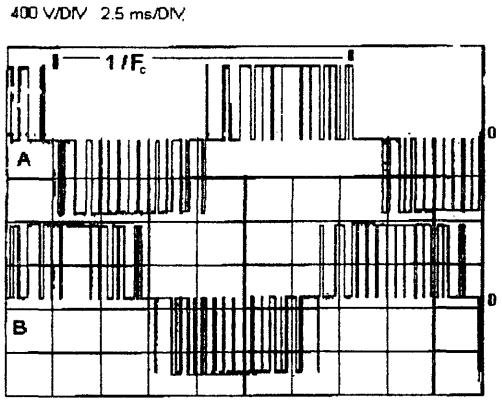

Figure 4.6. Observed Controller Output Voltage.

Figure 4.6 shows the pulse-width-modulated line-to-line controller output voltage traces A and B, each 1300 volts peak-to-peak and 120 degrees out of phase. In this example, the command frequency F_C = 60 Hz, the control base frequency F_b = 60 Hz, and the frequency of the triangular wave F_{pwm} = 1000 Hz. (Since this is a four-pole induction motor, the actual speed of motor rotation is 30 Hz.) As will be discussed in Chapter 7, the frequencies F_C, F_{pwm}, and F_b each affect motor controller EMI performance.

Chapter 5.

NOISE COUPLING IN ELECTRICAL CIRCUITS

Disturbances from various external energy sources can penetrate electrical circuitry and reappear as unwanted electrical noise and interference. The disturbances can be coupled to circuitry through conductance, common impedance, or via electromagnetic fields.

Conductive coupling occurs when spurious voltages are directly introduced into a circuit through wires, such as AC power leads. On the test bench, an investigation was run to quantify the amount of noise being conducted through the line voltage to the sensing circuitry. While the motor was active, it was evident that noise spikes were being conducted through the 110 V AC power line. When the motor was turned off, the spikes vanished. In Figure 5.1, the noise spike at the crest of the sinusoid is 24 mV, and the instantaneous line voltage is 155 V, giving an instantaneous signal-to-noise ratio of 76 dB. Conducted noise through the power lines is minimal here; in more serious cases isolation or conditioning of the line voltage may be required. In addition, the DC power supply used for instrumentation contains a ripple filter which reduces noise conducted via the AC line voltage.

Figure 5.1. Conducted Noise on 110 V AC Line Voltage.

Common impedance occurs when two circuits share a common ground, and the ground voltage of one is affected by the ground current of another (Ott, 1976). To safeguard against common impedance problems, the test bench chassis was grounded to structural building steel with a short, conductive ground strap. Good earth grounds were also established in the instrumentation circuits using short, low resistivity connections. Signal grounds were tied to a common point separate from the power grounds. All ground connections were checked with a voltmeter. Common impedance does not appear to be a major source of noise on the test bench sensor signals.

Electromagnetic noise coupling, however, introduces significant noise to the test bench sensor signals. The behavior of electromagnetic radiation is fully described by Maxwell's integral equations; however, the equations are unwieldy in practical applications as they require exact boundary conditions and are computationally and conceptually difficult. Practical solutions to EMI problems can more readily be

achieved through the use of network analysis. In this greatly simplified construction, the interaction of an electric field between two conductors is represented by a lumped capacitance and the interaction of a magnetic field between two conductors is represented by a lumped mutual inductance. From network theory, it can be shown that for electric field (capacitive) coupling,

$$Vnoise(s) = sRC(Vsource), \quad \text{or in the time domain,} \qquad \text{(Equation 5.1.1)}$$

$$Vnoise(t) = RC\frac{d(Vsource)}{dT}, \qquad \text{(Equation 5.1.2)}$$

where R is the resistance between the receiving conductor and ground, and C is the capacitance between the receiving conductor and the source conductor. Likewise, for magnetic field (inductive) coupling,

$$Vnoise(s) = sM(Isource), \quad \text{or in the time domain,} \qquad \text{(Equation 5.1.3)}$$

$$Vnoise(t) = M\frac{d(Isource)}{dT}, \qquad \text{(Equation 5.1.4)}$$

where M is the mutual inductance between source and receiver circuits (equations modified from Ott, 1976).

If the instrumentation is close to the noise source, as is the case in the test bench, electric and magnetic fields must be considered

separately. If the instrumentation is far from the source (far field), the radiation is considered combined EM radiation. Near and far fields are further discussed in Appendix D.

The theoretical noise voltage V_m developed across the ends of a loop antenna exposed to a magnetic field is

$V_m = 2\pi nfABcos\ \theta$ (Equation 5.1.5 from Johnson, 1984)

and the theoretical noise voltage V_e developed across the ends of a loop antenna exposed to an electric field is

$V_e = \frac{2\pi nAE}{\lambda} \cos \theta'$ where (Equation 5.1.6 from Johnson,1984)

f = the frequency of the magnetic field disturbance in Hz,

λ = the wavelength of the electric field disturbance in meters,

A = area of the loop in square meters,

B = incident magnetic field,

E = incident electric field,

n = number of turns of wire,

θ = angle between the magnetic field and a line normal to the loop, and

θ'= angle between the electric field and the plane of the loop.

When characterizing EMI it is useful to determine whether the noise field is predominantly electric or magnetic in nature, as shielding techniques depend on the type of radiation involved. Using two single-loop wire antennas simultaneously as shown in Fig. 5.2, it is possible to distinguish an electric field from a magnetic field. The antennas are identical, except that antenna A is shielded with an outer conductor which is gapped at the top to prevent the flow of noise current within the shield. Antenna A responds only to magnetic disturbances, while antenna B picks up noise voltage from both electric and magnetic disturbances (Ott, 1976). This relationship was useful in characterizing the EMI emanating from the test bench.

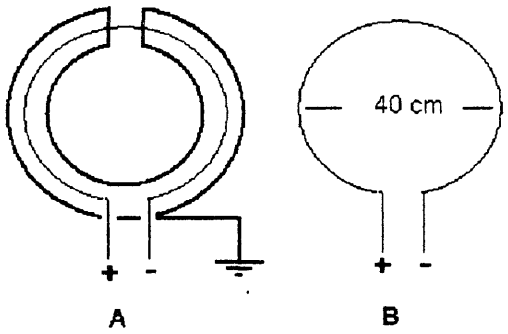

Figure 5.2. Antenna Configurations.

Chapter 6.

ANTENNA EXPERIMENTS

As depicted in Figure 6.1, experimentation with antennas was carried out in an attempt to 1) confirm that the mode of noise coupling to the sensor circuitry is indeed EMI emanating from motor control circuitry, and 2) to establish whether the nature of the postulated noise field is electric, magnetic, or some combination thereof. To eliminate the detection of ground potentials and to ensure that V is purely the result of radiated electromagnetic interference, the oscilloscope used to measure V was isolated from ground.

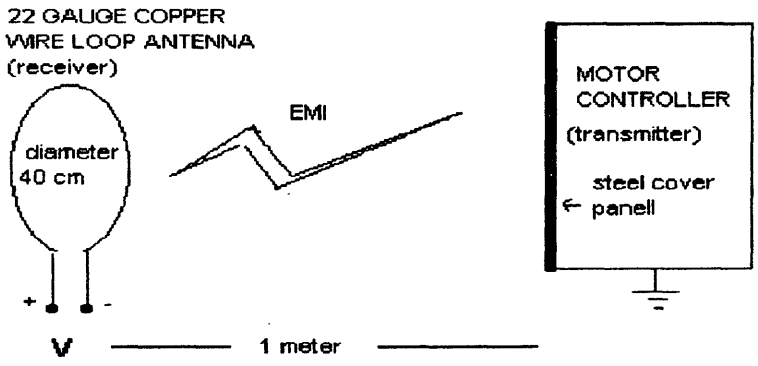

Figure 6.1. EM Field Measurements.

Six experiments involving antennas were carried out. In the first experiment, antenna voltage measurements were taken with and without the steel cover panel to determine if it has a shielding effect. In the second experiment, simultaneous measurements were taken with field-selective antennas to determine whether the noise field is principally electric or magnetic in nature. In the third experiment, antenna voltage measurements were collected with the motor under no-load and full-load conditions to determine the effect of motor current on the noise field. In the fourth experiment, simultaneous voltage measurements were taken using a) a single-turn loop antenna and b) multi-turn loop antennas, to determine the effect of antenna LRC on observed noise voltage. In the fifth experiment, direct line-to-line controller output phase voltage traces were collected simultaneously with antenna voltage traces. In the sixth experiment, the base controller frequency F_b was varied to determine its effect on antenna response. (F_b determines the slope of the V/Hz profile, as explained in Chapter 4 and Appendix B.)

Figure 6.2 shows the result of the first antenna experiment. A single loop unshielded antenna receiver was used to pick up controller EMI noise Traces A and B. The PWM carrier frequency F_{pwm} was set to 2500 Hz and the command frequency F_C was set to 2 Hz. (F_C and F_{pwm} are explained in Appendix B.) Trace A was collected with the controller cover panel installed; V_{pp} for Trace A is 38 mV. Trace B was collected with the cover panel removed; V_{pp} for Trace B is 62 mV. Operating the controller with the cover plate installed resulted in a noise attenuation of 20 log(62/38) = 4 dB. The first experiment confirms that the noise voltage is at least partially due to EM radiation originating from the motor controller.

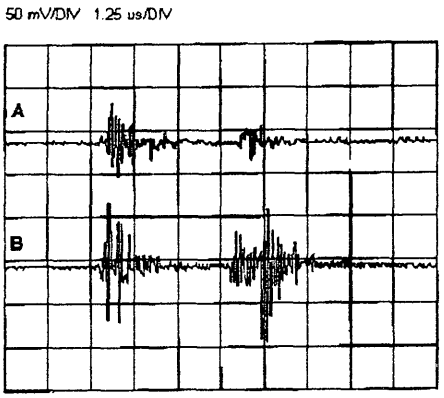

Figure 6.2.
Antenna Experinment 1.

In the second experiment, two antennas A and B (Figure 5.2) were used to simultaneously measure EM noise voltage. Antenna A was shielded with aluminum foil using the split-shield configuration and Antenna B was left unshielded. The voltage traces of A and B (Figure 6.3) were acquired with F_{pwm} set to 2500 Hz and F_C set to 2 Hz. V_{pp} for Antenna A is 48mV and V_{pp} for Antenna B is 544 mV. Clearly, the electric field is the dominating component of the noise field emanating from the motor controller circuits. The small residual voltages measured at the

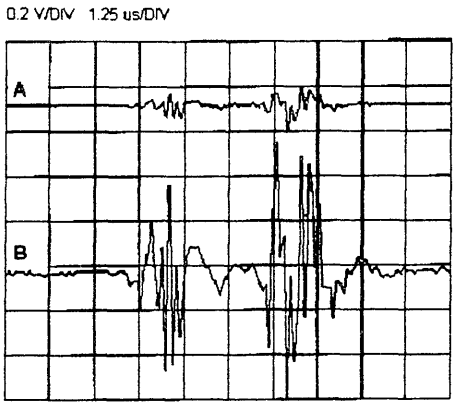

terminals of Antenna A may be either the result of magnetic induction or imperfect electric shielding.

Figure 6.3. Antenna Experiment 2.

In the next experiment, F_{pwm} was set to 2500 Hz, F_C was set to 10 Hz, and an unshielded wire loop antenna was used to measure field effects for a range of load conditions. In Figure 6.4, Trace A represents antenna response for no-load (valve R_O full open) and Trace B represents full-load (4,000 psig pump output pressure). Although the motor draws more current during loaded operation, no increase in antenna response was noted. This supports the conclusion that the noise coupling is principally capacitive. If the noise were inductively coupled, an increase in load would have caused an increase in the noise voltage.

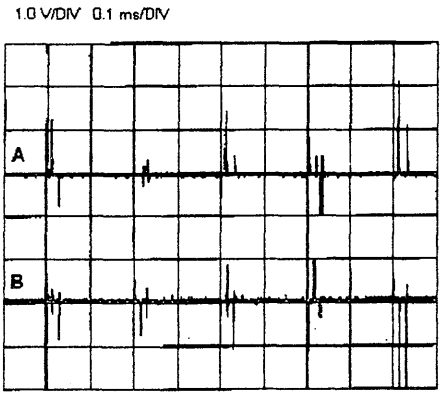

Figure 6.4.
Antenna Experiment 3.

The fourth antenna experiment was designed to investigate the effects of antenna LRC on the observed noise voltage waveform (Figure 6.5). As with the previous setup, F_{pwm} was set to 2500 Hz and F_C was set to 10 Hz. Antenna voltage Traces A and B were collected simultaneously. Trace A is the voltage developed at the terminals of a ten-turn loop, whereas Trace B is the voltage developed at the terminals of a single-turn loop. Trace A shows ringy, high-amplitude 1 MHz damped sinusoids with long decay time; Trace B shows low-amplitude 6MHz damped sinusoids with short decay time. This experiment shows that EMI noise voltages strongly depend on the LRC network characteristics of the receiving circuit, and in order to accurately characterize the EM field, the transfer function of the receiving antenna must be taken into account. As discussed in Chapter 2, this is one reason why the EMI noise characterization was done primarily in the time domain rather than in the frequency domain.

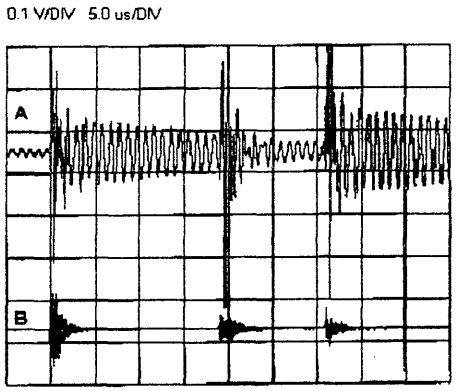

Figure 6.5.
Antenna Experiment 4.

In the fifth antenna experiment, F_{pwm} was set to 5,000 Hz and F_C was set to 60 Hz. In Figures 6.6 and 6.7, Trace A represents one phase (line-to-line) of the power converter output, and Trace B represents the voltage response of a single loop antenna. Both Traces A and B were

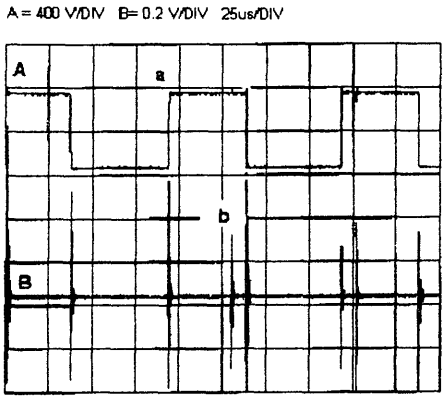

Figure 6.6

Antenna Experiment 5a.

acquired simultaneously. In Figure 6.6 at Point a, note that a step in one phase of the controller voltage results in a corresponding spike in the antenna voltage. However, at Point b, the spike in the antenna voltage does not correlate to the controller voltage. The spike at Point b originates from one of the other two controller phases. Figure 6.6 suggests that the noise voltage is related to the time-derivatives of each of the three-phase controller voltages.

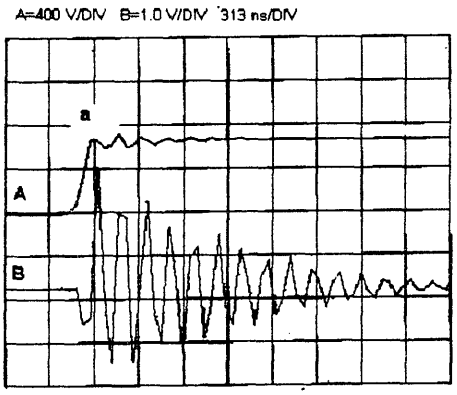

Figure 6.7.

Antenna Experiment 5b.

Figure 6.7 shows a single voltage switching event at an expanded time scale so that high-frequency behavior can be observed. Again, the antenna voltage (Trace B) appears as a derivative of the controller voltage (Trace A). The dominant frequency in both Traces is 6 Mhz.

Finally, in the sixth antenna experiment, (Figure 6.8), F_{pwm} was set to 2500 Hz and F_c was set to 10 Hz. Traces A and B in Figure 6.8 are single-loop unshielded antenna voltage responses. For Trace A, the controller was set to F_b = 240 Hz, and for Trace B, the controller was set to F_b = 60 Hz, which is the manufacturer's default setting. Notice that the parameter t decreases as F_b increases. (The parameter t is maximum duration of a 3-component noise pulse, which will be discussed in detail in Chapter 7.) From the perspective of noise reduction, Trace A is preferred over Trace B because a larger percentage of the signal is free of noise. The effect of F_c, F_b, and F_{pwm} on the noise trace will be further explored in Chapter 7.

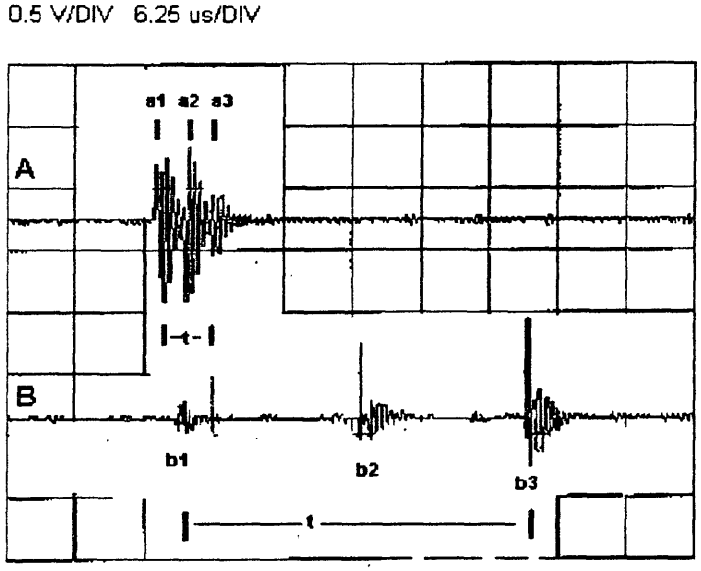

Figure 6.8. Antenna Experiment 6.

Chapter 7.

EMI NOISE CHARACTERIZATION

The raw oscilloscope voltage trace of each sensor was acquired under a range of operating conditions in order to illustrate and characterize signal and noise. The data presented in this chapter were collected prior to implementation of noise reduction measures. A five-meter length of shielded twisted pair cable for each sensor was used, except for S_h and S_v, in which case a five-meter length of coaxial cable was used. (S_h and S_v, are horizontal and vertical accelerometer traces. The accelerometer traces are described in Appendix B.) During data collection, the wrapped foil shield on the five-meter twisted pair cable was left ungrounded on both ends. The motor was allowed to run without load, except when specified otherwise.

7.1. Thermocouple Response.

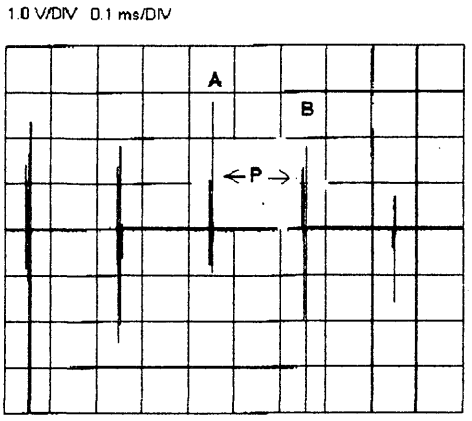

Figures 7.1.1, 7.1.2, and 7.1.3 all display the raw thermocouple signal at F_C = 2 Hz and F_{pwm} = 2500 Hz. (F_C and F_{pwm} are explained in Appendix B.) Voltage spikes of up to 4 volts occur at time intervals of $P = 1/(2F_{pwm}) = 0.2$ ms. Note Voltage Spikes A and B.

Figure 7.1.1.

Thermocouple Trace 1.

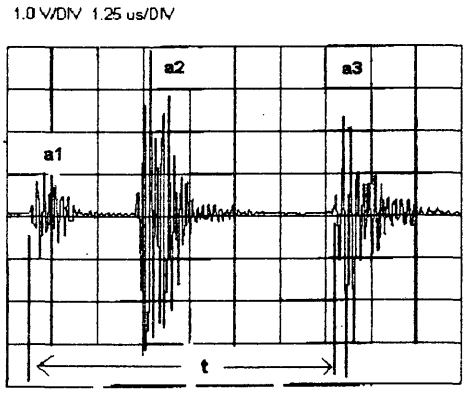

When viewed in an expanded time scale (Figure 7.1.2), Voltage Spike A can be seen to consist of up to three exponentially decaying Sinusoids a1, a2, and a3. The decaying 6 MHz sinusoids are more related to sensor circuit impulse response than to the actual EMI field. The parameter t is the maximum time interval between the onset of the first Component Waveform a1 and the onset of the last Component Waveform a3. Here, t= 8 μS.

Figure 7.1.2.

Thermocouple Trace 2.

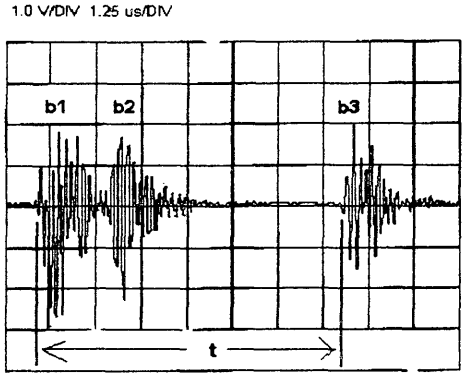

Figure 7.1.3.
Thermocouple Trace 3.

During normal motor operation, the component waveforms appear to systematically change their positions relative to one another while staying within the time interval t. Figure 7.1.3 shows the Component Waveforms b1, b2,and b3 of a second Voltage Pulse B. The parameter t has not changed, however the onset times of the component waveforms are now different. Note again that t is the maximum separation between b1 and b3, and that b3 can occur at separations of less than t. The three component waveforms are apparently related to switching events on separate phases of the inverter output.

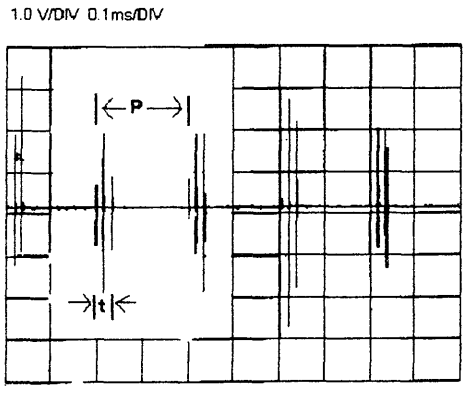

Figure 7.1.4.
Thermocouple Trace 4.

Figures 7.1.4, 7.1.5, and 7.1.6 show the effect of increasing F_C while holding all other control variables constant. When the motor is programmed to operate with a linear V/Hz curve, the parameter t increases linearly with F_C. Figure 7.1.4 is the oscilloscope trace at F_C = 10 Hz. For these settings, t = 35.5 μS.

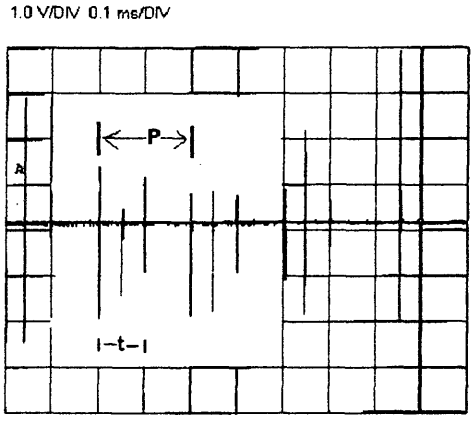

Figure 7.1.5 shows the thermocouple trace at F_C = 30 Hz. Notice that P remains unchanged, while t has increased to 100 μS.

Figure 7.1.5.

Thermocouple Trace 5.

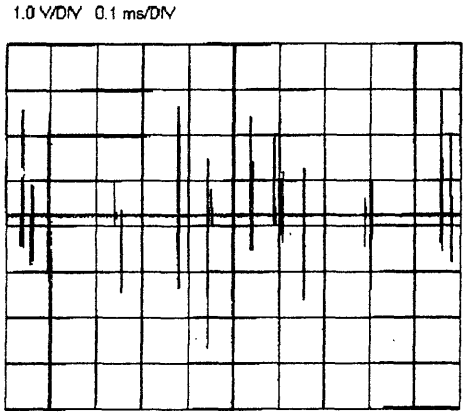

Figure 7.1.6 shows the thermocouple trace at F_C = 60 Hz. At higher motor speeds, the Component Waveforms a1, a2, and a3 overlap with b1, b2,and b3, and A and B can no longer be distinguished. The noise spikes now appear to be randomly distributed in time.

Figure 7.1.6.

Thermocouple Trace 6.

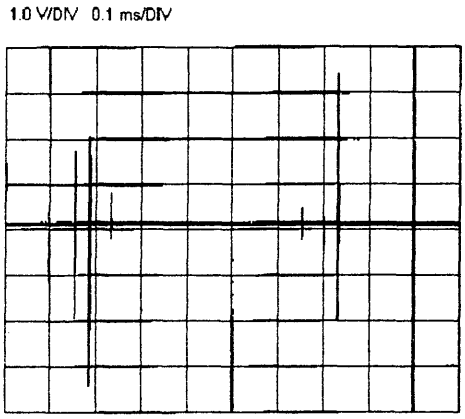

Figures 7.1.7 through 7.1.9 show the effect of changing F_{pwm} while holding all other control variables constant. In Figure 7.1.7, F_{pwm} = 1 kHz, F_C= 10 Hz, P = 500 μS, and t = 78 μS.

Figure 7.1.7.

Thermocouple Trace 7.

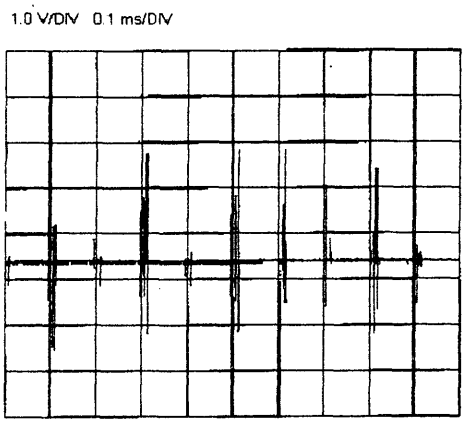

In Figure 7.1.8, F_{pwm} = 5 kHz, F_C = 10 Hz, P = 100 μS, and t = 15.8 μS.

Figure 7.1.8.

Thermocouple Trace 8.

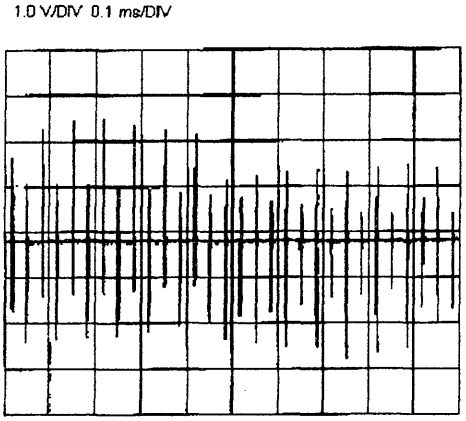

Figure 7.1.9.

Thermocouple Trace 9.

In Figure 7.1.9, F_{pwm} = 15 KHz, F_C = 10 Hz, P = 33.3 μS, and t = 4.28 μS.

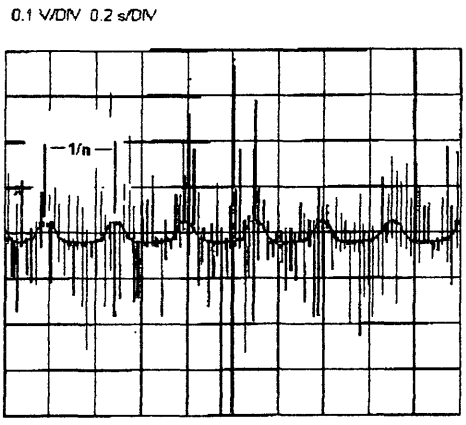

Figure 7.1.10.

Thermocouple Trace 10.

In Figure 7.1.10, F_{pwm} = 10 kHz and F_C = 10 Hz. The data is displayed in a compressed time scale to reveal a 3.3 Hz noise train. The noise frequency n increases with F_C and occurs only at those combinations of F_{pwm} and F_C which result in jerky motor operation. Grounding the shield of the twisted pair thermocouple leads to the bench frame eliminated the noise, but grounding the opposite side of the shield to the

instrument bench ground had no effect. This is not a typical grounding solution for capacitive-coupled noise. The above characteristics suggest that the low-frequency noise is a result of inductive coupling from unbalanced currents in the motor windings.

The thermocouple noise data summarized in Table 7.1 on the following page show that

$t = (F_c/2)/(k * F_{pwm})$ and (Equation 7.1.1)

$P = 1/(2F_{pwm})$. (Equation 7.1.2)

The constant k was empirically determined and is equal to 65. Later in the analysis, k was discovered to be equal to the control base frequency F_b, which was set to 60 Hz throughout the thermocouple analysis. The exact value of 60 Hz was not calculated due to difficulty in freezing rapidly changing traces on the oscilloscope screen.

The equation

$t = (F_c/2)/(F_b * F_{pwm})$ (Equation 7.1.3)

fully describes the parameter t as a function of motor controller variables. This result is useful in adjusting the controller for improved EMI performance.

Fpwm (Hz)	Fc/2 (Hz)	P (microsec)	t (microsec)	k	n (Hz)
1000	5	500	77	64.93506	no noise
1000	7.5	500			no noise
1000	10	500			no noise
1000	15	500			no noise
2500	1.0	200	5.7	69.80803	
2500	2.5	200	15.6	64.10256	
2500	5.0	200	31.8	62.89308	
2500	7.5	200	48.0	62.50000	
2500	10.0	200	63.3	63.19115	
2500	12.5	200	80.0	62.50000	
2500	15.0	200	95.2	63.02521	
5000	5	100	15.2	65.78947	no noise
5000	6	100			5.95
5000	7.5	100			6.76
5000	10	100			7.81
5000	12.5	100			no noise
10000	5	50	7.1	70.42254	3.33
10000	7.5	50			4.59
10000	10	50			6.71
10000	12.5	50			no noise
15000	5	33.33333	5.1	65.35948	2.18
15000	7.5	33.33333			3.82
15000	10	33.33333			4.36
15000	15	33.33333			6.21

Table 7.1. Noise Characteristics of Thermocouple Voltage Traces.

The frequency of the induction noise n appears to be linear with F_C and inversely related to F_{pwm}, although no simple mathematical relationship could be established with confidence. The induction noise is most likely to occur at high F_{pwm} and with F_C range of 10-20 Hz.

One hundred noise voltage peak amplitudes were measured and averaged in order to set a base value for decibel noise attenuation. Most of the voltage peaks occur in the range 0.5-4.0 volts. The algebraic mean is 2.4 volts. The maximum DC thermocouple signal is 10 volts, which establishes the present S/N ratio at 20 log(10/2.4) = 12.4 dB.

7.2. Pump Output Pressure Transducer Response.

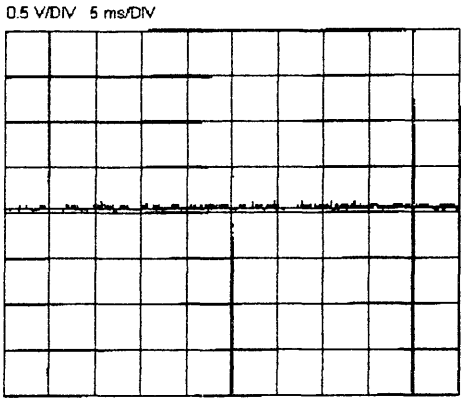

Figures 7.2.1 through 7.2.8 show the pump outlet pressure transducer response under a range of motor speed and load conditions. F_{pwm} was held constant at the default setting of 2500 Hz.
For Figure 7.2.1, F_C = 20 Hz, and the motor was not loaded.

Figure 7.2.1.

Pump Outlet Pressure Transducer Trace 1.

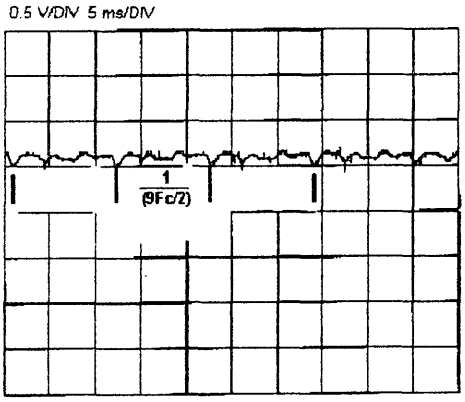

For Figure 7.2.2, F_C = 20 Hz, load = 3000 psi, and V_{pp} = 146 mV. Notice that under a loaded condition a frequency of 9(Fc/2) emerges. (F_C/2 is the angular velocity of pump rotation, and there are 9 pistons on the positive displacement pump).

Figure 7.2.2.

Pump Outlet Pressure Transducer Trace 2.

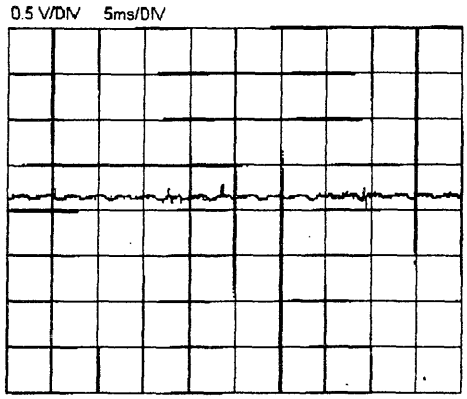

In Figure 7.2.3, F_C = 40 Hz, the motor was not loaded, and V_{pp} = 56 mV.

Figure 7.2.3.

Pump Outlet Pressure Transducer Trace 3.

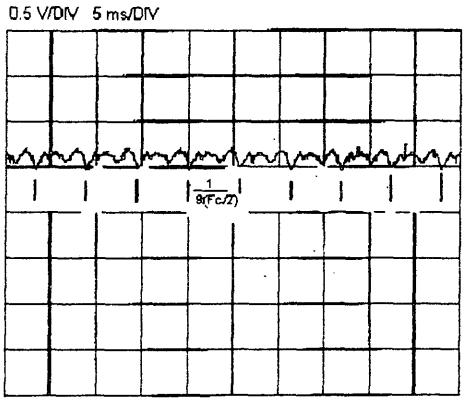

In Figure 7.2.4, F_C = 40 Hz, load = 3000 psi, and Vpp = 218 mV.

Figure 7.2.4.

Pump Outlet Pressure Transducer Trace 4.

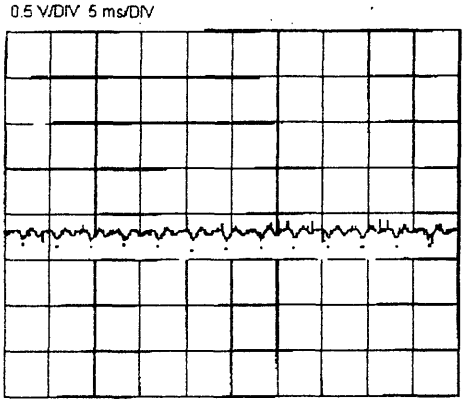

In Figure 7.2.5, F_C = 60 Hz, the motor was not loaded, and V_{pp} = 136 mV.

Figure 7.2.5.

Pump Outlet Pressure Transducer Trace 5.

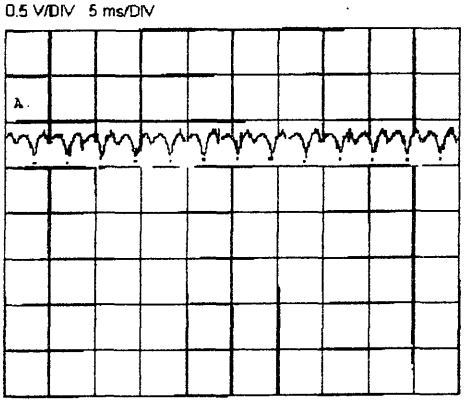

In Figure 7.2.6, F_C = 60 Hz, load = 3,000 psi, and V_{pp} =272 mV. Notice that the frequency $9(F_C/2)$ is maintained over a range of speeds, and the peak-to-peak amplitude increases with both speed and load.

Figure 7.2.6.

Pump Outlet Pressure Transducer Trace 6.

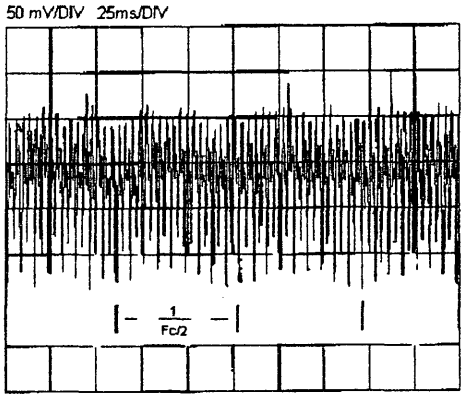

Figures 7.2.7 and 7.2.8 are displayed with a compressed time scale in order to observe frequencies Fc/2 and 9(Fc/2). In Figure 7.2.7, F_C = 30 Hz and the load is 3,000 psi.

Figure 7.2.7.

Pump Outlet Pressure Transducer Trace 7.

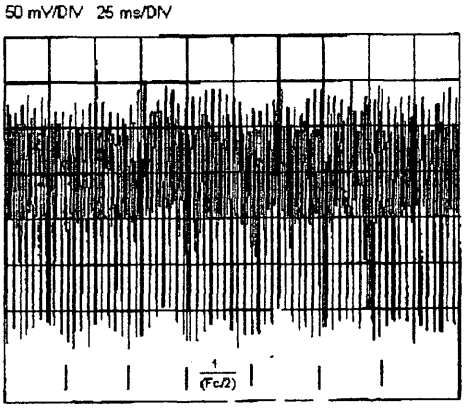

In Figure 7.2.8, F_C = 60 Hz and the load is 3,000 psi.

Figure 7.2.8.

Pump Outlet Pressure Transducer Trace 8.

The hydraulic pump features a tilted swashblock which actuates 9 individual pistons sequentially for every motor rotation, producing frequencies Fc/2 and 9(Fc/2) on the pressure trace. This effect offers encouraging possibilities for real-time system health monitoring. A similar effect can be seen on the input pressure trace which is discussed in the next section.

Early in the project, both pressure transducers provided by the manufacturer of the test bench failed, perhaps due to continued exposure to strong EM fields. While they were still operational, the transducers registered high levels of EM-induced noise and long voltage decay curves after each EMI burst. Unfortunately, hardcopy oscilloscope traces were not obtained before the sensors failed.

7.3. Pump Inlet Pressure Transducer Response.

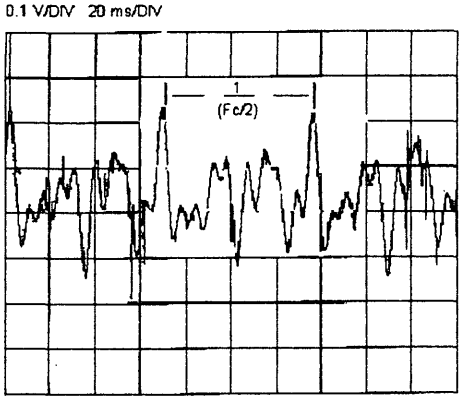

Figure 7.3.1.
Pump Inlet Pressure Trace 1.

Figures 7.3.1 through 7.3.5 show the oscilloscope voltage traces of the vacuum pressure transducer located at the pump hydraulic input. Sample traces were collected to show the effect of motor speed and pump cavitation . In Figure 7.3.1, F_C = 30 Hz, there is no cavitation occurring, and V_{pp} = 350 mV. Again, the frequencies $F_C/2$ and $9(F_C/2)$ are clearly visible.

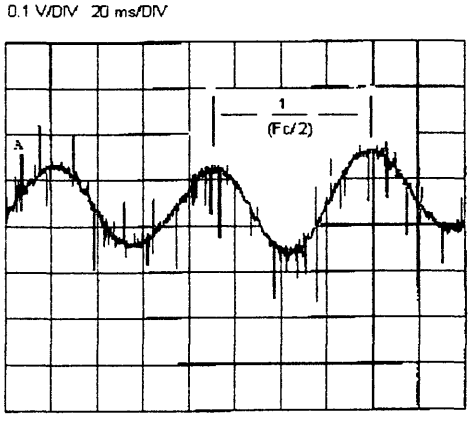

Figure 7.3.2.
Pump Inlet Pressure Trace 2.

In Figure 7.3.2, F_C = 30 Hz, cavitation is occurring, and V_{pp} = 212 mV. In a cavitated state, $F_C/2$ is readily observed, the individual piston events are obscured, and the overall signal amplitude is reduced.

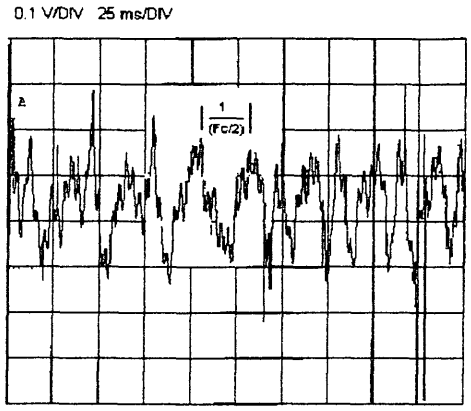

In Figure 7.3.3, F_C = 60 Hz, no cavitation is occurring, and V_{pp}=360 mV. F_C has little effect on V_{pp} in a non-cavitated state.

Figure 7.3.3.

Pump Inlet Pressure Trace 3.

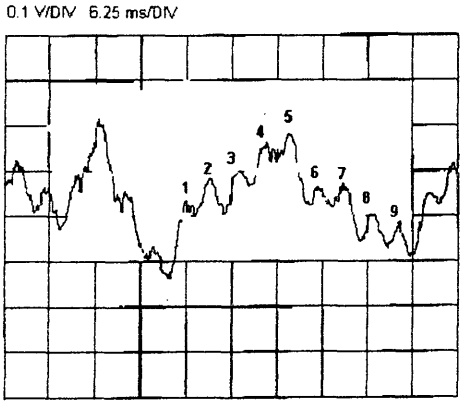

Figure 7.3.4 displays the data in Figure 7.3.3 with an expanded time scale to highlight the well-resolved piston events.

Figure 7.3.4.

Pump Inlet Pressure Trace 4.

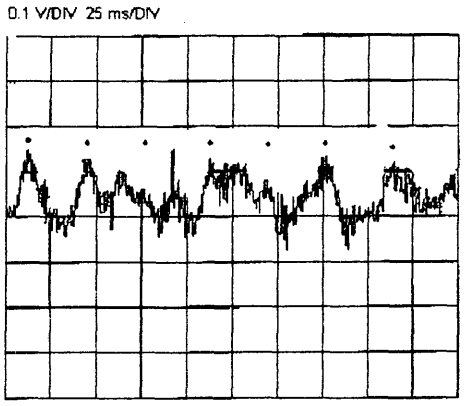

In Figure 7.2.5, F_C = 60, cavitation is occurring, and V_{pp} = 170 mV.

Figure 7.3.5.

Pump Inlet Pressure Trace 5.

Analysis of the low pressure trace led to the realization that the indicated motor speed F_C is twice the true motor speed, owing to the fact that the induction motor is four-pole.

7.4. Flowmeter Response.

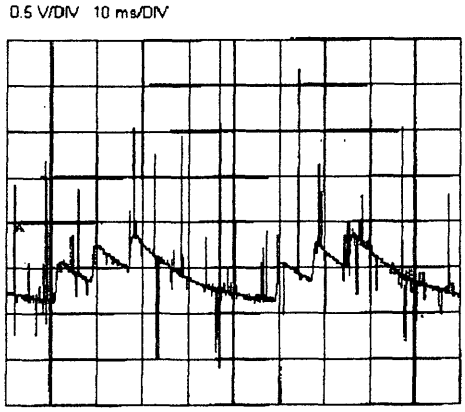

Figure 7.4.1.
Flowmeter Trace 1.

The volume flow rate is recorded by a turbine flow meter. The rotation of the turbine is recorded by a magnetic transducer which produces a series of voltage pulses with frequency proportional to the turbine rotation. The pulses are input to a pulse-rate-to-analog (f to V) converter mounted on the test bench frame. The converter output contains considerable ripple and PWM noise, as seen on these raw traces. Note the erratic sawtooth forms recorded at low flow rates. Zero flow was recorded below F_C = 20 Hz In Figure 7.4.1, F_C = 20 Hz and the pulse rate is 125 Hz.

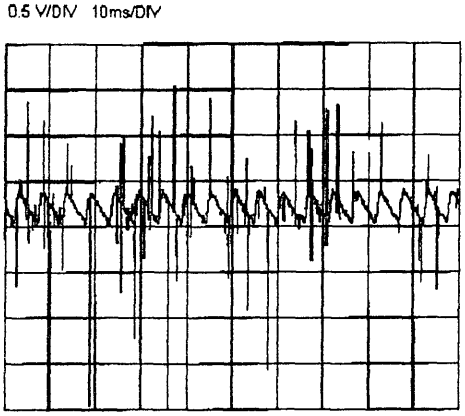

Figure 7.4.2.

Flowmeter Trace 2.

In Figure 7.4.2, F_C = 30 Hz and the pulse rate is 190 Hz.

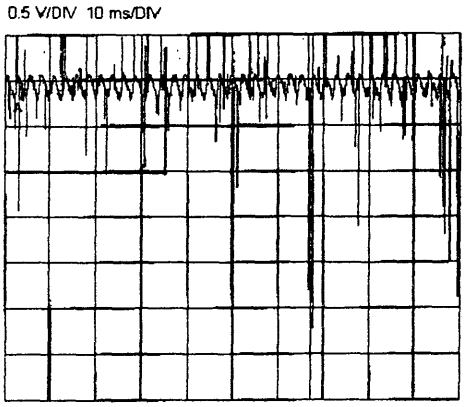

Figure 7.4.3.

Flowmeter Trace 3.

In Figure 7.4.3, F_C = 60 Hz and the pule rate is 380 Hz. The PWM noise spikes might be suppressed by moving the pulse-rate-to-analog converter unit away from the test bench chassis where it is currently mounted. Alternatively, the converter could be altogether removed and pulses could be counted digitally for a more direct measurement. Pulse rate appears to be strongly linear with motor speed.

7.5. Accelerometer Response.

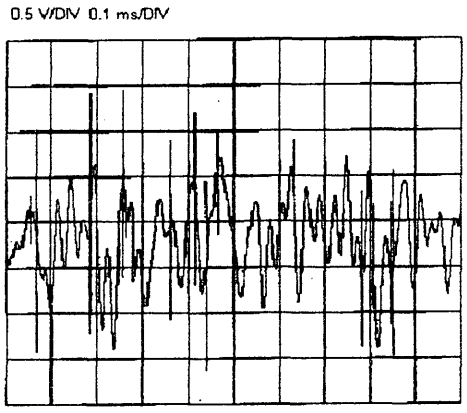

Figure 7.5.1. Accelerometer Trace (Instantaneous).

Two accelerometers are mounted on the pump housing. Both are radially mounted; one is horizontal and one is vertical. Each device is routed to a transmitter which provides two outputs. The first output voltage (Figure 7.5.1) is proportional to a directional component of instantaneous vibration acceleration, and the second output (Figure 7.5.2) is the RMS equivalent of the latter. The RMS value is a DC measure of the magnitude of acceleration experienced by the device. The data shown in Figures 7.5.1 and 7.5.2 were collected from the horizontally mounted accelerometer during pump cavitation and F_C = 60 Hz.

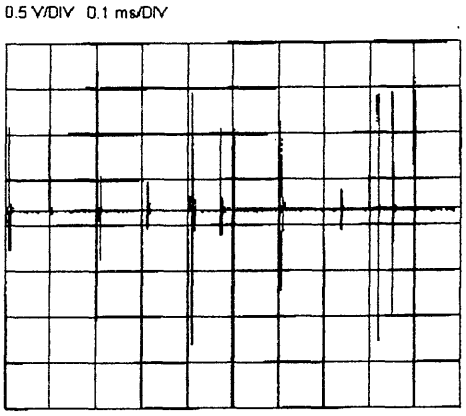

The transmitters for these accelerometers are mounted on the test bench chassis. As with the flowmeter, the severe PWM noise seen on these traces might be reduced by moving the transmitters to a location distal to the EMI source.

Figure 7.5.2.
Accelerometer Trace (RMS).

As with the pressure traces, the frequencies Fc/2 and 9(Fc/2) dominate the acceleration traces. Unlike the pump input pressure traces, the $9(F_C/2)$ piston event amplitudes increase during cavitation. A simplistic explanation for this effect follows: During normal pump operation, the forces developed on the piston faces react on the hydraulic fluid. If the supply of fluid to the pump is sufficiently restricted, the forces developed in the pistons must react on the mass of the pump, causing it to vibrate.

Chapter 8.

NOISE ATTENUATION TECHNIQUES

The Acromag AVME 932X Digitizing board features 16 Channel, 12 bit recording at sample rates of up to 67 kHz. It can be shown that an A/D recorder delivers a signal-to-noise ratio of 6dB per bit, or in this case 72 dB (Middleton, 1995). The aim of noise reduction techniques is to reduce the PWM-generated noise on the sensor voltages from its initial level of about 12 dB (Chapter 7) to a value below the quantization noise of 72 dB. Although this goal was not achieved, the signal-to-noise was measurably increased to a workable level of at least 40 dB by 1) relocating the noise source, 2) reducing length of high voltage leads, 3) shielding of the noise source, 4) grounding of the noise source, 5) adjusting motor controller settings, 6) conditioning the source voltage, 7) relocating network interface hardware, 8) shielding of sensor cabling and sensor circuitry, 9) grounding of shields, and 10) passive RC filtering of sensor signals.

8.1. Relocating the Noise Source.

When the test bench was delivered to CSM by its fabricators, the Baldor motor controller was mounted approximately 0.3 meters from the main sensor bank on the right side of the test bench chassis. The Baldor controller was removed and placed on the front of the test bench chassis near the motor. This modification increased the distance between the motor controller and the main sensor bank to 1.5 meters.

8.2. Reducing Length of High Voltage Leads.

When the test bench was delivered to CSM by its fabricators, the motor controller high voltage three-phase output was routed to the motor by about 3 meters of unshielded coiled wire. The long high-voltage line acted like a broadcasting antenna, overwhelming the sensors with EMI. Due to the relocation of the controller, it was possible to shorten the motor leads to about .5 meters.

8.3. Shielding of the Noise Source.

Shielding of the noise source was accomplished by 1) encasing the motor controller leads in 1.5 inch diameter flexible steel conduit,

grounded at both ends, 2) installing galvanized steel sheet on the back of the controller, and 3) replacing the front cover plate on the controller. Steel was chosen over aluminum and copper as the preferred shielding material based on the computer analysis given in Appendix D.

8.4. Grounding of the Noise Source.

The test bench chassis was solidly grounded to structural building steel using a special purpose, low resistivity copper braid.

8.5. Adjusting Controller Settings.

Referring to Figure 7.1.4 in the previous chapter, it has been demonstrated from empirical data that

$P = 1/(2F_{pwm})$ and (Equation 7.1.2)

$t = (F_c/2)/(F_b*F_{pwm})$, where (Equation 7.1.3)

P = the time between two successive 3-component noise bursts,

t = the maximum duration of a single 3-component noise burst,

F_c = the motor controller command frequency,

F_b = the motor controller base frequency, and

F_{pwm} = the motor controller PWM carrier frequency.

Again referring to Figure 7.1.4, notice that the ratio of noisy-trace-segment to clean-trace-segment is t/P. It is desirable to maximize P while minimizing the ratio t/P so that the greatest possible percentage of the sensor trace will be free of noise. It is not possible to eliminate the noise spikes, but it is possible to bundle them into tight, widely separated groups by adjusting the motor controller variables. Between these groups, the trace is virtually free of EMI noise. It is possible to sample only those points from the noise-free trace segments, but implementation of such a tuned system is beyond the scope of this thesis.

From equations 7.1.2 and 7.1.3, one obtains

$t/P = F_c/F_b$ (Equation 8.5.1)

Therefore, for improved signal quality, F_{pwm} should be small, F_c should be small, and F_b should be large. Fpwm, Fc, and Fb should be changed only to the extent that they do not compromise safety and overall motor performance.

Note also that the ratio t/P is the fraction of digitized samples which are contaminated by interference. This ratio is unaffected by the

sample rate or PWM carrier frequency (Fpwm). For example, if F_C = 20 Hz F_b = 60 Hz, one third of the samples will be affected by some PWM interference voltage.

It is believed that the intense EMI generated by the motor controller interferes with digital data transfer. During the early phases of testing, digital data transmission from the Ethernet interface to the host computer was often interrupted, resulting in lost data. Loss of information packets only occurred while the motor controller was operating. The number of interrupts per unit of time was found to increase with F_{pwm}. After F_{pwm} was reduced from its factory setting of 8 kHz to its minimum of 1 kHz, the number of Ethernet interrupts sharply decreased, although some interrupts still occurred.

8.6. Conditioning Source Voltage.

At this point, Baldor corporation technical service personnel recommended that a line reactor (also called a choke coil or three-phase inductor) be installed between the motor controller and the motor, in order to condition the PWM input voltage. This was an expensive option, so other alternatives were explored.

8.7. Relocating Network Interface Hardware.

The physical location of the Ethernet network interface was also found to have an effect on the number of interrupts. Through trial and error, a suitable location for the interface unit was found (on the floor against the west wall of Brown Hall Room 154), and interrupts have not been a serious problem since. The noise level on the sensor traces, however, was still unacceptable.

8.8. Shielding of Sensor Cabling and Sensor Circuitry.

Satisfied that we had done all we could within our means to attenuate the noise at its source, our attention shifted to the noise-receiving circuitry. As with the high voltage lines, the sensor cables were shortened and shielded with steel conduit, and the SCMS circuits were encased in a grounded Faraday cage. Steel was chosen over aluminum and copper as the preferred shielding material based on the computer analysis given in Appendix D.

8.9. Grounding of Shields.

Each twisted-pair sensor cable is shielded by flex conduit as well as the braided foil exterior of the twisted pair. At each end, the shields can be grounded or left floating, giving sixteen possible grounding configurations. Through trial and error, the most effective grounding combination was selected. The winning configuration has each end grounded except the twisted pairs on the test bench side (Figure C.11). Initially, the twisted pair shields were left to float inside the junction box, but improvements were realized by extending the floating shield terminations all the way up to the sensor casing (Fleischer, 1995).

8.10. Passive RC Filtering of Sensor Signals.

Simple first-order low-pass analog filters were constructed to condition the sensor signals. The filters can be enabled with dip switches inside the SCMS unit (Figure 3.3). The filter schematics are documented in Appendix C.

A short review of filter theory follows. As shown in Figure 8.10.1, each filter was constructed from a capacitor and a resistor. The transfer function of the filter is given by $1/(1+sCR)$, the time constant

τ is equal to RC, and the cutoff frequency f_C is equal to $1/(2\pi RC)$ Hz. (The command frequency F_C is not to be confused with the cutoff frequency f_C. Impedances at the input and output terminals of the filter will not be considered in this simple analysis.)

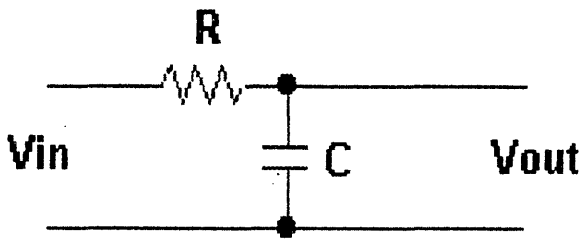

Figure 8.10.1. First Order Low-Pass Filter.

The Bode plot for this circuit (Figure 8.10.2) shows a flat frequency response for $f<f_C$, 3 dB attenuation for $f=f_C$, and 20 dB/decade roll-off for $f>f_C$.

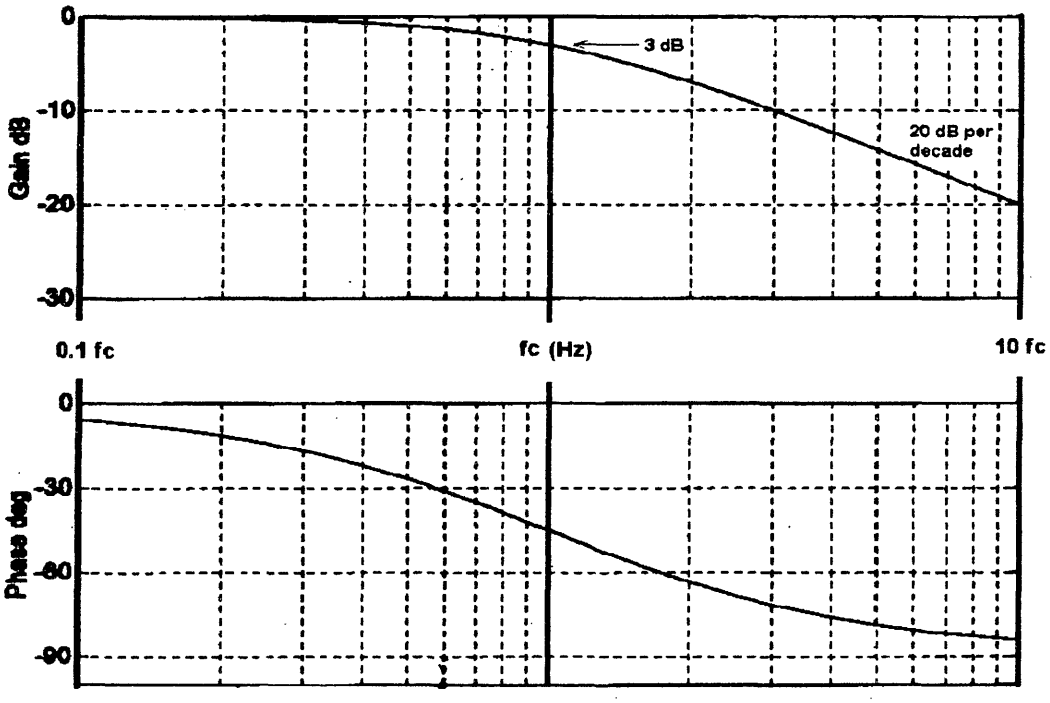

Figure 8.10.2. Bode Plot for a First Order Filter.

Table 8.10.1 gives a summary of the signal bandwidth and filter characteristics for Channels 1 through 9. Ideally, the analog filter bandwidth should be matched to that portion of the signal bandwidth

which contains the information of interest, and the sample rate should be set to at least twice the analog filter high-cut frequency. The sample rate for this initial setup was fixed at 12 Hz; however, the Acromag A/D board is capable of sampling at speeds of up to 67 kHz. The RC filter components are intentionally removable so that they can be tuned to provide anti-aliasing filtration for any sampling speed.

Channel Number	Sensor Variable	Sensor Bandwidth (Hz)	R (Ohms)	C (uF)	Cutoff Frequency (Hz)	Filter Time Constant (seconds)
1	To	DC	180	10	88	0.0018
2	Ti	DC	180	10	88	0.0018
3	Pi	3000	180	10	88	0.0018
4	Po	3000	180	10	88	0.0018
5	Q	DC	1000	10	16	0.01
6	Av	DC	180	10	88	0.0018
7	Ah	DC	180	10	88	0.0018
8	Sv	5000	300	0.1	5308	0.00003
9	Sh	5000	300	0.1	5308	0.00003

Table 8.10.1. Sensor Signal Bandwidths and High-Cut Frequencies.

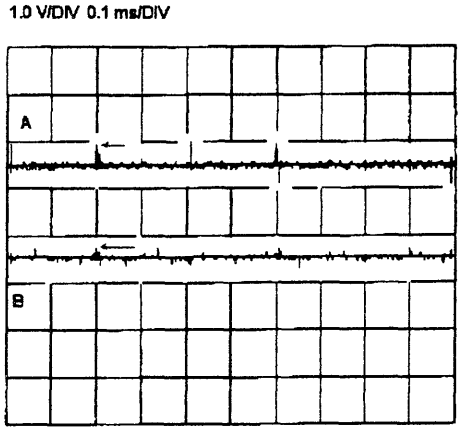

Figure 8.10.3
Thermocouple Response.

Figure 8.10.3 shows two traces A and B collected simultaneously from the same thermocouple. In this figure, F_C = 2 Hz, F_{pwm} = 2500 Hz, F_b = 60 Hz, and the motor is not loaded. Trace A shows the effects of grounding and shielding alone, whereas Trace B shows the combined effects of grounding, shielding, and filtering. Compare these to the raw, unshielded, unfiltered signals in Figure 7.1.1. The average magnitude of the EMI noise bursts for Trace A is approximately 500 mV, and the average magnitude of the EMI noise bursts for Trace B is approximately 100 mV. Greater attenuation could have been achieved by setting the high-cut to the recommended value of 6 Hz (half the sample rate). However, increasing R indiscriminately can 1) reduce the DC level of the signal and throw it out of calibration, and 2) increase system response time. Rather than simply calculating the values to be used for R and C, they were carefully selected for each channel while using an oscilloscope to monitor the AC and DC attributes of the filtered signal.

The Acromag AVME 932X A/D board is equipped with differential inputs for all 16 channels. However, in order to maintain a common point ground for all the sensors, the negative terminals of each channel

were connected. This signal ground was referenced to the negative terminal of the floating instrument power supply, as shown in Figure C.11. This step had the added benefit of simplifying the wiring in the SCMS channel selector switches.

Lastly, it was discovered that the high-frequency performance of the electrolytic capacitors could be marginally improved by adding .1 uF polystyrene capacitor in parallel. This modification was applied to each electrolytic filter capacitor.

Chapter 9.

RESULTS

1) The interference which has been contaminating the sensor signals has been identified as near-field EMI (electromagnetic interference).

2) The noise coupling is predominantly capacitive rather than inductive.

3) The noise voltage occurs as the derivative of 3-phase PWM motor control voltage.

4) EMI noise voltage frequencies depend on the LRC characteristics of the receiving circuit.

5) The approximate average amplitude of the noise spikes, as observed on the oscilloscope thermocouple trace, was reduced from 2.4 volts to 500 millivolts through relocation of system components, grounding, and shielding. For a 10 volt signal, this represents an improvement in S/N from 12 dB to 26 dB.

6) Additional attenuation was achieved using a first-order low-pass RC filter. For the thermocouple traces, R = 180 ohms, C = 10 μF, giving a

cutoff frequency of 88 Hz. This further suppressed the approximate average magnitude of the noise spikes to about 100 millivolts, increasing S/N to 40 dB for a 10 volt signal. Greater attenuation could be achieved by increasing R, but this would sacrifice response time and possibly throw the DC signal out of calibration.

7) The noise cannot be completely removed. Although the noise on the filtered signal is still greater than the quantization noise, it was reduced to a workable level of 40 dB. This means that the filtered signal has a resolution of almost 7 bits.

8) Using an empirical approach, equations 7.1.3 and 8.5.1 were developed, which relate the duration of noise trains directly to motor controller command frequency (F_C), the motor control PWM carrier frequency (F_{pwm}), and the base control frequency (F_b). The pattern of noise spikes (as seen on the thermocouple oscilloscope trace) can be modified using the above motor control settings. For optimum noise performance, F_{pwm} and F_C should be small, while F_b should be large. Although it is not possible to eliminate the noise, it is possible to group the noise bursts into tight, widely spaced packets. Such grouping reduces the likelihood of spike voltage sampling, and reduces the number of Ethernet interrupts during digital data transmission. The probability of sampling an interference spike is equal to the ratio F_C/F_b, and is independent of F_{pwm} or sample rate.

9) Specific piston pump events occurring at a rate of $9(F_C/2)$ were identified on the AC pressure and accelerometer traces which may prove useful in system health diagnoses.

10) Cavitation has the effect of obscuring the $9(F_C/2)$ piston events on the vacuum sensor at the pump input, while increasing the amplitude of the $9(F_C/2)$ events on the acceleration traces.

Chapter 10.

CONCLUSIONS

1) The interference from PWM controllers can contaminate measurement systems to the extent that measured data are rendered useless.

2) Prior to this research, the entire system health monitoring project was at a standstill due to EMI problems. A literature search failed to uncover analogous case studies, so experimentally-derived techniques were developed using the sentinel publication by H.W. Ott as a guide. These efforts were successful; the health monitoring system is now functional.

3) PWM-generated EM interference can be improved by changing motor controller variables.

4) A new relationship between motor command frequency, base control frequency, PWM carrier frequency, and the duration of the interference pulse was developed (equations 7.1.3 and 8.5.1). The equations are useful in improving motor controller EMI performance, and provide a means of computing the probability of sampling an interference spike.

5) Any filtering implementation should be preceded by proper shielding and grounding exercises.

6) Electromagnetic compatibility (EMC) problems are insidious and should be addressed early in the design phase. Good systems engineering practices should be applied in projects where EMI is expected to be a problem.

7) Persistent diagnostics and remediation of cause and effect phenomena in detecting and suppressing interference require patience, skill, and determination.

8) Based on this research project, the following outline was developed to serve as a guide for future interference reduction efforts. When faced with a noise problem of an unknown nature, it may be useful to follow each step in chronological order, keeping in mind that the solutions to noise problems are not always found by following a set of hard-and-fast rules.

I. Identify the source or sources of the interference and the mode or modes of noise coupling.

A. Check line voltages for conducted noise with an isolated oscilloscope.

B. Check connections to ground for common impedance noise with an isolated oscilloscope.

C. Check for EMI with a loop antenna connected to an isolated oscilloscope.

D. Correlate oscilloscope noise traces (from steps one through three) with suspected source voltages to identify the origin of the interference. In the case of capacitively-coupled EMI, the antenna response will appear as the time-derivative of the source voltage.

II. Eliminate or suppress interference at its source.

A. Remove the noise source if possible.

B. Replace the noise source with a quieter equivalent if possible.

C. Relocate the noise source away from the receiving circuitry if possible.

D. Place the source circuitry in a Faraday cage.

E. Reduce the length of all leads which conduct the source voltage (especially those which conduct PWM voltage) and avoid loops or coils.

F. Encase all source voltage leads in steel conduit.

G. Provide a good single-point earth ground for the noise source using a short, conductive connection, such as heavy gauge copper braid connected solidly to building steel.

H. If the interference source is a PWM motor controller, set controls to minimize the PWM carrier frequency, minimize the command frequency, and maximize the control base frequency, to the extent that motor safety and performance are not compromised.

I. Condition the source voltage using a three-phase line reactor (choke coil).

III. **Suppress interference at the receiver.**

A. All sensor signal conditioning circuitry should be shielded inside a Faraday cage.

B. Use shielded twisted-pair or coaxial sensor cabling.

C. Minimize cable lengths and avoid coils and loops.

D. All cable shields for analog signal transmission should be tied to a common point near the A/D board. The individual foil shields should extend all the way to the sensor, where they should be terminated and allowed to float independently.

E. All cables should be encased in steel conduit.

F. Instrumentation power supply cases should be grounded to the common-point ground in step D. The power terminals should float with respect to this ground. Each of the analog signal grounds should be referenced to the negative terminal of the power supply.

G. Minimize the length of the signal conductor that extends beyond the cable shield. Aluminum foil works well to extend/modify cable shields.

IV. Apply special techniques.

A. Implement first-order passive RC filters to suppress interference on the sensor voltages prior to digitization.

1. Passive filters should reject all but necessary bandwidths.

2. Choose a small-valued R for the first-order passive filter so that the voltage drop does not affect signal calibration. A small value for R will also reduce Johnson noise.

3. View the filtered signal oscilloscope trace before choosing the final R and C values.

4. Electrolytic filter capacitors should be paralleled with small-valued ceramic or polystyrene capacitors.

5. Sample rate should be at least twice the high-cut frequency.

B. Consider tuned-sampling so that only EMI-free segments of the sensor voltage are digitized.

REFERENCES

Acromag Inc., 1994. Analog I/O Boards. Technical specifications published by Acromag Inc., 30765 Wixom Road, P.O. Box 437, Wixom, MI 48393-7037.

Archuleta, Michelle. 1996. Intelligent On-Line Real-Time Oil Condition Monitoring. Colorado School of Mines Engineering Division thesis (in preparation).

Baldor, Inc. 1994. Baldor Motor and Drives - Series 15H - Inverter Control Installation and Operating Manual. Published by Baldor Electric Company, Inc., P.O. Box 2400, Fort Smith, AR 72902-2400.

Brady, T. and Thomas, M. 1995. Reactive, Preventive, and Predictive Maintenance Cost Benefit Analysis. Colorado School of Mines Economics Department. Submitted to Journal of Engineering Economics.

Brown, G. 1996. Preliminary Investigation of Using an Expert System for On-Line Near Real-Time System Health Monitoring of a Remote Hydraulic Circuit. Colorado School of Mines Engineering Division thesis (in preparation).

Fleischer, Karl. 1995. Evaluation of a Data Acquisition System for Electrical Noise Immunity. Unpublished technical report for engineering course EGES 501. Colorado School of Mines, Golden Colorado.

Flett, F., ed. 1994. A Tutorial in AC Induction and Permanent Magnet Synchronous Motors - Vector Control with Digital Signal Processors. Published by Analog Devices, Inc. and Infosys Technologies, Ltd.

Heraeus Sensor Inc. 1994. TK-244 RT Series 2-Wire Head Mout Transmitters. Technical specifications published by Heraeus Sensors Instruments, 9901 Blue Grass Road, Philadelphia, PA 19114.

Johnson, R.C. and Jasik, H. 1984. Antenna Engineering Handbook. McGraw - Hill, Inc.

Lindsay, J.F. and Rashid, M.H. 1986. Electromechanics and Electrical Machinery. Prentice Hall, Inc., Englewood Cliffs, N.J. 07632

Metrix Instrument Company Inc. 1990. Accelerometers Rated Up to 120 C Model 5514 and 5522 and Vibration Transmitters for Remote Sensors. Technical specifications published by Metrix Instrument Company, 11711 Townhurst Drive, Houston, Texas 77043.

Middleton, N. 1995. EGES 501 - Engineering Measurement. Unpublished notes from course taught by Dr. Nigel Middleton, Colorado School of Mines, Golden, Colorado.

N.V. Philips. 1990. 60 MHz Digital Storage Oscilloscope PM3335/3337 Test Measurements. Published by N.V. Phillips, Eindhoven, The Netherlands.

Oilgear Inc. 1990. Hydura PVWH Open Loop Pumps - Technical Bulletin 47015B. Published by The Oilgear Company, 2403 South 51st Street, Milwaukee, WI 53219.

Ott, H. W. 1976. Noise Reduction Techniques in Electrical Systems. John Wiley & Sons, Inc., New York.

Seifert, T. 1996. Dynamic Alarm Handling Using Fuzzy Logic for SHARP. Colorado School of Mines Engineering Division thesis (in preparation).

Sensotech Inc. 1993. Universal Inline Transducer Amplifier +/- 10 Volts Output Model User's Guide. Published by Sensotech Inc., 1200 Chesapeake Avenue, Colombus, Ohio 43212-2288.

Sensotech Inc. 1995. Calibration of Absolute Pressure Transducers by Shunt Calibration Using Change. Doc. 008-0262-00. Published by Sensotech Inc., 1200 Chesapeake Avenue, Colombus, Ohio 43212-2288.

Steele, J.P.H. 1995a. System Health Monitoring and Prediction Program Technology Assessment Report. Laboratory for Intelligent Automated Systems technical report LIAS-TR-950701. Colorado School of Mines, Golden, Colorado.

Steele, J.P.H. 1995b. System Health Monitoring and Prediction Program Test Plan. Laboratory for Intelligent Automated Systems technical report. Colorado School of Mines, Golden, Colorado.

Thornton, E. 1991. Electrical Interference and Protection. Ellis Horwood Limited, New York.

Webster Instruments, Inc. 1990. LTE Series Turbine Flowmeters User's Guide. Published by Webster Instruments, Inc., 1290 East Waterford Avenue, Milwaukee, WI 53235.

Williams, B.W. 1992. Power Electronics - Devices, Drivers, Applications, and Passive Components. McGraw - Hill, Inc. Second edition.

Zhong, E. and Lipo, T.A. 1995. Improvements in EMC Performance of Inverter-Fed Motor Drives. IEEE Transactions on Industry Applications, vol. 31, no.6, PP 1247-1256.

Appendix A.

TEST BENCH COMPONENT SPECIFICATIONS

This section documents the serial number, model number, manufacturer, and key specifications for each test bench component. Copies of manufacturer specification sheets and installation/operation/calibration notes may also be attached.

A.1. Motor.

Manufacturer:	Baldor
Serial Number:	494C
Catalog Number:	CM2539T
Spec. Number:	42B02413
Frame:	324TC
Voltage Raring:	230/460 V
Current Rating:	102/51 Amps
Speed Rating:	1760 RPM, 60 Hz
NEMA Nominal Eff:	90.2%
Power Factor:	82

A.2. Motor Controller.

Manufacturer:	Baldor
Serial Number:	2994RX028
Type:	4 Pole Induction
Catalog No:	ID15H440-EO
Input Voltage:	460 VAC 3PH 50/60 Hz, WYE*
Output Voltage	460 VAC 3PH, WYE*
Control Method:	Sinewave Carrier Input, PWM Output
Carrier Frequency:	1 KHz- 15 Khz adjustable
Transistor Type:	IGBT
Analog Outputs:	2 Assignable
Digital Outputs:	4 Assignable
Reference Document:	Baldor Inc.,1994

*The fourth wire is grounded to the controller frame and motor chassis.

A.3. Pump.

Manufacturer:	Oilgear
Serial Number:	94164431
Type:	9 Piston Swashblock, Fixed Displacement
Model:	PVWH11LSAYCNNN
Flow Rate:	11 GAL/MIN at 1800 RPM
Reference Document:	Oilgear Inc., 1990

A.4. Thermocouples.

Manufacturer:	Heraeus
Type:	J (Iron-Constantan)
Reference Document:	Heraeus Sensor Inc., 1994

A.5. Thermocouple Transmitters.

Manufacturer:	Heraeus
Type:	W/TK244-J HINGE HD
Model Number:	82000
Catalog Number:	XIJ51002U000B
Range:	0C = 4 MA, 270C = 10 MA
Reference Document:	Heraeus Sensor Inc., 1994

TK-244 R-T-SERIES

2-WIRE HEAD-MOUNT TRANSMITTERS

- Off-the-Shelf Delivery
- High Accuracy (+/-0.05%)
- Fully-Scaleable
- Economical
- Small Size
- RFI-Tested

The TK-244 R-T 2-Wire Link-Scaleable Temperature Transmitters offer the most effective price/performance ratio in the industry. Easily scaled by a simple solder link on the top of the unit, it can even be scaled in the field. And, because the TK-244 R-T is only 1.0"H x 1.7" Dia., they can be used with industry-standard connection heads.

Precision 20-turn potentiometers provide fine adjustment of ZERO and SPAN. RTD units are completely linearized. Thermocouple units are voltage linear. RFI-tested to rugged SAMA PMC 33-1 Standard.

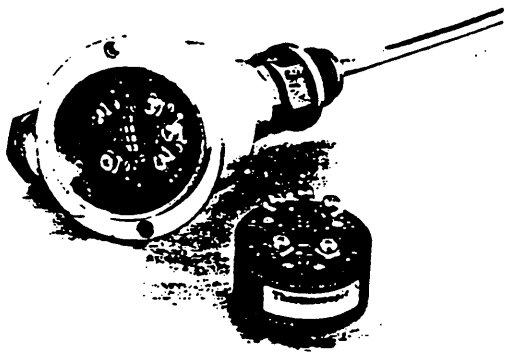

SPECIFICATIONS

V_{nom} = 24VDC T_{amb} = 25°C

$Span_{nom}$ = 100°C (Pt100 RTD); 250°C (T/C)

Output:	4-20mADC
Supply:	10-36VDC, polarity-protected
Zero Drift:	+/-0.01%/°C
Span Drift:	+/-0.01%/°C
Voltage Effect:	+/-0.002%/V
Ambient Range:	-10° to 70°C
Storage:	-20° to +100°C
Load Capability:	V - 10V/20mA
Sensor Burn-Out:	Upscale, >23mA Limited to 40mA, max.
Accuracy:	+/-0.05%

Model TK-244 R-T (Pt100 RTD Input)
Input: Pt100 RTD (α = 0.00385)
Zero Adjustment: -50° to +50°C
Span Adjustment: 50° to 800°C
Linearization: +/-0.1%

Model TK-244 R-T (T/C Input)
Input: Type K or Type J
Zero Adjustment: 0°C+/-25°C, approx.
Span Adjustment: Type K: 150°-1200°C
Type J: 150°-600°C
Cold Junction: 0.05°C/°C
Linearization: voltage linear

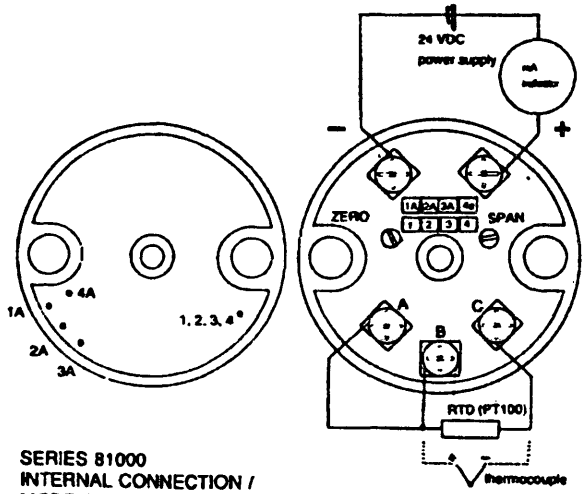

SERIES 81000
INTERNAL CONNECTION /
MODELL 81000
INNENLIEGENDE VERBINDUNGEN

SERIES 81000 /
MODELL 82000

DESIRED SPAN /
PROGRAMMIERBARE
MEßSPANNEN IN °C

Connect: / Verbindung:	Thermoelement Typ		
	Pt100	K	J
1-1A	50-100	150-300	150-300
2-2A	100-200	300-600	300-600
3-3A	200-400	600-1200	–
4-4A	400-800	–	–

Note: fine adjustment by potentiometer
Example: to make a range of 0-60°C with Pt100:
connect 1 and 1A and adjust to desired value with
zero and span potentiometers.

Beispiel: Meßbereich 0-+60°C Pt100.
Lötstützpunkte 1 mit 1A verbinden
Mit Potentiometern für ZERO (Anfangswert) und
SPAN (Meßspanne) fein justieren.

A.6. High Pressure Sensor.

Manufacturer:	Sensotech
Serial Number:	470896
Model Number:	LM/2345-14
Pressure Range	0-5000 PSIG
Excitation:	10.0 VDC
Input Resistance:	350 Ohms
Output Resistance:	350 Ohms
Cal. Factor:	2.3532 MV/V
Shunt Cal. Factor	1.4793 MV/V
Reference Document:	Sensotech Inc., 1993

A.7. Low Pressure Sensor.

Manufacturer:	Sensotech
Serial Number:	459300
Model Number:	TJE/-713-26TJA
Pressure Range:	0-15 PSIA
Excitation:	10.0 VDC
Input Resistance:	401 Ohms
Output Resistance:	350 Ohms
Calibration Factor:	3.0080 MV/V
Shunt Resistance:	59 KOhm
Shunt Cal. Factor:	1.4768 MV/V
Reference Document:	Sensotech Inc., 1993

A.8. Pressure Transducer Inline Amplifiers.

Manufacturer:	Sensotech
Serial Numbers:	485263 (Channel 3), 485268 (Channel 4)
Part Number:	060-6827-04
Power Supply:	18-28 VDC
Output:	10 V
Reference Document:	Sensotech Inc., 1993

Chapter 1
INTRODUCTION

1.1 OVERVIEW

The Sensotec Universal Inline Amplifier is housed in a small plastic package, which is connected between the transducer and a readout instrument. The amplifier supplies a highly regulated bridge excitation voltage for the transducer and converts the millivolt signal of the transducer to a + / - 10-volt, high level output. The inline features include three selectable excitation voltages, programmable gain settings, a wide adjustment range on the zero and a buffered solid state shunt cal relay for quick calibration.

1.2 SPECIFICATION

Power Requirements	18 - 32 volts DC
Bridge Excitation	10, 5 or 3 volts DC @ 70 ma. User selectable
Output voltage range	+ / - 10 volts @ 2.5 ma.
Frequency response	DC - 3000 HZ
Zero Balance range	+/- 30 % coarse,+/- 15 % fine adjustment range.
Gain Adjustment Range	Switch selectable (1 to 10 mV/V), +/- 25 % fine adjust.
Short circuit protected	+ Output to - Output/Common
Environment Protection	IP-66 or NEMA 4
Shunt calibration	Solid State Relay
Long Term Zero Drift	.1% of Full Scale per 6 months

1.3 LAYOUT

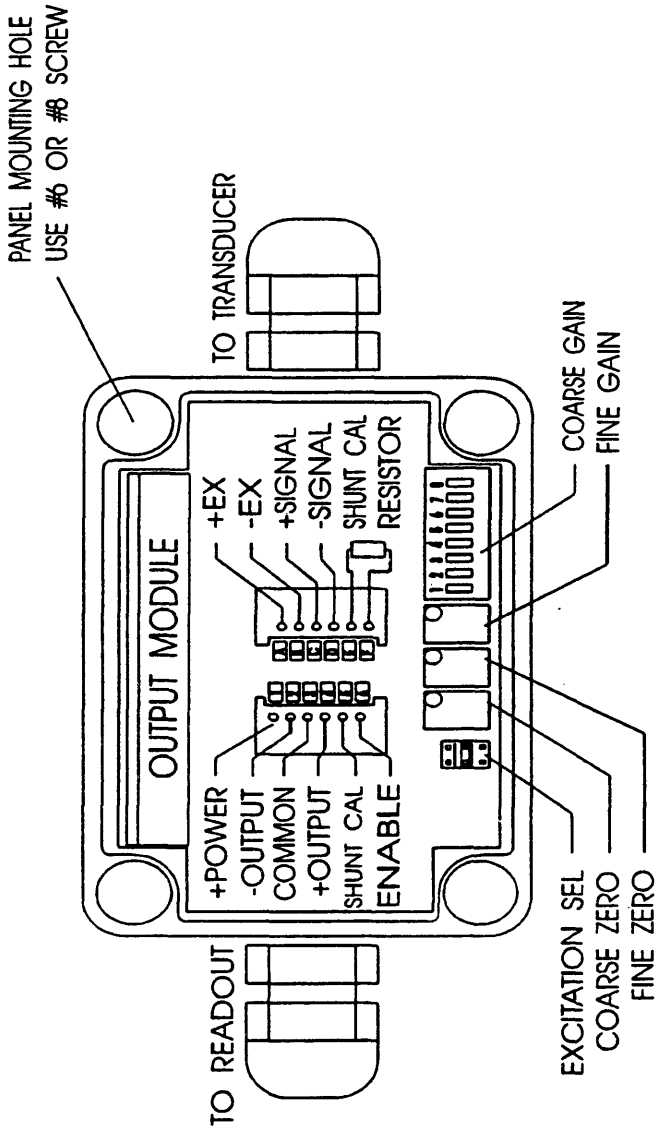

Figure 1-1. Layout of Inline Amplifier

Chapter 2
INSTALLATION / SET UP

2.1 WIRING

The 060-6827-04 INLINE amplifier can be powered from a 18 to 32 volt single voltage supply. The following diagrams show the wiring to the supply and readout.

Cables should be stripped back 3 inches with the wires stripped and tinned 1/2 inch. Connections to the terminal block are made by pressing the orange levers and inserting the wires into the hole next to the levers. The terminal block will accept wire up to AWG 20.

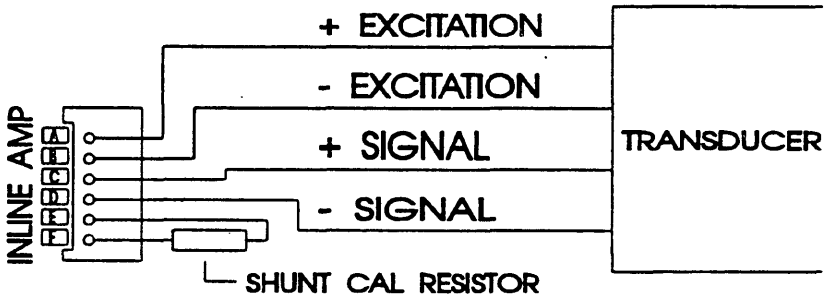

Install shunt cal resistor value specified on the transducer data sheet.

Figure 2-1. Transducer to Inline Wiring

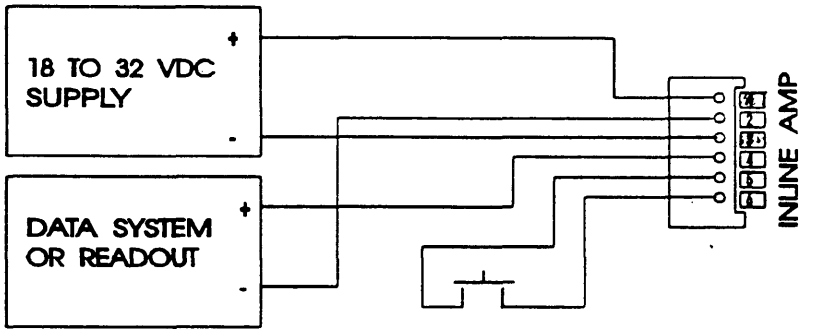

Figure 2-2. 18 to 32 Volt Power Supply to Inline Wiring

2.2 EXCITATION AND COARSE GAIN SWITCH

COARSE GAIN SETUP

SWITCH POSITION on	EXCITATION		
	10	5	3
1	1 mV/V	2 mV/V	3.3 mV/V
2 & 4	1.5 mV/V	3 mV/V	5 mV/V
2	2 mV/V	4 mV/V	6.6 mV/V
3 & 6	2.5 mV/V	5 mV/V	7.5 mV/V
3	3 mV/V	6 mV/V	10 mV/V
4 & 7	3.5 mV/V	7 mV/V	1.6 mV/V
4	4 mV/V	8 mV/V	13.3 mV/V
5 & 8	4.5 mV/V	9 mV/V	15 mV/V
5	5 mV/V	10 mV/V	16.6 mV/V
6	6 mV/V	12 mV/V	20 mV/V
7	7 mV/V	14 mV/V	23.3 mV/V
8	8 mV/V	16 mV/V	26.6 mV/V

Figure 2-3. Coarse Gain Setup Table

PROCEDURE FOR SETTING UP EXCITATION AND COARSE GAIN SWITCH:

1. Determine the EXCITATION VOLTAGE required by the transducer being used.

2. Set the EXCITATION SELECT JUMPER as shown below: (See Fig.1-1 for location of jumper)

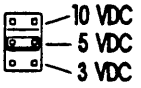

3. Determine the sensitivity of the transducer in mV/V from the transducer calibration sheet.

4. Set the COARSE GAIN SWITCH (See Fig.1-1 for location of switch) to the nearest mV/V setting in the corresponding excitation column in Fig. 2-3.

Chapter 3
CALIBRATION

3.1 CALIBRATION

Step 1. Apply power and allow unit to stabilize for 10 minutes.

Step 2. With zero load or pressure on the transducer adjust the ZERO potentiometers to indicate zero on the readout instrument.

Step 3. Apply full scale pressure or load to the transducer and adjust the SPAN potentiometer to indicate full scale on the readout instrument.

Step 4. Recheck zero and full scale (repeat steps 2 & 3).

3.2 USING SHUNT CALIBRATION

Sensotec transducers feature a calibration technique called shunt calibration. This method applies a known resistance across one leg of the transducer, which simulates an output, as if a load or pressure was applied to the transducer. When performing shunt calibration, the transducer should be at ZERO pressure or load. The full scale output and shunt cal output is found on the TRANSDUCER CALIBRATION SHEET. This information can be used to calibrate the amplifier's output voltage and the readout's display with the following equations.

TRANSDUCER CALABRATION DATA

Full Scale Output = _____ mV/V.

Shunt Resistor Value of _____ OHMS

Shunt Cal Output = _____ mV/V.

The following equations are used to calculate output current and display units:

3.3 FORMULA TO CALCULATE OUTPUT CURRENT

$$\frac{\text{SHUNT CAL OUTPUT}}{\text{FULL SCALE OUTPUT}} \times \text{FULL SCALE VOLTAGE (10 V)} = \text{OUTPUT VOLTAGE}$$

_____ x _____ = _____

3.4 FORMULA TO CALCULATE DISPLAY UNITS

$$\frac{\text{SHUNT CAL OUTPUT}}{\text{FULL SCALE OUTPUT}} \times \text{FULL SCALE UNITS} = \text{DISPLAY UNITS}$$

_____ x _____ = _____

Step 1. Apply power and allow the amplifier to warm up.

Step 2. With zero load or pressure on the transducer, adjust the ZERO potentiometer to indicate zero on the readout instrument.

Step 3. Connect a jumper across PINS 5 & 6 of the power terminals (See Fig. 1-1) or wire in a switch as shown in wiring section. Adjust the SPAN potentiometer to the calculated voltage or calculated units on the readout instrument.

Step 4. Disconnect the shunt cal jumper or release the shunt cal switch and repeat steps 2 & 3 if needed.

SENSOTEC, INCORPORATED
1200 Chesapeake Avenue
Columbus, Ohio 43212
(614) 486-7723

Instructions for

CALIBRATION OF ABSOLUTE PRESSURE TRANSDUCERS BY SHUNT CALIBRATION USING CHANGE

1.0 Introduction

Shunt calibration is used to verify transducer bridge continuity and amplifier gain. In this technique, the transducer has no stimulus (no pressure or load), and a known value of precision resistor is placed across one leg. This causes an unbalance of known proportion, which should cause a known amplifier response. The amplifier is then adjusted to provide that result. A problem comes about, however, when the transducer cannot be unloaded, that is, a no-stimulus condition cannot be obtained. The bridge impedance will not be exactly what it was in the unloaded condition, and therefore the application of the shunt calibration resistor will not produce exactly the same effect.

Another problem results from the inability to unload the transducer, as well. Amplifiers for strain gage transducers are linear devices, producing output according to the straight line equation

$$y = mx + b$$

where y is the output (volts)
x is the input (mv)
m is the span
b is the zero (volts)

When the ZERO control of an amplifier is adjusted, it is the "b" term that is affected. When SPAN is adjusted, the "m" term is affected, which means that the slope of the calibration curve is changed. Thus, SPAN changes the slope, but ZERO moves the curve parallel to itself without changing the slope. Ideally, the calibration curve passes close to the origin, but in an absolute transducer we cannot be certain of this with a single adjustment because we cannot (physically) set $x = 0$ in the equation. Further, a second calibration point is needed to establish the line. If we have this point, setup can be obtained, though it is necessary to move into it in small increments. This has been termed "rocking" the adjustment.

Refer to Figure 1-1. This figure graphically illustrates the problem. The desired calibration curve is shown, with two points marked on it: today's atmospheric pressure (obtained from the weather bureau), and the shunt calibration output (obtained by evacuating the transducer, then applying shunt calibration). Let

us assume that the circuitry is actually set up with curve #2. Because he cannot evacuate the transducer, the user calls the local aviation weather station and obtains the local barometric pressure. His instrument is reading low, so he adjusts the SPAN control to give the proper reading. Graphically, he has shifted the curve's slope, without changing its zero; he is closer, but not there yet. Repeated adjustments are needed, but he finds himself in difficulty, because he has no established second point. The problem is very much in evidence.

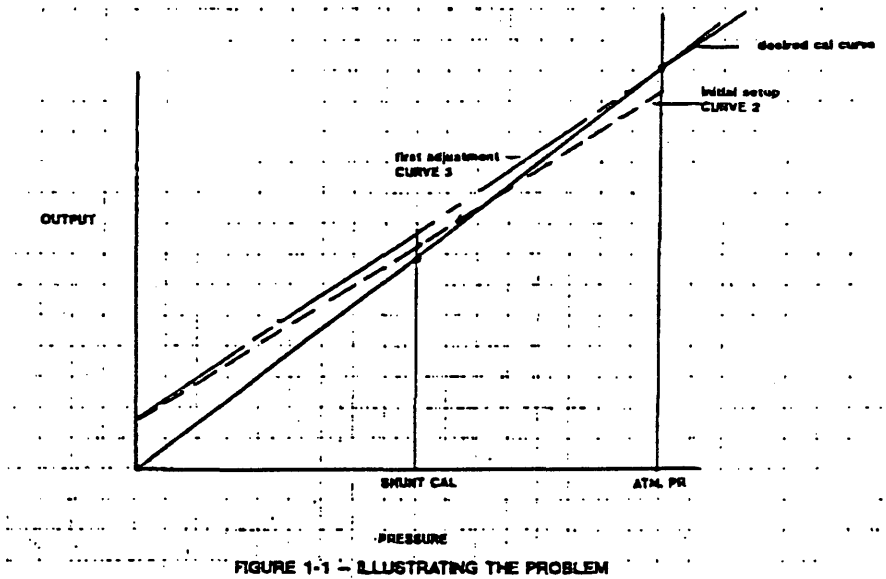

FIGURE 1-1 – ILLUSTRATING THE PROBLEM

2.0 A Solution using Change in Shunt Calibration

A second point can be easily obtained if the effect of the shunt calibration technique is measured in the change it produces, rather than in its effect on the absolute value.

Using some numbers for illustration, let us assume that, when testing a 15 psia absolute pressure transducer, the factory calibration shows a shunt calibration value of 7.500 psi. (When evacuated, the transducer is shunted with a known resistor which causes the output to look as if the pressure was 7.500 psi.) If an instrument is being used, it is then accurately set up so that the output at vacuum is 0000, and at 15 psia is 5.000 volts. At atmospheric pressure (about 14.5 psia) the amplifier output would be about

$$\frac{14.5}{15.0} \times 5.000 \text{ volts} = 4.833 \text{ volts}$$

If the shunt calibration circuit is wired to produce a negative change starting from atmospheric pressure, when the shunt calibration is performed, we would expect to see a drop of pressure to about

$$14.5 - 7.500 = 7.0 \text{ psia,}$$

indicated by an output voltage of

$$\frac{7.000}{15.00} \times 5.000 \text{ volts} = 2.333 \text{ volts}$$

However, this assumes that the change in shunt calibration value is the same as the shunt calibration value itself. This is not true, except when the bridge impedance is the same as at zero. The actual change in value will be different.

But what if the amplifier is carefully set up, atmospheric pressure applied, then the change created by the shunt calibration process noted? The resulting change could be used as the second point in a setup procedure. If atmospheric pressure were about the same, the resulting error would be very small.

Thus, the rationality of using the change in shunt calibration value from atmospheric pressure is established.

3.0 Procedure

Figure 3-1 illustrates the calibration procedure being used in setting up an amplifier using the change in shunt cal value technique.

1. Determine the uncorrected atmospheric pressure.

2. Adjust the SPAN control to cause the instrument to read this value. If you are using the analog voltage output instead, adjust the SPAN control to yield this value:

$$\frac{\text{Atmospheric Pressure}}{\text{Transducer Full-Scale Pressure}} \times 5 \text{ volts}$$

3. Press the SHUNT CAL button, and by subtraction, note the change. Compare it with the change given by the Transducer Calibration Record. Adjust the ZERO control until the change noted when using the SHUNT CAL button is what is expected.

4. Repeat steps 2 and 3 until the correct atmospheric pressure and correct change in shunt calibration value are obtained. This will generally be about three passes through the procedure, getting closer to the

desired conditions with each pass. See Figure 3-1 to see why this value approaches the correct value with each pass.

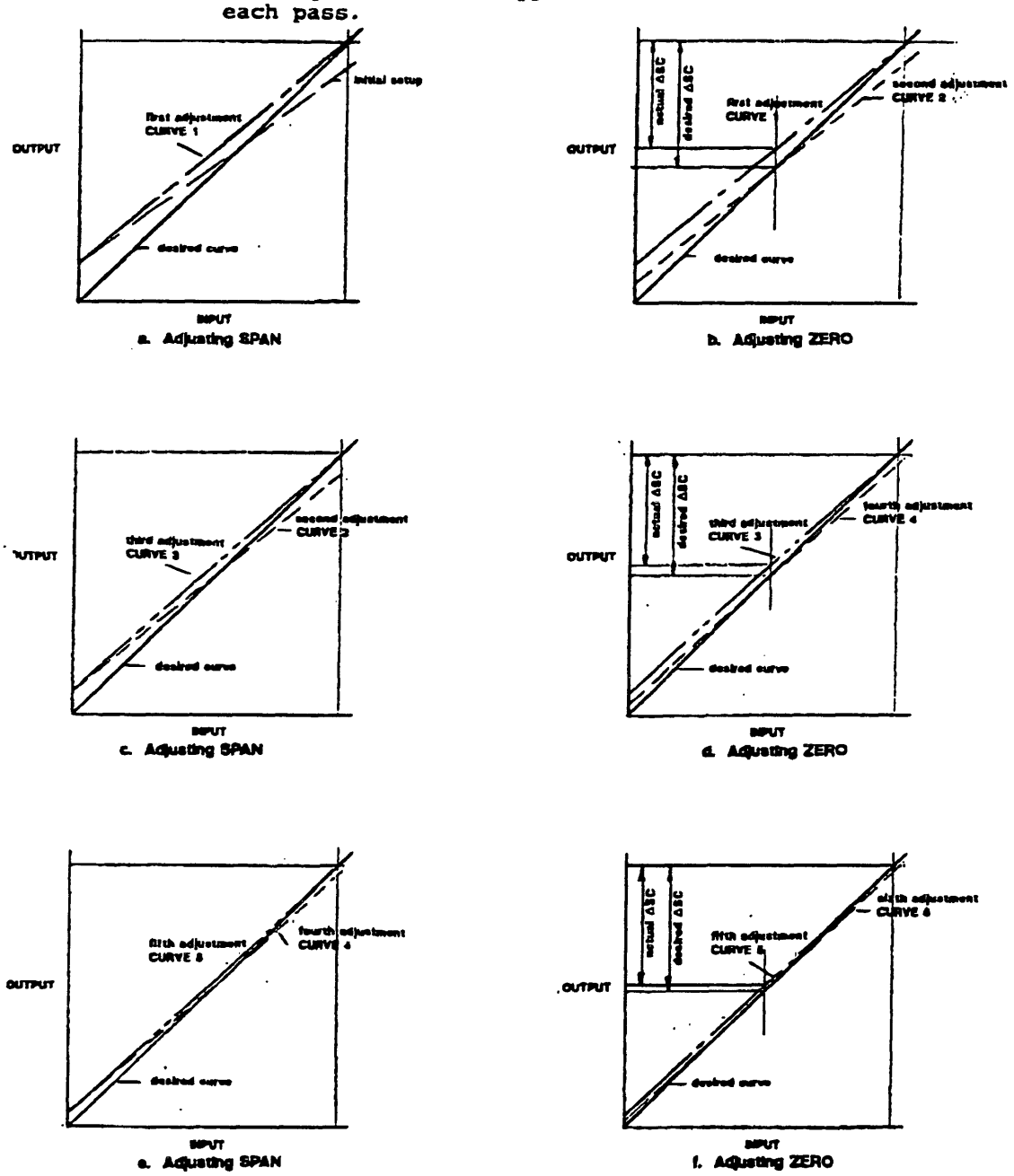

FIGURE 3-1 "ROCKING" THE ADJUSTMENTS

A.9. Flowmeter.

Manufacturer:	Webster
Serial Number:	35774
Model Number:	LTE50
Cal. Number:	680.09
Reference Document:	Webster Istruments Inc., 1990

WEBSTER INSTRUMENTS
A DIVISION OF WEBTEC PRODUCTS

LTE Series
Turbine Flowmeters

Features

- **FLOW RANGE:** 0.5 to 100 GPM
- **ACCURACY** within 1% of full scale over normal range
- **COMPACT** design allows installation with 90° elbows were space is limited
- **PRESSURE** up to 6000 psi, 420 bar
- **BI-DIRECTIONAL** operation
- **FLUIDS** wide range of hydraulic, lubrication oil, fuels and water - oil emulsions
- **TEMPERATURE** sensor built-in

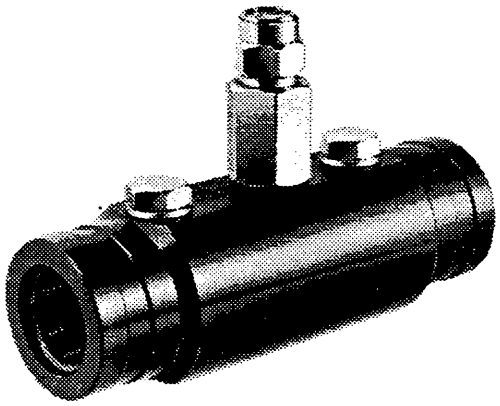

The LTE series Turbine Flowmeters provide a complete solution for the flow measurement requirements of hydraulic systems on Test Stands, Machine Tools and other fixed or mobile applications. The flowmeter is electrically connected to a readout to provide remote indication of flowrate. The flowmeter can be installed anywhere in the hydraulic circuit for production testing, commissioning, development testing and control systems. The compact design and unique built-in flow straighteners allows installation without the conventional lengths of straight pipe.

A wide range of readouts and signal conditioning devices are available from Webster Instruments to provide the instrumentation needed to analyze the performance of pumps, motors, valves and hydrostatic transmissions.

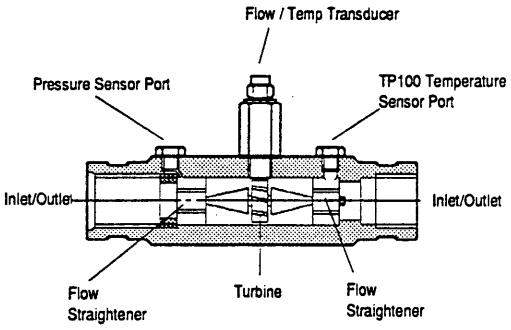

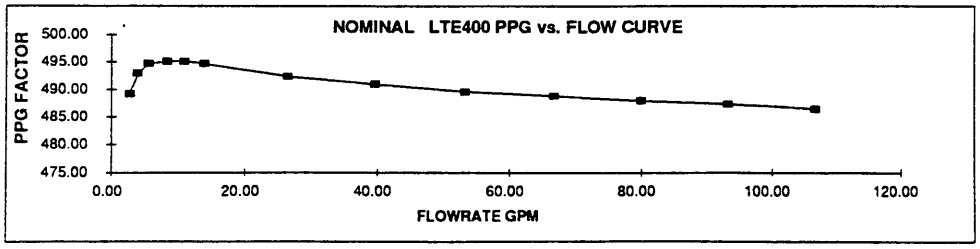

LTE TURBINE FLOWMETER SPECIFICATIONS

MODEL NUMBER	FLOW RANGE NORMAL	MAXIMUM	NOMINAL PULSES PER GAL.	PER LTR.	MAX PSI	PORT SIZE
LTE50	2 - 12	5 - 15	2380	630	6000	1 1/16" -12 #12 SAE O-RING
LTE125	3 - 25	1- 30	2380	630	6000	
LTE250	5 - 50	2 - 65	551	146	6000	1 5/16" -12 #16 SAE O-RING
LTE400	8 - 80	3 - 100	55	146	6000	

MEASUREMENT AND INDICATION

Flow
Measured by the electronic count of an axial turbine which is designed to minimize the effects of variations in temperature and viscosity. The speed of the turbine is monitored by a magnetic transducer. Built in flow straighteners reduce flow turbulence and allow flow measurement in either direction.
Accuracy: +/- 1% of full scale over normal range.
+/- 2% of full scale outside normal range.

Temperature
Sensed by a thermistor housed in the transducer for fast response and simplified cable connection.
Resistance: 30K Ohms at 30 °C.
Accuracy: +/- 1 °C over range 0-90 °C.

Consult sales office for linear output temperature sensors.

CONSTRUCTION

Flow Block
High tensile aluminum block houses a six blade turbine rotating on a stainless steel bearing and shaft. The flow straighteners and turbine design eliminates the effects of turbulence and swirl, allowing the LTE series flowmeters to be connected with 90° fittings on the inlet and outlet ports. The flowmeter block has 1/4" BSPP ports for pressure and temperature sensors. Optional loading valves, readouts and signal conditioners are available.

Transducer
The self energized magnetic reluctance transducer has a minimum output voltage of 80 mV RMS at minimum rated flow. The transducer output frequency is proportional to flow rate and is typically 20 pulses/second (Hz.) at minimum rated flow. Resistance is 4.3 K Ohms.

Seals
Turbine - Viton (static) seal compatible with oil, fuels, phosphate-ester, water glycol and water - oil emulsions.

INSTALLATION

LTE series Turbine Flowmeters have built-in flow straighteners so the normal recommended length of straight tube can be eliminated where space is limited. Inlet and outlet connections can be elbows but should always be of adequate size to prevent venturi constriction effects. The Webster Instruments' range of flowmeters can be used for intermittent or continuous testing of flow in either direction. Standard transducer output connection is 5 pin DIN. Pin - out #1 flow signal, #2 flow common, #3 & #4 Temp. thermistor. Cannon MS type connectors are available, consult sales office. Standard connecting cable part # FT6685, 20 foot, for flow and temperature output connection.

ALL DIMENSION IN INCHES							
A	B	C	D	E	F	G	H
2.0	6.5	1.81	3.98	3.13	1.75	1.39	1.12
2.0	6.5	1.81	3.98	3.13	1.75	1.39	1.12
2.34	6.5	2.06	4.25	3.14	1.75	1.39	1.12
2.34	6.5	2.06	4.25	3.14	1.75	1.39	1.12

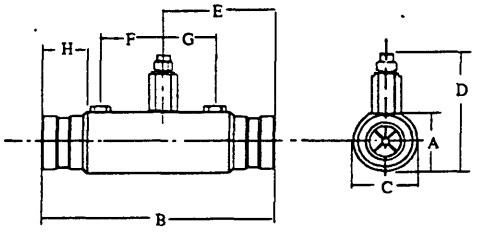

WEBSTER INSTRUMENTS, 1290 East Waterford Avenue, Milwaukee, WI 53235 Phone: (414) 769-6400 or Toll Free (800) 932-8378 Fax: (414) 769-6591

WEBSTER INSTRUMENTS

FLOW TEST REPORT

Date: 03/12/93 Operator: R.D.

Model No. LT50 Serial No. 35774

Test Fluid: ESSO NUTO H32 Viscosity 28 Centistokes at 48°C

Test Temperature: 46°C Test Pressure: 200 PSI

Maximum Test Pressure: 6000 PSI

Recommended Calibration Factor k 2574.40PPUSG

Test Flow USGPM	Frequency Hz	Calculated Flow USGPM	Flow Error USGPM	F.S Error %
0.53	16.90	0.394	-0.134	-1.02
1.08	40.90	0.953	-0.130	-0.98
1.61	64.50	1.503	-0.108	-0.82
2.14	86.80	2.023	-0.117	-0.88
2.72	113.00	2.634	-0.087	-0.66
3.94	168.30	3.922	-0.014	-0.10
5.39	231.30	5.391	0.002	0.01
7.87	339.30	7.908	0.036	0.27
10.57	458.80	10.693	0.126	0.95
13.21	571.40	13.317	0.109	0.82

Engineering Department Production Department

Signature _____ Signature _____

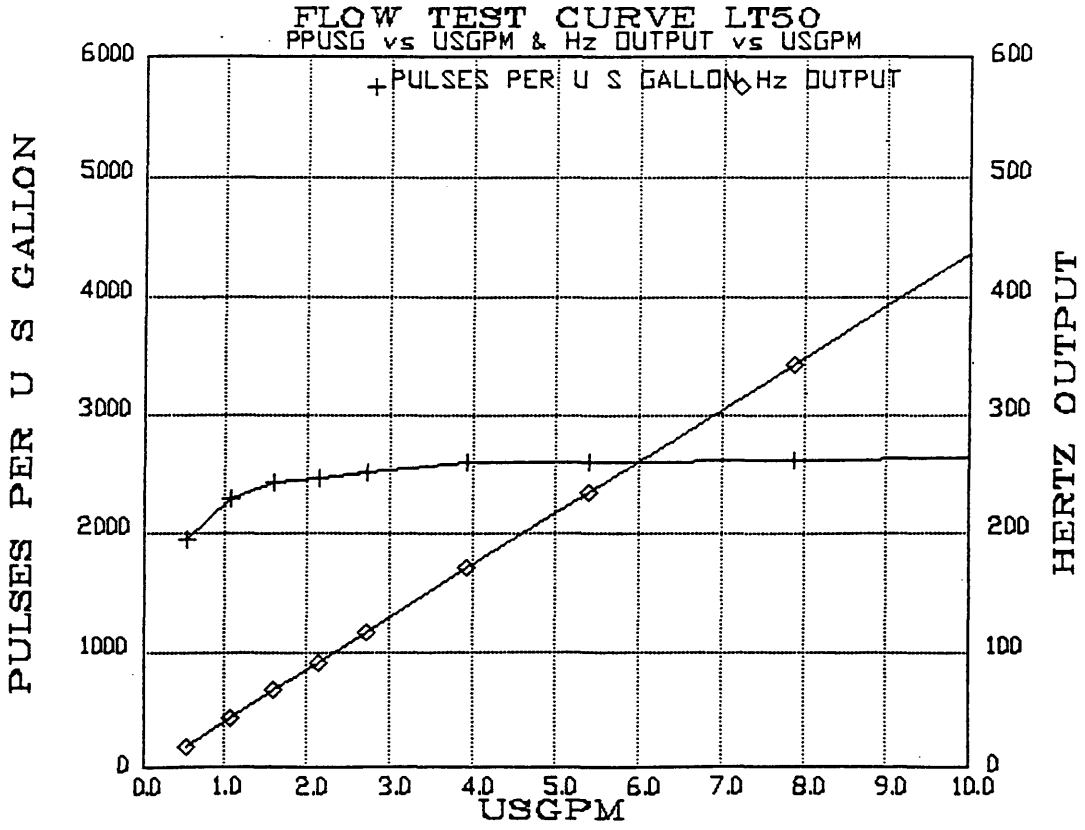

A.10. Flowmeter Pulse Rate to Analog Converter.

Manufacturer: Webster

Model Number: PRA1-1021-3094

Reference Document: Webster Instruments Inc., 1990

WEBSTER INSTRUMENTS
A DIVISION OF WEBTEC PRODUCTS

RA2
Pulse Rate to Analog Converter

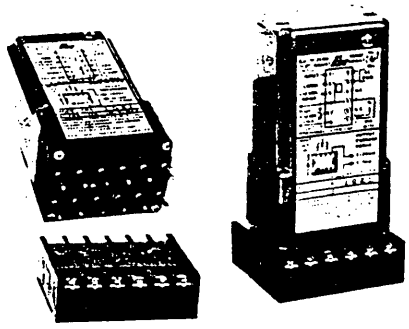

The RA2 is a convenient plug-in module that provides voltage or current output signals proportional to the pulse rate (frequency) of flow or speed input signals. In typical applications the RA2 input is supplied by a turbine flowmeter, positive displacement flowmeter or magnetic speed sensor which generates a signal proportional to the flowrate or RPM. The RA2 converts the frequency content of the input signal to analog form which can be used to drive strip chart recorders, feedback to speed control circuits, input to a PLC or data acquisition device.

The RA2 develops a "constant-area" pulse from the trailing (negative going) edge of each input pulse. These "constant-area" pulses are fixed in voltage amplitude and time duration. The RA2 takes an average of a train of these pulses to generate an analog output level proportional to the input frequency.

Since the analog output is generated by averaging pulses, an inherent response time is involved. When using the RA2 to provide feedback in closed-loop systems, response time must be considered to avoid stability problems. Internal filtering is kept to a minimum to provide the fastest practical response time. Additional external capacitance may be added to provide the desired degree of filtering.

The plug-in module mates with a heavy duty CSA approved base mounting socket with pressure clamp screw terminals that accept stripped wires without lugs. Closed back construction allows mounting directly on metal panel without an insulation barrier.

Features

- **FACTORY CALIBRATED**
- **DELIVERS ANALOG OUTPUT PROPORTIONAL TO INPUT PULSE-RATE**
- **ACCEPTS INPUT FROM A VARIETY OF FLOWMETERS AND SPEED SENSORS**
- **MULTIPLE SIGNAL OUTPUT, 0-10 VDC AND 4-20 mA OR 0-1 mA**
- **ACCURACY (LINEARITY) 0.25%**

Specifications

Primary Supply Voltage: 110 VAC or 230 VAC, +/- 10%, 50/60 Hz. (see ordering info)
Signal Voltage Output: 0-10 VDC @ 10 mA
Signal Current Output: (selectable)
0-1 mA into load resistance range 0-4K Ω
4-20 mA into load resistance range 0-200 Ω
Linearity: +/- 0.25% FSD.
Voltage/Current Output Tracking: Current signals follow voltage signals within +/- 3% FSD.
Response Time: See next page
Input Sensitivity: 250 mV P-P
Operating Temperature: 0-140 °F
Weight: RA2 & socket 10 oz.

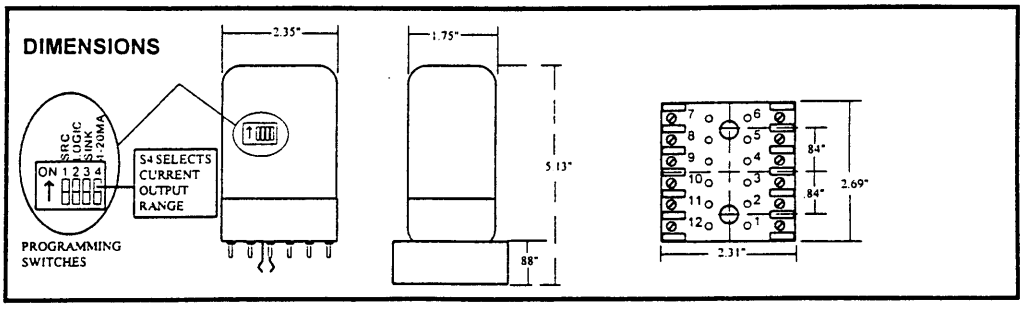

COMPATIBLE TURBINE & POSITIVE DISPLACEMENT FLOWMETERS

MODEL #	FLOW RANGE	PRESSURE	MAX FLOW SIGNAL
LT5*	0.04 - 2.5 GPM	6000 PSI	1200 Hz.
LT10*	0.05 - 4.0 GPM	6000 PSI	1500 Hz.
LT20*	0.06 - 5.0 GPM	6000 PSI	2000 Hz.
LT50*	0.5 - 15 GPM	6000 PSI	600 Hz.
LT125*	1.0 - 30 GPM	6000 PSI	1200 Hz.
LT250	2.0 - 65 GPM	6000 PSI	500 Hz.
LT400	3.0 - 100 GPM	6000 PSI	750 Hz.
LT500	4.0 - 130 GPM	5000 PSI	750 Hz.
LT750	6.0 - 170 GPM	5000 PSI	600 Hz.
LT760	7.0 - 210 GPM	5000 PSI	750 Hz.

* May require use of ASTC in-line amplifier to boost low flow signal to acceptable level

CONNECTIONS & SET-UP ADJUSTMENTS

When supplied with a flowmeter or magnetic speed sensor as a matched set, the RA2 will be supplied factory calibrated to that specific sensor. No field adjustments are required. Consult the calibration sticker affixed to the RA2 to determine the model number, serial number and proportional output range.

The required electrical connections detailed in figure 1 are as follows;
110 VAC mains power: pins 5 & 6
Sensor input signal: pins 7 & 8
(7,8 & 9 for ASTC In-Line Amplifier)
Proportional output:
0-10 VDC, pins 10 (comm) & 12 (pos)
4-20 mA, pins 3 (neg) & 1 (pos)
OR
0-1 mA, pins 3 (neg) & 1 (pos)

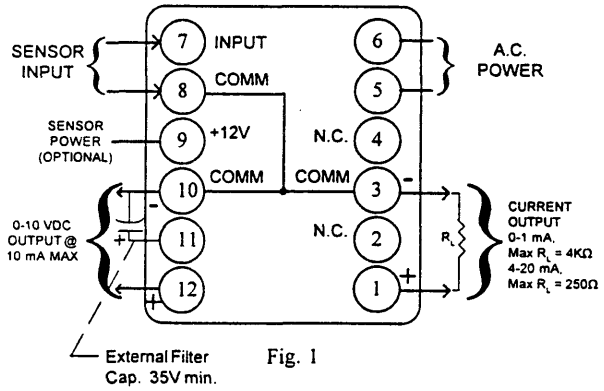

Fig. 1

FIELD CALIBRATION

The RA2 is shipped with a matched sensor as a factory calibrated set. If the sensor is changed or damaged and replaced with a new sensor, the RA2 can be calibrated in the field.

VOLTAGE OUTPUT ADJUSTMENT:

Only the RANGE ADJUSTMENT is effective when the voltage output is used.
(Zero adjustment affects only current output)
Procedure:
Apply the maximum input frequency and set the RANGE ADJUSTMENT to obtain the desired output voltage.

CURRENT OUTPUT ADJUSTMENT:

When current output is used, the ZERO ADJUSTMENT must be set before RANGE ADJUSTMENT setting is attempted.
Procedure:
1. Select current range with switch S4 (0-1 mA or 4-20 mA)
2. Connect milliammeter in series with the current loop circuit from pin 1 to pin 3. CAUTION: do not exceed the maximum load resistance specified for the current range.
3. ZERO ADJUSTMENT
a) 0-1 mA RANGE - With input signal removed turn zero adjust CW until positive current is indicated. Turn back CCW until the current flow just reaches zero. Stop turning the adjustment at this point.
b) 4-20 mA RANGE - turn zero adjust until current is current is 4 mA.
4. *RANGE ADJUSTMENT - Apply maximum frequency input signal and set RANGE ADJUSTMENT to the desired output (10 V, 20 mA, 1 mA)

** RANGE ADJUSTMENT - Turning CW decreases output at a given frequency (increases range) and turning CCW increases output (decreases range).*

OUTPUT RESPONSE & RIPPLE CHARACTERISTICS

Response time: Time required for the output to reach 90% of final value when the input is instantly changed from 0 to full-scale is typically 25 milliseconds.

Ripple: Typical ripple values do not exceed 1V P-P.

External Capacitance: Ripple can be decreased by adding external capacitance. A .22 mfd tantalum capacitor will reduce ripple approximately 50% and roughly double response time. Larger capacitance values can be added for higher degree of ripple reduction, however this will increase response time. Capacitors with voltage rating of 35V or more are recommended with installation as in Fig. 1.

How To Order

Specify flowmeter model number from table above together with RA2 and output required.
Webster Model LT250-RA2-4-20mA is a 2-65 GPM flowmeter with 110 VAC powered RA2 calibrated for 4-20 mA proportional output. Specify 230 VAC powered RA2 as separate line item.

WEBSTER INSTRUMENTS 1290 E. Waterford Ave. Milwaukee, WI 53235 Toll Free: 800-932-8378 Fax: 414-769-6591 Phone: 414-769-6400

WEBSTER INSTRUMENTS
A DIVISION OF WEBTEC PRODUCTS

RA2 APPLICATION CONSIDERATIONS

CONNECTIONS & SET-UP ADJUSTMENTS

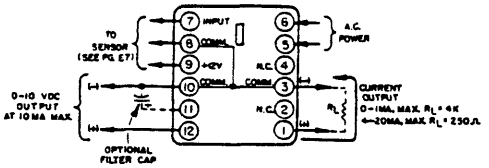

VOLTAGE OUTPUT ADJUSTMENT:

Only the RANGE ADJUSTMENT is effective when voltage output is used. (Zero Adjustment affects only current output.)

PROCEDURE

Apply the maximum input frequency and set the *RANGE ADJUSTMENT to obtain the desired output voltage.

CURRENT OUTPUT ADJUSTMENTS:

When current output is used, the ZERO ADJUSTMENT must be set before RANGE ADJUSTMENT setting is attempted.

PROCEDURE

1. Select current range (0-1, or 4-20ma) with switch S4.
2. Connect a milliammeter in series with the current loop circuit from Term 1 to Term 3. CAUTION: DO NOT exceed maximum load resistance specified for the current range.
3. ZERO ADJUSTMENT
   A) 0-1MA RANGE - With input signal removed (zero frequency) turn ZERO ADJUST CW until positive current flow is indicated. Then, turn back CCW until the current flow just reaches zero. Stop turning the adjustment at that point.
   B) 4-20MA RANGE - Set ZERO ADJUST until current is 4ma.
4. *RANGE ADJUSTMENT - Apply maximum frequency input signal and set RANGE ADJUSTMENT to get desired output.

* *RANGE ADJUSTMENT - Turning CW decreases output at a given frequency (increases range) and turning CCW increases output (decreases range). To calibrate the RANGE ADJUST, apply a known oscillator frequency to the input, or operate the sensor-equipped machine at a known speed and frequency. Then set the output as required.*

ADJUSTABLE RANGE RATINGS & OVER RANGE OPERATION

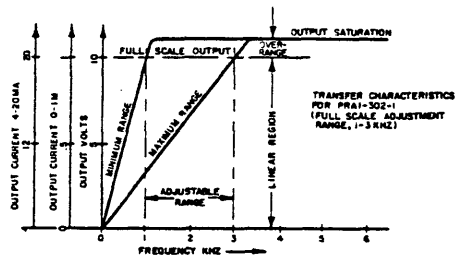

The Transfer Curve (at left) shows the frequency-input/voltage-output relationship for the PRA1-302-1 for both Min. Range (0-1KHZ) and Max. Range (0-3KHZ) adjustment. These curves are typical and apply to all PRA1 ranges.

As shown by these curves, the PRA1 RANGE ADJUSTMENT allows the unit to be calibrated to deliver full scale output for any input frequency from the min. to max. range ratings. As long as the input frequency is equal-to or less-than the full-scale range setting, the PRA1 is operating in its linear region and the output voltage or current will be proportional to input frequency. If the input frequency exceeds the full-scale range setting (over range) the output will flatten out and saturate at some level above 10V at all higher frequencies.

CAUTION: Maximum input frequency for PRA1 modules is 10KHZ. At input frequencies in excess of 10KHZ, the frequency roll-off characteristics of the input circuit will cause signal drop out and result in discontinuous operation.

OUTPUT RESPONSE & RIPPLE CHARACTERISTICS

PRA1 Modules are supplied with a minimum amount of output ripple filtering in order to avoid compromising response-time. The data presented below permits a reasonable estimate of the amount of ripple and the response-time that will be experienced in a particular application. As shown by the curves below, the amount of output ripple depends on the range setting and the input frequency.

Ripple voltage can be reduced by adding external filter capacitance, but ripple-reduction is a trade-off against increased response times. This must be kept in mind, especially if the PRA1 is to be used to supply feedback control signals. The values of capacitance given in the table are for reference only and do not imply a limit to the amount of capacitance that can be added. For example an external filter capacitance may be 10 times the reference values shown for a very high degree of ripple reduction, provided that the resulting long response time is acceptable.

NOTE: If large capacitor values are required to achieve a high degree of ripple reduction, tantalum capacitors rated at 35V or more are recommended. (Proper polarity must be observed. See Connection Drawing above.)

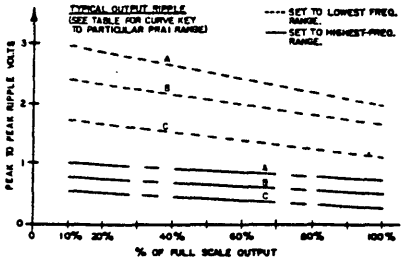

PART NUMBER	FULL SCALE RANGE ADJUSTMENT MIN	FULL SCALE RANGE ADJUSTMENT MAX	RESPONSE TIME (1)	RIPPLE CURVE (2)	EXT CAP (REF) (3)
PRA1-101-1 or -2	30HZ	100HZ	250msec	A	2.2mfd
PRA1-301-1 or -2	100HZ	300HZ	75msec	A	.56mfd
PRA1-102-1 or -2	.3KHZ	1KHZ	25msec	A	.22mfd
PRA1-302-1 or -2	1KHZ	3KHZ	10msec	B	.1mfd
PRA1-103-1 or -2	3KHZ	10KHZ	8msec	C	.047mfd

(1) RESPONSE TIME - Time required for the output to reach 90% of final value when the frequency is instantly changed from 0 to full-scale range frequency.

(2) See "Typical Output Ripple" Curves (at left).

(3) External Capacitance can be added between terminals 10 and 11 to decrease ripple. Reference values shown in MFD, will reduce ripple approximately 50% and will roughly double response times.

A.11. Accelerometers.

Manufacturer: Metrix

Model Number: 5514B

Reference Document: Metrix Instrument Co., 1990

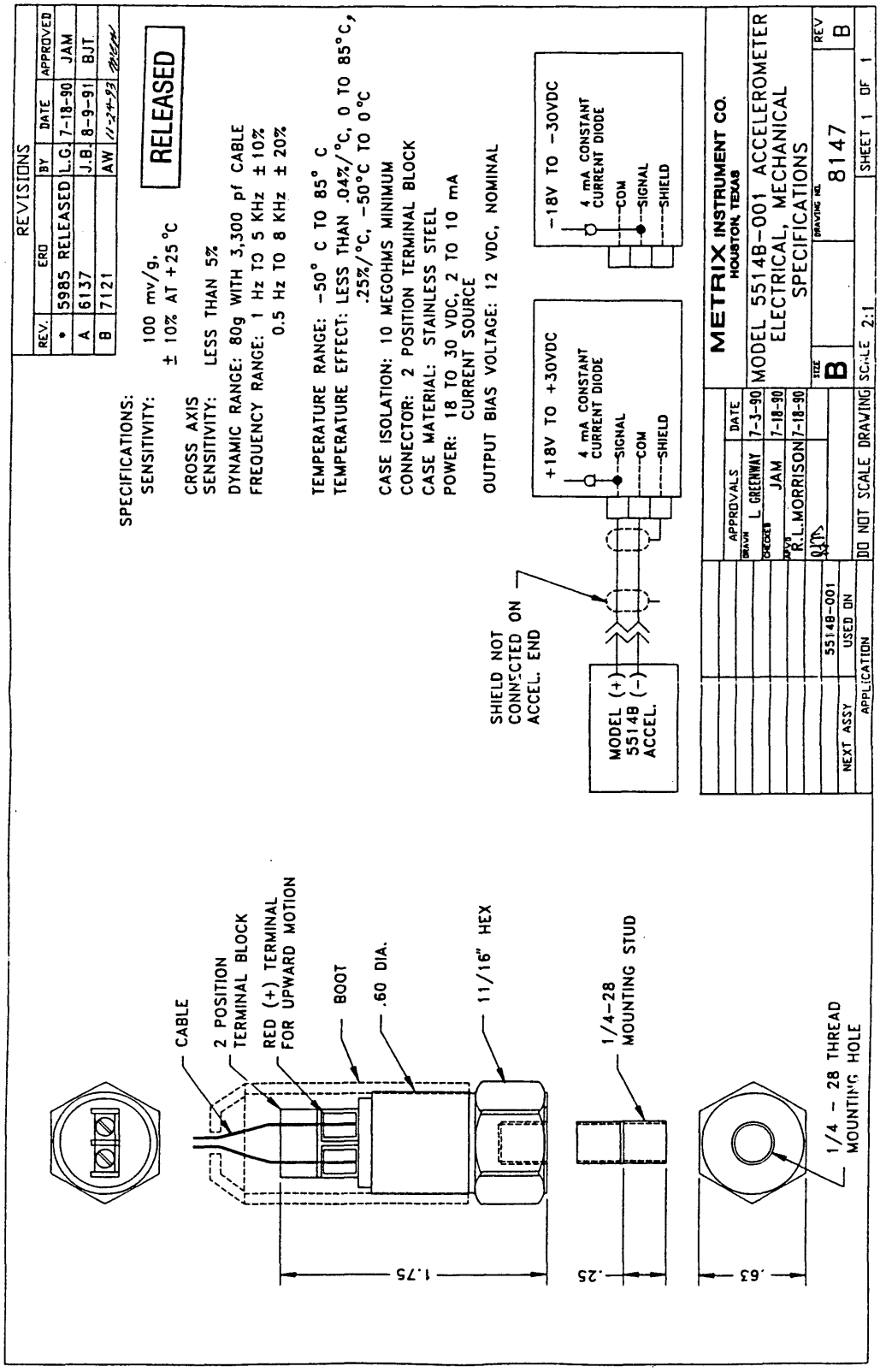
REVISIONS
REV. | ERD | BY | DATE | APPROVED
• | 5985 RELEASED | L.G. | 7-18-90 | JAM
A | 6137 | J.B. | 8-9-91 | BJT
B | 7121 | AW | 11-24-93
RELEASED
SPECIFICATIONS:
SENSITIVITY: 100 mv/g, ± 10% AT +25 °C
CROSS AXIS SENSITIVITY: LESS THAN 5%
DYNAMIC RANGE: 80g WITH 3,300 pf CABLE
FREQUENCY RANGE: 1 Hz TO 5 KHz ± 10%
0.5 Hz TO 8 KHz ± 20%
TEMPERATURE RANGE: -50° C TO 85° C
TEMPERATURE EFFECT: LESS THAN .04%/°C, 0 TO 85°C, .25%/°C, -50°C TO 0°C
CASE ISOLATION: 10 MEGOHMS MINIMUM
CONNECTOR: 2 POSITION TERMINAL BLOCK
CASE MATERIAL: STAINLESS STEEL
POWER: 18 TO 30 VDC, 2 TO 10 mA CURRENT SOURCE
OUTPUT BIAS VOLTAGE: 12 VDC, NOMINAL
CABLE
2 POSITION TERMINAL BLOCK
RED (+) TERMINAL FOR UPWARD MOTION
BOOT
.60 DIA.
11/16" HEX
1/4-28 MOUNTING STUD
1/4 - 28 THREAD MOUNTING HOLE
1.75
.25
.63
+18V TO +30VDC
4 mA CONSTANT CURRENT DIODE
SIGNAL
COM
SHIELD
-18V TO -30VDC
4 mA CONSTANT CURRENT DIODE
COM
SIGNAL
SHIELD
SHIELD NOT CONNECTED ON ACCEL. END
MODEL (+) 5514B (-) ACCEL.
METRIX INSTRUMENT CO.
HOUSTON, TEXAS
APPROVALS DATE
DRAWN L. GREENWAY 7-3-90
CHECKED JAM 7-18-90
APPD R.L. MORRISON 7-18-90
MQ/A
MODEL 5514B-001 ACCELEROMETER ELECTRICAL, MECHANICAL SPECIFICATIONS
SIZE B
DRAWING NO. 8147
REV B
55148-001
NEXT ASSY USED ON
APPLICATION
DO NOT SCALE DRAWING
SCALE 2:1
SHEET 1 OF 1

ACCELEROMETERS RATED UP TO 120 °C
MODEL 5514 & 5522

- **Integral amplifier - low source impedance**
- **Conforming to API standard 678**

Capable of sensing a wide range of vibration frequencies, these accelerometers are ideal for use on variety of machines, including low speed fans and high speed turbines and gear boxes. A built-in amplifier provides a high level, low impedance output for driving a remote monitor.

Each model consists of a temperature stabilized piezo-electric sensor and an amplifier packaged together in a stainless steel case, from which the sensing circuit is electrically isolated. A 1/4-28 mounting stud is provided. Two models are offered:

Model 5514: This reliable, general purpose industrial accelerometer features a 2 position terminal block for easy field wiring. A silicone rubber boot is provided to protect cable termination.

Model 5522: This high performance accelerometer features a wider frequency range, greater temperature stability and a hermetically sealed case.

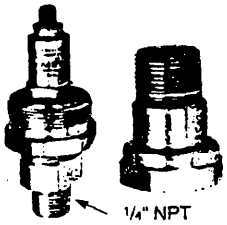

Sensor Housing Model 7295

Provides physical protection of sensor and wiring. Explosion-proof in NEC Class I (A, B, C, & D), Divisions 1 and 2 hazardous locations. 1/4 NPT stud base provides single hole, rigid mounting to machine case. 1" NPT conduit union provides convenient termination of signal cable conduit and easy access to accelerometer.

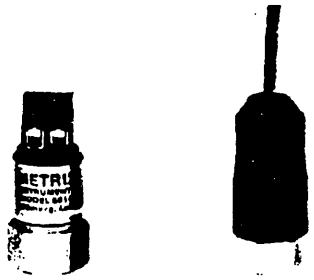

5514 | 5514 with boot | 5522

pending

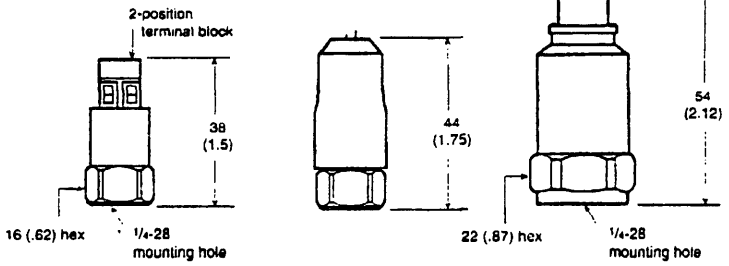

SPECIFICATIONS	5514	5522	Units
Sensitivity, 25°C	100 ± 10	100 ± 5	mv/g
Acceleration Range	40	50	g
Equivalent Noise	.0002	.0005	g
Frequency Response, ± 10%	2 to 5000	2 to 12000	Hz
Cross Axis Sensitivity	7	5	%
Temperature Range	-20 to +80	-50 to +120	°C
Sensitivity vs Temperature	+.12	+.07	%/°C
Case Isolation, minimum	100k	100K	ohms
Connector	terminals	bayonet	3 pins
Case Seal	epoxy	hermetic	
Power	20 to 28	18 to 30	volts
Current Regulating Diode	2 to 6	2 to 10	mA
Weight	32	80	grams
Associated Monitors	See Section 4		

HOW TO ORDER

5514-001 Accelerometer - complete with silicone rubber boot and (1/4"-28) stud.
93800-017 Cable - 2 conductor (AWG 22) with shield and PVC jacket, for use with 5514-001.
5522-001 Accelerometer - complete with 3719-02 mounting stud.
8426-XXX Connector/Cable Assy - complete with mating connector and 3 conductor cable (AWG 20) with shield and PVC jacket, for use with 5522-001.
7295-002 Sensor Housing - complete as shown. Zinc plated steel.

ACCESSORIES: See last page this Section for wiring accessories

Dimensions in mm (inches)

METRIX INSTRUMENT CO.
1711 TOWNHURST DRIVE, HOUSTON, TEXAS 77043 USA
PHONE: 713-461-2131 FAX: 713-461-8223

A.12. Accelerometer Vibration Transmitters.

Manufacturer	Metrix
Model Number:	5505B-005-100
Serial Number:	1721 (vert) and 1722 (hor)
Sensor In:	100 MV/g
Signal Out:	100MV/g
Full Scale Vibr:	4-20 MA= 0 to 1.0 IPS (25mm/s) PK
Passband:	5 to 10,000 Hz
Reference:	Metrix Instrument Co., 1990

VIBRATION TRANSMITTERS FOR REMOTE SENSORS

- **Use with velocity transducers, accelerometers or proximity sensors**
- **Provides 4-20 mA signal proportional to vibration level**
- **Seismic sensor models offer true RMS response per ISO 2954**

These transmitters accept signals from remote vibration sensors and produce a 4-20 mA output current proportional to the measured variable. They are the most efficient way to interface a vibration sensor with a milliamp monitor, data logger, PLC or computer. Four models are offered:

Models 5504 and 5519: These units operate with velocity transducers (see Section 2) and are available with response proportional to either vibration velocity or displacement.

Model 5505: This unit provides power to and accepts the signal from a low impedance accelerometer (see Section 2) and is available with response proportional to either acceleration or velocity.

Model 5510: This unit provides power to and accepts the signal from a proximity probe driver (see Section 2). The response is proportional to peak to peak displacement.

All models feature a buffered input signal for dynamic analysis and for probe gap indication (Model 5510). In the event of a sensor failure, the output current from the transmitter is driven below 4 mA, thereby signaling a malfunction. Bandpass filtering is optional.

The units are supplied with adapters for surface mounting or for mounting on a 35 mm DIN rail. The polymer housing is internally coated for EMI protection.

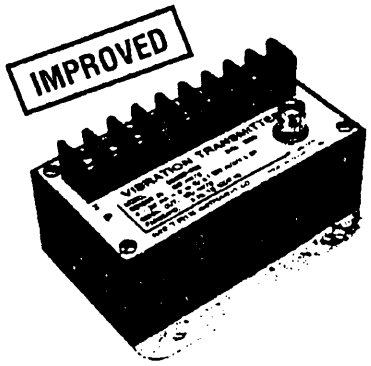

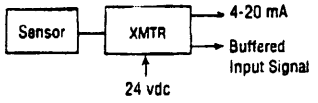

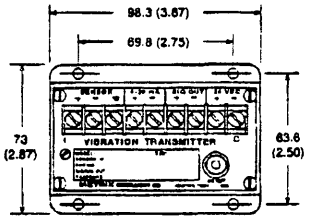

height: 68.6 (2.70)
weight: .27 kg (0.6 lbs.)

SPECIFICATIONS

Input Signal:
Models 5504 & 5519: 100 to 500 mv/ips (4 to 20 mv/mm/s)
Model 5505: 10 to 100 mv/g
Model 5510: 200 mv/mil (8 mv/micron)
Sensor Excitation Provided:
Model 5504: not required
Model 5519: 4 mA constant current
Model 5505: 4 mA constant current
Model 5510: -24 vdc, standard
-18 vdc available
Vibration Ranges: see table
Output: 4-20 mA dc
Maximum Load Resistance: 600 ohms
Frequency Response (Filter Out):
Model 5504: 5 Hz to 2000 Hz
Model 5505: 5 Hz to 10000 Hz (g's)
Model 5510: 5 Hz to 3000 Hz
Model 5519: 5 Hz to 2000 Hz
Signal Output: buffered input signal
Filters: optional low pass and high pass filters (18 db/octave slopes) can be specified. Part 7992-XXX
Isolation: 500V, circuit to case
Temperature Limits: -40°C to 66°C
Power: 18 to 30 VDC, 60 mA

ACCESSORIES:
See last page of Section 2 for enclosures and wiring accessories.

HOW TO ORDER

Input Sensor	Transmitter Model		Full Scale Vibration
	Flat Base	DIN Rail[1]	
Self Generating Velocity Transducer (see Section 2)	5504B-002	5504B-102	1.0 ips (25 mm/s), pk*
	5504B-003	5504B-103	2.0 ips (50 mm/s), pk*
	5504B-004	5504B-104	5 mils (125 um), pk-pk
	5504B-006	5504B-106	20 mils (500 um), pk-pk
Piezo-Velocity Transducer (see Section 2)	5519B-002	5519B-102	1.0 ips (25 mm/s), pk*
	5519B-003	5519B-103	2.0 ips (50 mm/s), pk*
	5519B-004	5519B-104	5 mils (125 um), pk-pk
	5519B-006	5519B-106	20 mils (500 um), pk-pk
Voltage Mode Accelerometer (see Section 2)	5505B-002	5505B-102	10 g (100 m/s²), pk*
	5505B-007	5505B-107	50 g (500 m/s²), pk*
	5505B-005	5505B-105	1.0 ips (25 mm/s), pk*
	5505B-006	5505B-106	2.0 ips (50 mm/s), pk*
Proximity Sensor (see Section 2)	5510B-001	5510B-101	5 mils (125 um), pk-pk
	5510B-002	5510B-102	10 mils (250 um), pk-pk
	5510B-003	5510B-103	20 mils (500 um), pk-pk

* For RMS calibration add 30 to dash number, ie -102 becomes -132.
[1] Specify DIN rail type when mounting in enclosure.

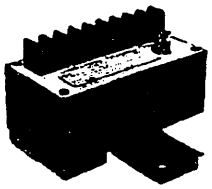

DIN Rail Adapter

Dimensions in mm (inches)

METRIX INSTRUMENT CO.
1711 TOWNHURST DRIVE, HOUSTON, TEXAS 77043 USA
PHONE: 713-461-2131 FAX: 713-461-8223

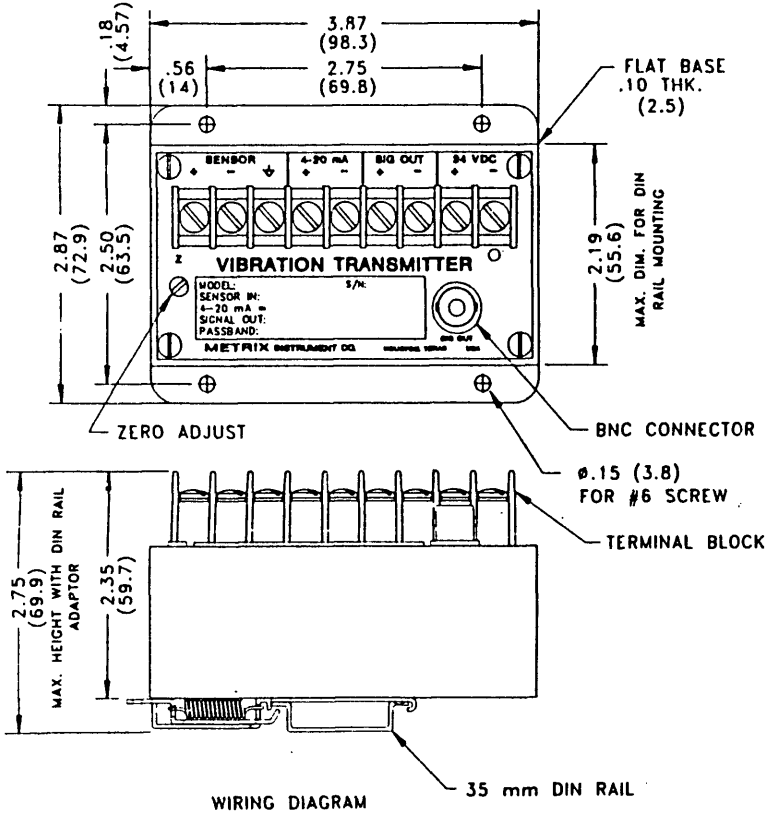

WIRING DIAGRAM

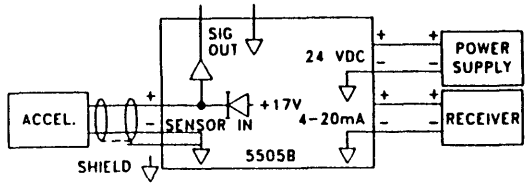

5505B
TRANSMITTER SPECIFICATIONS:

FUNCTION:

VIBRATION TRANSMITTER WITH ACCELEROMETER TRANSDUCER INPUT AND 4-20 mA CURRENT SOURCE OUTPUT.4-20 IS PROPORTIONAL TO THE TRUE RMS VALUE OF THE VIBRATION EXPRESSED IN PEAK OR RMS ACCELERATION (G), PEAK OR RMS VELOCITY (IPS) OR THE METRIC EQUIVALENTS.

INPUT (SENSOR) SENSITIVITY: 10 TO 100 mV/G (4.7 mA CONSTANT CURRENT SOURCE)

CURRENT OUTPUT (4-20mA): 4-20mA DC CURRENT SOURCE

MAXIMUM LOAD RESISTANCE: 600 OHMS

CURRENT OUTPUT ADJUSTMENT; FRONT PANEL ZERO POTENTIOMETER

VIBRATION RANGES: SEE TABLE

FREQUENCY RESPONSE (FILTER OUT): 5Hz TO 10KHz, -3db

OPTIONAL FILTERS: LOW PASS, HIGH PASS, AND BANDPASS FILTERS CAN BE SPECIFIED.

SIGNAL (SIG) OUTPUT: BUFFERED INPUT SIGNAL (ACCELERATION)

SENSOR FAILURE: CAUSES OUTPUT TO FALL BELOW 3.5mA

ISOLATION: 500V, CIRCUIT TO CASE

TEMPERATURE LIMITS: -40° C TO +66° C

POWER (24VDC): +20 TO +30VDC, 60mA

MOUNTING: FLAT BASE INSTALLED.
FOR 35mm DIN RAIL MOUNTING ADAPTOR INSTALLED, ADD 100 TO DASH NUMBER, I.e., -001 BECOMES -101.

MODEL	INPUT SENSOR	FULL SCALE VIBRATION
5505B-001	ACCELEROMETER	5 G (50 m/s^2), PK*
5505B-002	ACCELEROMETER	10 G (100 m/s^2), PK*
5505B-003	ACCELEROMETER	20 G (200 m/s^2), PK*
5505B-004	ACCELEROMETER	0.5 IPS (12.5 mm/S), PK*
5505B-005	ACCELEROMETER	1.0 IPS (25 mm/S), PK*
5505B-006	ACCELEROMETER	2.0 IPS (50 mm/S), PK*
5505B-007	ACCELEROMETER	50 G (500 m/s^2), PK*

*FOR RMS CALIBRATION ADD 30 TO DASH NUMBER, I.e., -001 BECOMES -031

A.9. A/D Board.

Manufacturer:	Acromag
Model Number:	AVME 932X
Reference:	Acromag Inc, 1994

Analog I/O Boards

Series AVME932x

High Speed Analog I/O Boards

- **Model AVME9320** Analog Input
- **Model AVME9321** Analog Input/Output

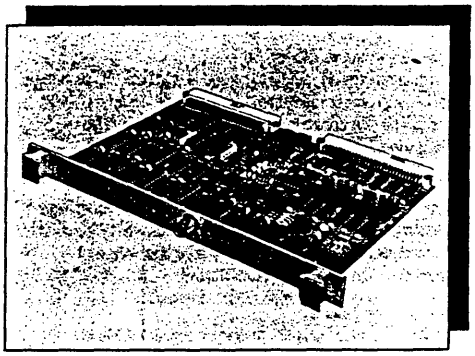

Description

General

These boards provide a means for interfacing analog input signals to the VMEbus. They are an easy and convenient solution to high-level analog signal interfacing in measurement and control applications. Typical uses include applications with external signal conditioning where rapid A/D conversion is needed. They are ideal for low-cost, high-speed data collection applications.

Model AVME9320

This board contains several features that reduce host processing to achieve system throughput rates equal to the board throughput rate.

Two channel selection schemes and three trigger sources offer operational flexibility and high throughput. In the individual channel mode, the input channel defined by the user undergoes an A/D conversion for each conversion trigger. The sequential scanning mode automatically increments to the next input channel after each conversion to eliminate host processing time.

Software and hardware trigger sources are generated directly by the user for precise synchronization with individual external events. An internal programmable timer provides self-triggering for scanning and precise interval timing without host intervention.

Nine unique input ranges enable easy adaptation to your application (+/-10, +/-5, +/-2.5, +/-1.25, +/-.625, 0 to 1.25, 0 to 2.5, 0 to 5, and 0 to 10 Volts). They are selectable with three jumper positions and four programmable gains. The programmable gain is selectable on an individual channel basis. Other gains are available on special order.

Zero drift correction circuitry allows the user, on command, to short the input signal and to read and store any value present. This value can then be used to correct measured inputs, eliminating the entire effect of offset errors, drift, etc.

Model AVME9321

This board provides the same analog input capability as the Model AVME9320 board with the added capability of two high-speed analog output channels for driving external devices. Each channel performs digital-to-analog conversions in 7 microseconds. Five jumper-selectable output ranges are available up to +/-10 volts with short circuit protection.

Features

Model AVME9320:

- 16 differential or 32 single-ended nonisolated inputs
- Throughput of 67,000 channels per second (15uS A/D conversions)
- 12-bit A/D resolution
- Three jumper-selectable input ranges:
  +/-5V, +/-10V, and 0 to 10V
- Two channel selection schemes:
  Individual channel
  Sequential scanning
- Three trigger sources:
  Software
  Internal programmable timer
  External trigger
- Three data formats, jumper selectable:
  Unipolar Straight Binary
  Bipolar Offset Binary
  Bipolar Two's Complement
- Four software programmable gains: 1, 2, 4, 8
- Zero drift correction circuitry
- Support for seven-level bus interrupt

Model AVME9321:

Analog input features same as the AVME9320 plus:

- Two independent analog outputs
- 12-bit D/A resolution
- 7 microsecond settling time
- Five jumper-selectable output ranges up to +/-10V with short circuit protection
- Three jumper selectable data formats, similar to the input, but independent of the analog input data format

Specifications

The following specifications are given for 25C ambient temperature and nominal power supply values unless otherwise noted.

Analog Input

Analog input type: nonisolated voltage

Number of analog input channels:
16 differential, 32 single ended

Input ranges:
+/-5 and +/-10 volts bipolar, 0 to 10 volts unipolar

Software programmable gains: x1, x2, x4, x8

Input overvoltage protection: +/-32 volts continuous

Input resistance: 9,000 megohms

Input bias current: 150pA typical

Common mode rejection ratio (60Hz): 71dB

Channel to channel rejection ratio (60Hz): 71dB

RFI resistance: <0.25% of full scale range at field strengths of 10V/m at 27, 151, and 467MHz

Monotonicity guaranteed over temperature

System accuracy: 0.04% of full scale range

A/D resolution: 12 bits

A/D accuracy: 12 bits

No missing codes over temperature: 12 bits

A/D nonlinearity: +/-1/2 LSB

Overall throughput rate: 67,000 channels per second max, or 15uS per conversion

Gain temperature coefficient: 50 ppm/C max

Offset temperature coefficient: 24 ppm/C max (without zero-drift correction)

Analog Output

Model AVME9321 Only

Analog output type: nonisolated voltage

Number of analog output channels: 2

Output ranges: +/-10, +/-5, +/-2.5, 0 to 5, and 0 to 10 volts

Resolution: 12 bits

Accuracy: 12 bits

Monotonicity guaranteed over temperature

Nonlinearity: +/-1/2 LSB

Output noise: 3mV p - p max

Capacitive loading without overshoot: 0.01uF max

Short circuit protection: continuous

Resistance to RFI: <0.25% of full scale range

Settling time (20V Step): 6uS to 0.01% of full scale range

Default output on reset: 0V or minus full scale (jumper-selectable)

Gain temperature coefficient: 25 ppm/C max

Offset temperature coefficient: 15 ppm/C max

VME Compliance

Meets or exceeds all written VME Specifications per revision C.1 dated Oct., 1985 and IEC 821-1987

Data transfer bus: A16: D16/D08 (EO) DTB slave

Address modifier code: 29(HEX) and 2D(HEX)

Interrupts: I(1) - I(7) jumper-programmable interrupt level; software-programmable interrupt vector

Memory map: short I/O space, occupying 1K consecutive byte locations, base address jumper-configurable within 64K short I/O space

Board size: Double Eurocard (NEXP) (233.5mm X 160mm)

Power Supply Requirements

+5 volts +0.25/-0.125 @ 2.5 Amps max

+/-12 volts = no load

Environmental

Operating temperature: 0 to 70C (32 to 158F)

Storage temperature: -25 to 85C (-13 to 185F)

Relative humidity: 5 to 95%, noncondensing

Connectors

P1: IEC Type 603-2-C096MX-xxx (96 pin DIN)

P2: IEC Type 603-2-C096MX-xxx (96 pin DIN)

P3: BNC jack

Ordering Information

Specify the Analog Board desired:

AVME9320: High speed analog inputs

AVME9321: High speed analog I/O

For special input ranges using fixed resistor gains, contact the factory.

***Specify the Termination Panel desired**

6924-16Dx: 16 differential inputs

6924-32Sx: 32 single-ended inputs

6925-16Dx: 16 filtered differential inputs

***Specify the Analog Signal Cable desired:**

9940-x: Unshielded cable

9941-x: Shielded cable

Where x is the length in feet; 12 feet maximum.

* For complete details of Termination Panels and Cables, see Page 46.

A.10. Ethernet Interface.

Manufacture:	Force 30
Model:	SYS68k CPU 307BE

A.11. Computer.

Manufacturer:	Silicon Graphics
Model:	Indigo 2,
Software:	Gensym G-2

A.12. Oscilloscope.

Manufacturer:	Phillips
Model:	PM 3335
Type:	60 MHz Digital Storage Oscilloscope
Reference Document:	N.V. Philips 1990

Appendix B.

TEST BENCH PHYSICAL DESCRIPTION, VARIABLES,AND OPERATING INSTRUCTIONS

The test bench is a hydraulic circuit with overpressure protection, fitted with a control system, a sensor array, and a data acquisition/interpretation system. The test bench simulates a hydraulic power unit (HPU) used to provide power to a robotic device. The main drive components are attached to an 8' x 4' x 4' metal chassis with protective Plexiglas walls. The test bench is located at CSM in the lower level of Brown Hall in the garage adjacent to Room 154.

The main components of the test bench are 1) hydraulic piston pump, 2) oil reservoir, 3) hydraulic valves and motorized valve control system, 4) motor and motor controller, 5) cooling fan, 6) sensor array, 7) Signal Conditioning/Monitoring/Speed control unit (SCMS), 8) ACROMAG analog-to-digital converter, 9) Force 30 Ethernet network interface, and 10) SGI Indigo 2 Extreme host computer workstation running G-2, a real-time expert system shell. Figure B.1 is a diagram of the main system components, Table B.1 lists the operator control variables, Table B.2 lists the sensor variables, and Figure B.2 shows the data acquisition hardware configuration. Individual component descriptions and specifications are given in Appendix A.

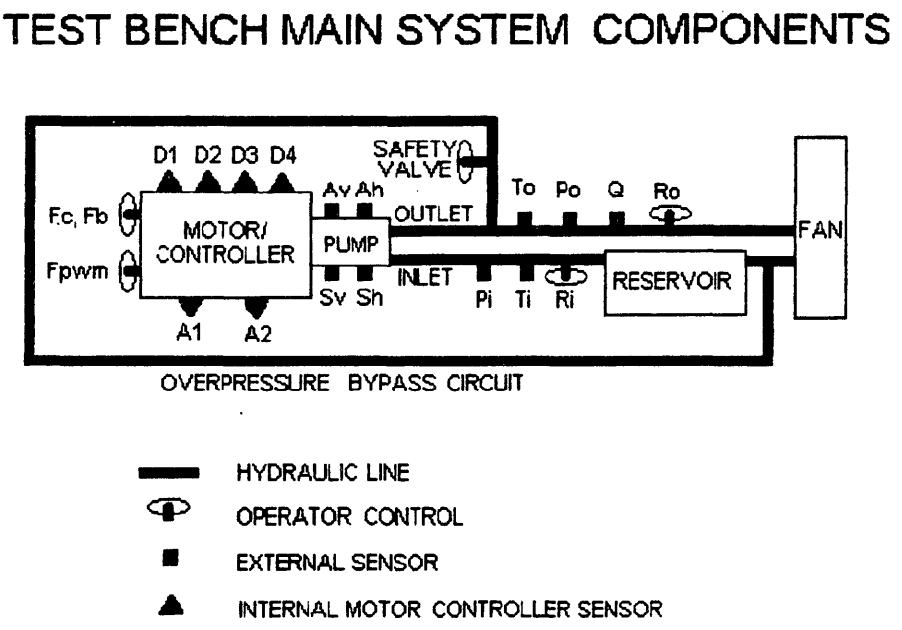

Figure B.1. Test Bench Main System Components.

F_c	COMMAND FREQUENCY (2*motor speed)
F_b	CONTROL BASE FREQUENCY (motor control parameter)
F_{pwm}	CARRIER FREQUENCY (motor control parameter)
R_i	PUMP INPUT HYDRAULIC IMPEDANCE (pump inlet valve)
R_o	PUMP OUTPUT HYDRAULIC IMPEDANCE (pump outlet valve)

Table B.1. Operator Controlled Variables (independent).

T_i	FLUID TEMPERATURE AT PUMP INPUT
T_o	FLUID TEMPERATURE AT PUMP OUTPUT
P_i	HYDRAULIC PRESSURE AT PUMP INPUT
P_o	HYDRAULIC PRESSURE AT PUMP OUTPUT
Q	VOLUME FLOW RATE AT PUMP OUTPUT
A_v	VERTICAL PUMP ACCELERATION MAGNITUDE (RMS)
S_v	VERTICAL PUMP VIBRATION ACCELERATION (AC)
A_h	RADIAL HORIZONTAL PUMP ACCELERATION MAGNITUDE (RMS)
S_h	RADIAL HORIZONTAL PUMP VIBRATION ACCELERATION (AC)
*A_1,A_2	MOTOR CONTROLLER DIAGNOSTIC ANALOG OUTPUT SIGNAL
*D_1,D_2,D_3,D_4	MOTOR CONTROLLER DIAGNOSTIC DIGITAL OUTPUT SIGNAL

* The motor controller is equipped with internal programmable diagnostic output signals which can be selected using the motor controller keypad. Refer to Appendix B for a detailed description of each of these variables.

Table B.2. Sensor Variables (dependent).

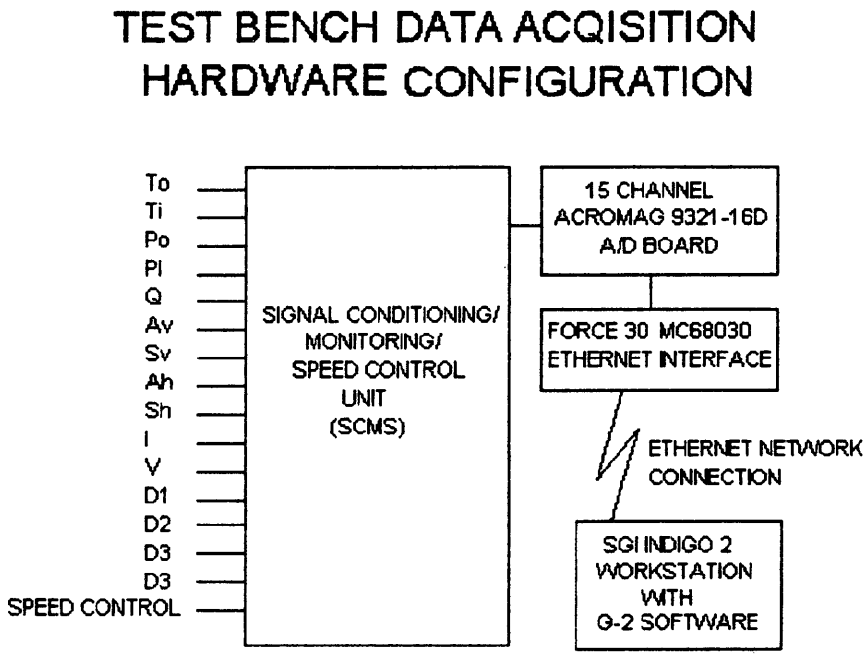

Figure B.2. Test Bench Data Acquisition Hardware Configuration.

The test bench data acquisition hardware measures sensor variables as a function of operator variables while providing on-line, real-time data access via an Ethernet network connection. For example, the relationship of pump input pressure (P_i, an independent operator controlled variable) on pump horizontal acceleration (A_h, a dependent sensor variable) can be observed at multiple remote locations for a wide range of operating conditions in real time. Rules which relate combinations of independent and dependent variables for normal machine operation could be developed. Abnormal conditions, such as pump cavitation, could be detected in real time by independent analysts using

expert systems, and specific predictive maintenance actions could be proposed. A recent cost-benefit analysis conducted by the CSM Economics Department has indicated that such a predictive tool would allow cheaper, faster and safer operations, particularly in hazardous applications such as nuclear remediation (Brady, T. and Thomas, M, 1996).

There are two main classifications of test bench variables: independent and dependent. Independent variables are directly controlled by the operator; dependent variables are functions of the independent variables. Dependent variables are classified as either external sensor variables or internal motor controller variables. The internal motor control variables are further subdivided into analog or digital categories (Figure B.3). The highlighted (bold) variables in Figure B.3 are available at the SCMS unit (Chapter 3) as signals in the range of 0 to 10 V for digitization and real time analysis during test bench operation. Each variable and will be discussed in detail in the remainder of this appendix.

Where possible, the external sensors have current outputs (4-20 mA) rather than voltage outputs in order to eliminate the resistive effects of long sensor leads. The current outputs are then converted to voltage signals in the SCMS unit prior to digitization.

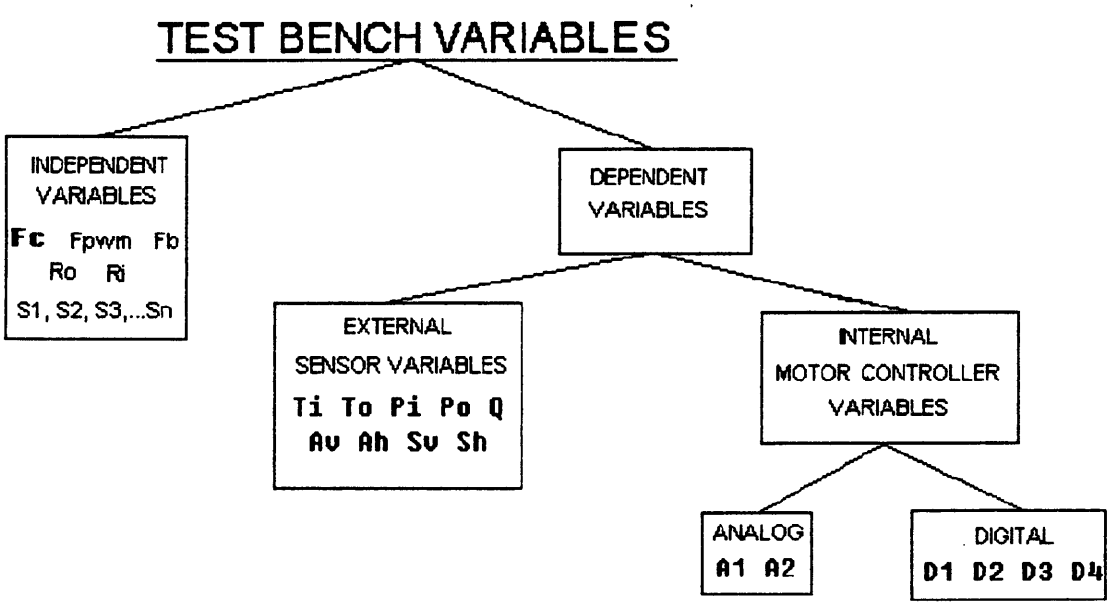

Figure B.3. Classification of Test Bench Variables.

B.1. Command Frequency (Fc).

F_C is an independent control variable which determines the desired speed of motor angular rotation, and can be set either by the SCMS unit or at the controller keypad (Chapter 3). F_C is indicated on the controller digital display above the keypad. It is important to note that F_C is relative to the motor controller, not the motor itself. The general relationship of F_C to motor speed F_m is given by the equation $F_m = 2F_C/P$, where P = the number of poles (Linday, 1986). The test bench has a four pole induction motor, giving $F_m = F_C/2$. However, the

desired motor speed ($F_C/2$) may differ slightly from the actual motor speed (F_m) depending on load conditions. In the current configuration of the test bench, the maximum speed F_C is limited to 60 Hz, or F_m = 30 Hz. In this report, the words 'motor speed' refer to F_C, unless otherwise indicated.

B.2. Carrier Frequency (Fpwm).

F_{pwm} is an attribute of the motor controller which is discussed in detail in Chapter 4. It can be set by the operator in the range of 1 kHz to 15 kHz. F_{pwm} is a main factor in determining the EMI performance of the test bench.

B.3. Control Base Frequency (Fb).

F_b is an attribute of the motor controller which is discussed in Chapter 4. It can be set by the operator in the range of 10 to 400 Hz. F_b is a main factor in determining the EMI performance of the test bench.

B.4. Pump Input Hydraulic Impedance (Ri).

R_i is controlled by a screw valve at the pump input (Fig. 3.1). The valve is fitted with a servo-mechanism to allow operation from the host computer. R_i is a relative measure, non-linearly correlated to the area of valve opening.

Excessive restriction of fluid flow using this valve will result in pump cavitation, an undesirable state in which fluid pressure drops below the vapor pressure of the hydraulic fluid, resulting in the implosion of void bubbles within the liquid. Cavitation can be identified by the high intensity of audible mechanical vibrations in the pump ('squealing' sound). Cavitation causes excessive erosion of pump components, and the accompanying vibrations can loosen nuts, bolts, etc. In one case, false temperature changes were recorded because the vibrations broke an electrical connection to the thermocouple transmitter.

B.5. Pump Output Hydraulic Impedance (Ro).

R_o is controlled by a screw valve at the pump output. (Fig 3.1). The valve was fitted with a servo-mechanism to allow operation from the

host computer. As with R_i, R_o is a relative measure, non-linearly correlated to the area of valve opening.

B.6. Machine Components (S1, S2, S3,. . . Sn).

S_1, S_2, S_3,. . . S_n indicate machine components such as pump type, fluid viscosity, hose bend radii, etc., which are in direct control of the test bench operator. By changing these variables, it is possible to study the system response of 1) different pump types (piston vs. gear pump), 2) old, worn, or damaged components, 3) various hose bend radii, 4) contaminated or improper viscosity fluid, 5) weakened mechanical connections, etc. The relative health state of worn components could be assessed based on comparison with equivalent new components, and specific failure responses could be simulated by purposely substituting broken components.

B.7. Fluid Temperature At Pump Input (Ti).

A J-type (iron-constantan) thermocouple unit senses the temperature of the hydraulic fluid at the pump input and returns an electric signal in the millivolt range. The voltage is input to a co-located transmitter which 1) provides a reference voltage (cold junction), 2)

adjusts for non-linearity, and 3) and converts the signal to an electrical current in the range of 4-20 mA. This current range linearly corresponds to temperature limits of -17.78 to 132.2 degrees Celsius (0 to 270 degrees Fahrenheit). The temperature resolution is 0.037 degrees Celsius (0.066 degrees Fahrenheit).

B.8. Fluid Temperature At Pump Output (To).

A second identical thermocouple monitors the temperature of the hydraulic fluid on the high pressure line, thus allowing comparative temperature measurements. The temperature difference between pump input and output gives an indication of the work done by the pump. At equilibrium, the thermocouples can be calibrated to a Weston dial readout thermometer mounted on the reservoir tank.

B.9. Hydraulic Pressure At Pump Input (Pi).

P_i is measured by a Sensotech Model TJE vacuum pressure transducer mounted on the same low-pressure hydraulic line as the pump input. The detector therefore yields useful diagnostic information on the pump's cavitation characteristics. The device senses fluid vacuum pressures in the range of 0 to -103 kPa (0 to -15 psia) and produces a proportionate

voltage signal in the millivolt range. The sensor signal is routed to a packaged in-line amplifier located in the SCMS unit (Figure 3.3). The in-line amplifier supplies a scaled, calibrated high-level signal output to the A/D board. A separate standard dial-readout vacuum gauge on the same hydraulic line provides redundancy.

Initially, the test bench was delivered with an Ashcroft M1 Pressure Transducer, which was particularly susceptible to motor controller electromagnetic noise emanations. The sensor eventually failed and had to be replaced. The fabricators of the test bench later informed CSM that that particular sensor was designed for gas pressure detection rather than fluid pressure detection.

B.10. Hydraulic Pressure At Pump Output (Po).

P_O is obtained by a Sensotech Model LM pressure transducer mounted on the same high-pressure line as the pump output. The detector senses fluid pressures in the range 0 to 34.5 kPa (0 to 5000 psig) and produces a proportionate voltage signal in the millivolt range. As with P_i, the sensor signal is routed to a packaged in-line amplifier located in the SCMS unit. The in-line amplifier supplies a scaled, calibrated high-level signal output to the A/D board. The test bench is capable of producing pressures of up to 41.4 MPa (6000 psi), however a safety

bypass valve will open if the pressure exceeds 34.5 MPa (5000 psi). P_O should not exceed 27.5 MPa (4000 psig) during normal operation. A separate standard dial-readout pressure gauge on this line provides redundancy.

Initially, the test bench was delivered with a Webster LPT-6000 transducer, which failed and had to be replaced by the more expensive Sensotech device. Continued exposure to intense EMI may have damaged the Webster sensor.

B.11. Volume Flow Rate At Pump Output (Q).

Q is obtained with a Webster LTE 50 Turbine Flowmeter and Model PRA1 Pulse Rate to Analog Converter. The flowmeter is connected in series with the high pressure hydraulic line at the pump output, and the PRA module is mounted on the test bench chassis. The meter detects flow rates ranging from 1.9 to 56.8 liters per minute (0.5 to 15 gallons per minute) and returns a pulse rate modulated signal which is converted by the PRA1 module to an analog current in the range of 4-20 mA. Sometimes the turbine gets stuck; in this case free it using high motor speed. Also, be wary of possible loose connections on the SCMS input signal screw-terminal.

B.12. Vertical Pump Vibration AC Acceleration (Sv).

S_V is obtained from a Metrix Accelerometer Model 5514 mounted vertically and radially to the pump axis. The accelerometer is capable of sensing mechanical acceleration magnitudes of up to 40 gravitational units and frequencies in the range of 2-5000 Hz. The acceleration voltage trace is routed to the SCMS unit where it is biased for compatibility with ACROMAG A/D board input requirements. Specifically, the acceleration voltage trace must be limited to the range of 0 to 10 volts. In order to accomplish this, a blocking capacitor first removes the existing DC component of the acceleration trace (Figures C.9, C.10). Next, bias is added so that the acceleration trace is 5 volts when acceleration is zero. This insures that the full unclipped waveform is available as a voltage signal even during maximum pump vibration experienced during cavitation. The acceleration trace is then optionally filtered prior to digitization.

B.13. Vertical Pump Vibration Acceleration RMS Magnitude (Av).

The raw accelerometer output is routed to a Metrix vibration transmitter mounted on the test bench chassis (Figure C.10). In addition to providing a buffered signal (S_V) to the SCSM unit, the

transmitter also provides an RMS signal (A_V). The sensor variable A_V is a measure of the RMS magnitude of the vertical component of pump vibration acceleration, and is routed to the SCMS as an electrical current in the range of 4-20 mA.

B.14. Radial Horizontal Pump Vibration AC Acceleration (Sh).

As with S_V, S_h is measured by a second identical accelerometer mounted horizontally and radially to the pump.

B.15. Radial Horizontal Pump Vibration Acceleration RMS Magnitude (Ah).

As with A_V, A_h is provided by a second identical vibration transmitter which routes the horizontal RMS vibration magnitude to the SCMS unit as a current signal.

B.16. Motor Controller Analog Outputs (A1, A2).

Two analog outputs (A_1 and A_2) are available on terminals J6 and J7 of the terminal strip mounted on the controller panel (Figure C.2).

Using the keypad, the operator may select any two of the following nine analog output variables for monitoring on SCMS Channels 10 and 11:

1) COMMAND FREQUENCY. Although F_C is an independent control variable, it can also be chosen as an analog output signal. A value of zero volts on this channel corresponds to zero motor speed, a value of 5 volts corresponds to maximum motor speed. Forward and reverse motor rotation both result in a positive voltage at this terminal.

2) FREQUENCY. Under constant current conditions, a motor turning a heavy load will rotate slower than the same motor turning a light load. The controller compensates for the effect of load by driving the motor at a frequency higher than the command frequency. This adjusted frequency is available as an analog output.

Note that 1) and 2) do not represent the true angular frequency of motor rotation, and are not slip compensated.

3) AC RMS CURRENT. This is the line current I drawn by the motor. A value of zero volts on this channel corresponds to zero current draw; a value of 5 volts corresponds to the full load current of 51 amperes.

4) AC RMS VOLTAGE. This is the line voltage V supplied by the controller to the motor. A value of 5 volts DC at this terminal corresponds to a value of 460 volts RMS at the motor leads.

5) POWER. Horsepower is given by the equation V*I*(SQRT 3)*(POWER FACTOR)*(EFFICIENCY)/746. For this motor, the power factor is 0.82 and the efficiency is 0.902, giving a horsepower rating of 40. A value of zero volts on this channel represents -40 horsepower and a value of 5 volts on this channel represents a value of 40 horsepower. The negative sign does not indicate reverse rotation, rather it indicates a situation when electricity is being generated by the motor. This can occur during deceleration while the inertial energy of the load is being dissipated after the motor input power is cut off.

6) TORQUE. Torque is proportional to motor power divided by motor speed. A value of 5 volts DC on this channel represents 100% rated torque of 120 ft-lbs.

7) BUS VOLTAGE. The three phase current is rectified prior to modulation. The resulting rectified DC voltage is the bus voltage. A value of zero volts on this channel represents zero bus voltage; a value of 2.5 volts represents a rated bus voltage of 650 volts DC.

8) ZERO CAL. The output of this channel is simply zero volts and is used as a ground reference for external meters.

9) 100% CAL. The voltage on this channel is always 5 volts above ground and is used to calibrate external meters.

AC RMS CURRENT (I) and AC RMS VOLTAGE (V) are currently assigned to the two analog controller outputs A1 and A2.

B.17. Motor Controller Digital Outputs (D1, D2, D3, D4).

Digital outputs are available on terminals J19, J20, J21, and J22 (Figure C.3) of the terminal strip mounted on the controller panel. The digital outputs require an external voltage source and are either "on" or "off " according to a specific test condition. Using the keypad, the operator can assign four of the following nine parameters to be output to the terminal strip for monitoring:

1) READY CONDITION. On if controller is receiving power and no faults exist.

2) ZERO SPEED. On if the motor is operating below a prescribed set point speed.

3) AT SPEED. On if the controller is operating within a set speed range.

4) AT SET SPEED. On if the speed is at or above the set point speed.

5) OVERLOAD. On if the output current is above the control rated current.

6) KEYPAD CONTROL. On if the motor is being controlled locally at the keypad.

7) DRIVE ON. On if the controller is ready and commanding the motor to operate.

8) REVERSE. On if the motor is running in reverse.

9) FAULT. On if a fault condition is present, such as power failure, ground fault condition, overload, controller memory failure, etc.

The current four selections for the digital variables are shown in Table B.3.

DIGITAL VARIABLE	LED NUMBER (FIG. 3.3)	SCMS CHANNEL NUMBER	FUNCTION
D1	1	12	READY CONDITION
D2	2	13	ZERO SPEED (10 Hz)
D3	3	14	AT SET SPEED (50 Hz)
D4	4	15	AT SPEED (0.1 Hz)

Table B.3. Digital Variable Assignments.

B.18. Powering Up (Figure 3.1).

1) Visually inspect test bench. Check for disconnected hoses, unsafe electrical connections, oil leaks, etc.

2) Engage primary power switch. The cooling fan in the motor controller will turn on. A red LED will appear on the lower left of the STOP button on the controller keypad.

3) Engage secondary power switch. The flowmeter sending unit, motorized pressure valves, and main cooling fan will not operate if this switch remains off.

4) Leave the test bench area and go to the SCMS unit. Turn on 24 volt power supply, oscilloscope, and 9 V battery saver switch. The red LED indicator (labeled 24 V) on the SCMS unit will turn on.

5) Using the toggle switches on the front of the SCMS unit, set ENABLE on, FORWARD on, REVERSE Off, and set all four speed control toggle switches off.

6) Go back to the test bench motor controller keypad and press LOCAL until the word REMOTE appears on the controller digital display. Press FWD on the controller keypad. The red stop light should turn off and a green light will appear at the lower left of the FWD button. The test bench is now ready. Reverse the procedure to power down.

B.19. Programmable Remote 15 Speed Selection (Figure 3.2).

After powering up, select motor speed using the four speed toggle switches located on the front panel of the SCMS unit. The motor speed can be selected from Table B.4. (Note that listed speed (F_C) is referenced to the motor controller, not the motor itself.)

SWITCH 1	SWITCH 2	SWITCH 3	SWITCH 4	SPEED Hz
DOWN	DOWN	DOWN	DOWN	0.0
UP	DOWN	DOWN	DOWN	2.5
DOWN	UP	DOWN	DOWN	5.0
UP	UP	DOWN	DOWN	7.5
DOWN	DOWN	UP	DOWN	10.0
UP	DOWN	UP	DOWN	15.0
DOWN	UP	UP	DOWN	20.0
UP	UP	UP	DOWN	25.0
DOWN	DOWN	DOWN	UP	30.0
UP	DOWN	DOWN	UP	35.0
DOWN	UP	DOWN	UP	40.0
UP	UP	DOWN	UP	45.0
DOWN	DOWN	UP	UP	50.0
UP	DOWN	UP	UP	55.0
DOWN	UP	UP	UP	60.0
UP	UP	UP	UP	RESET

Table B.4. Test Bench Motor Speed Selection.

B.20. Continuous Remote Speed Control.

The motor controller can be reconfigured for continuous remote speed operation from a 5K potentiometer on the front panel of the SCSM unit (Figure 3.2) as follows:

1) Press the red STOP button on the motor controller keypad.

2) Press PROG.

3) Scroll with arrow key until PRESS ENTER FOR INPUT appears on the keypad display, and press ENTER.

4) Scroll until OPERATING MODE appears, and press ENTER.

5) Scroll until STANDARD RUN appears, and press ENTER.

6) Scroll until ANA CMD SELECT appears and press ENTER.

7) Scroll until POTENTIOMETER appears and press ENTER.

8) Scroll until MENU EXIT appears, and press ENTER.

9) Scroll until PROGRAMMING EXIT appears and press ENTER.

10) Press LOCAL until REMOTE appears. Set SCMS unit to ENABLE on, FORWARD on, Speed Toggle Switch # 1 on, all others off. Motor speed can now be controlled remotely and continuously with the potentiometer speed control knob on the SCMS unit.

B.21. Local Keypad Speed Control.

The motor can be controlled locally at the keypad by configuring the controller as follows:

1) Press STOP on the keypad.

2) Press PROG on the keypad.

3) Scroll with arrow key until PRESS ENTER FOR INPUT appears on the keypad display, and press ENTER.

4) Scroll until OPERATING MODE appears, and press ENTER.

5) Scroll until KEYPAD appears, and press ENTER.

6) Scroll until MENU EXIT appears, and press ENTER.

7) Scroll until PRESS ENTER FOR PROGRAMMING EXIT appears and press ENTER.

8) Press FWD. Motor speed can now be controlled locally at the keypad using the arrow keys.

B.22. Pulse Width Modulation Carrier Frequency Selection.

The PWM carrier frequency (F_{pwm}) is explained in Chapter 4. F_{pwm} can be set to any value from 1 kHz to 15 kHz as follows:

1) Press STOP on the controller keypad.

2) Press PROG.

3) Scroll to LEVEL 2 BLOCKS and press ENTER.

4) Scroll to OUTPUT LIMITS and press ENTER.

5) Scroll to PWM FREQUENCY and press ENTER.

6) Set PWM FREQUENCY using SHIFT to select a decimal place, and arrow keys to select a decimal value. Press ENTER.

7) Scroll to MENU EXIT and press ENTER.

8) Scroll to PROGRAMMING EXIT and press ENTER.

B.23. Select Motor Controller Outputs.

The Baldor series 15H motor controller provides nine independent programmable analog outputs and seven independent programmable digital outputs for monitoring motor controller functions. However, the controller only supports a maximum of two analog outputs (A_1, A_2) and four digital outputs (D_1, D_2, D_3, D_4) during continuous operation. The LEDs provided in the SCMS unit (Figure 3.2) show the logic states of D_1, D_2, D_3, and D_4. This section describes how to select A_1, A_2, D_1, D_2, D_3,and D_4 from the controller keypad.

1) Press STOP.

2) Press PROG.

3) Scroll to PRESS ENTER FOR OUTPUT and press ENTER.

4) Select four digital outputs and 2 analog outputs.

5) Scroll to MENU EXIT and press ENTER.

6) Scroll to PROGRAMMING EXIT and press ENTER.

B.24. Recovering Factory Settings.

At some point it may be desirable to default to standard factory settings. This can be achieved as follows:

1) Press PROG
2) Scroll to LEVEL 2 BLOCKS and press ENTER.
3) Scroll to MISCELLANEOUS and press ENTER.
4) Scroll to FACTORY SETTINGS and press ENTER.
5) Scroll to YES and press ENTER.
6) Scroll to MENU EXIT and press ENTER.
7) Scroll to PROGRAMMING EXIT and press ENTER.

B.25. Analog Signal Monitoring and Filter Controls.

The SCMS allows simultaneous oscilloscope observation of any two sensor signals. The selected sensor signals can be observed before or after signal conditioning. It is also possible to simultaneously observe the pre- and post- conditioned traces of a given channel. The channel selection switches are located on the front panel of the SCMS (Figure 3.2). The two 12-position switches are labeled RAW SIGNAL and

FILTERED SIGNAL. Table B.5 shows which channel positions correspond to which sensor variables.

SWITCH POSITION (CHANNEL NUMBER)	SENSOR VARIABLE
0	left open for test purposes
1	T_i
2	T_o
3	P_i
4	P_o
5	Q
6	A_v
7	A_h
8	S_v
9	S_h
10	A_1
11	A_2

Table B.5. Selector Switch Positions.

The dip switches located inside the SCSM (Figure 3.3) activate the signal conditioning circuit for each channel. Suppose one wishes to

view the unfiltered traces R_i and R_o. Simply set the dip switches for Channels 3 and 4 to the OFF position and set the RAW SIGNAL and FILTERED SIGNAL selectors to 3 and 4, respectively. Now suppose one wishes to view the raw and filtered versions of Q, the volume flow rate. Set Dip Switch Number 5 to ON and select Channel 5 on both channel selector switches. Another useful configuration is to use the X-Deflection feature of the oscilloscope (in analog mode) to display one channel as a function of another channel. This mode of operation is useful in simultaneously observing S_v and S_h to detect pump cavitation, or observing the delay effects of the analog filter for a given channel.

B.26. Fluid Pressure Controls.

The pressure of hydraulic fluid at the pump inlet (R_i) ranges from zero to approximately -15 psia, and is controlled by a red-handled lever valve mounted near the base of the oil reservoir (Figure 3.1). The high pressure at the pump outlet (R_o), which can exceed 4,000 psig, is controlled by a rotary valve mounted on the test bench chassis. Extreme caution should be exercised while operating the test bench at elevated fluid pressures. Subsequent to the noise analysis project, both of the fluid pressure valves were automated with stepper motors controlled by a dedicated computer located near the SCMS unit.

Appendix C.

CIRCUIT DIAGRAMS

This section contains schematics for the SCMS circuits, including signal conditioning, speed control, motor analog and digital outputs, and grounding/shielding schematics. In the RC filter circuits, an additional 0.1 UF tantalum capacitor was placed in parallel with the main filter capacitor in order to improve rejection of high frequencies.

MOTOR SPEED CONTROL SCHEMATIC

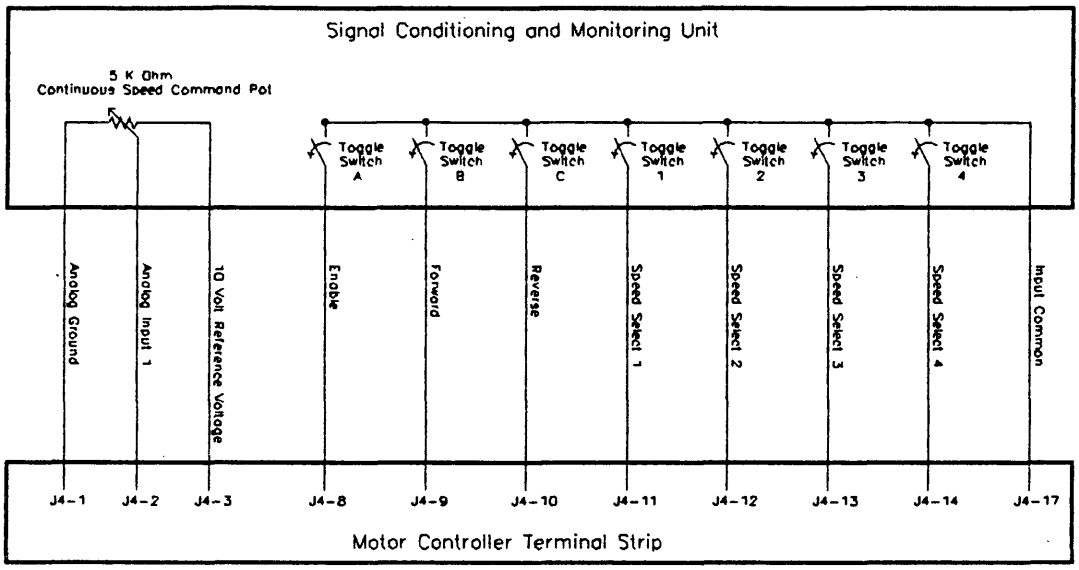

Figure C.1. Motor Speed Control Schematic.

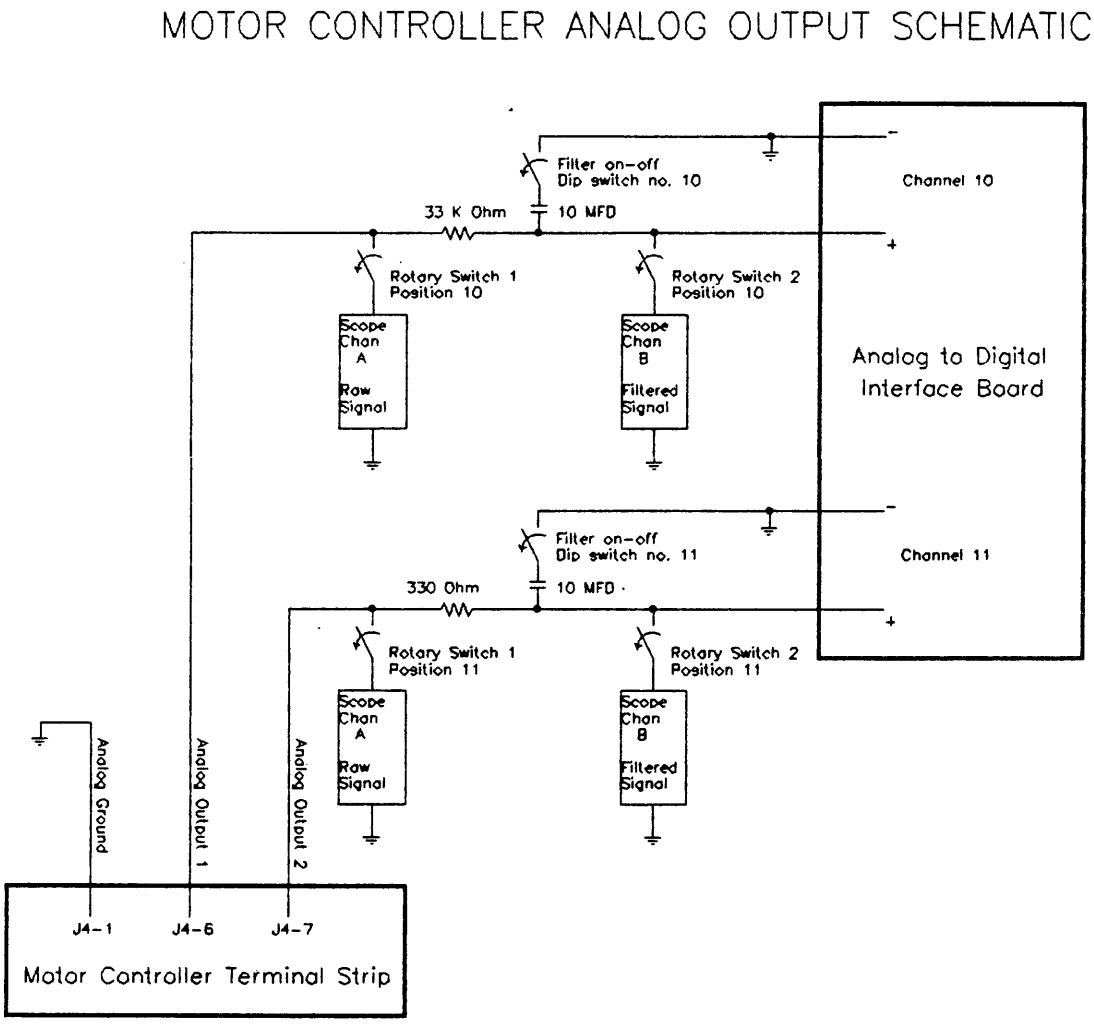

Figure C.2. Motor Controller Analog Output Schematic.

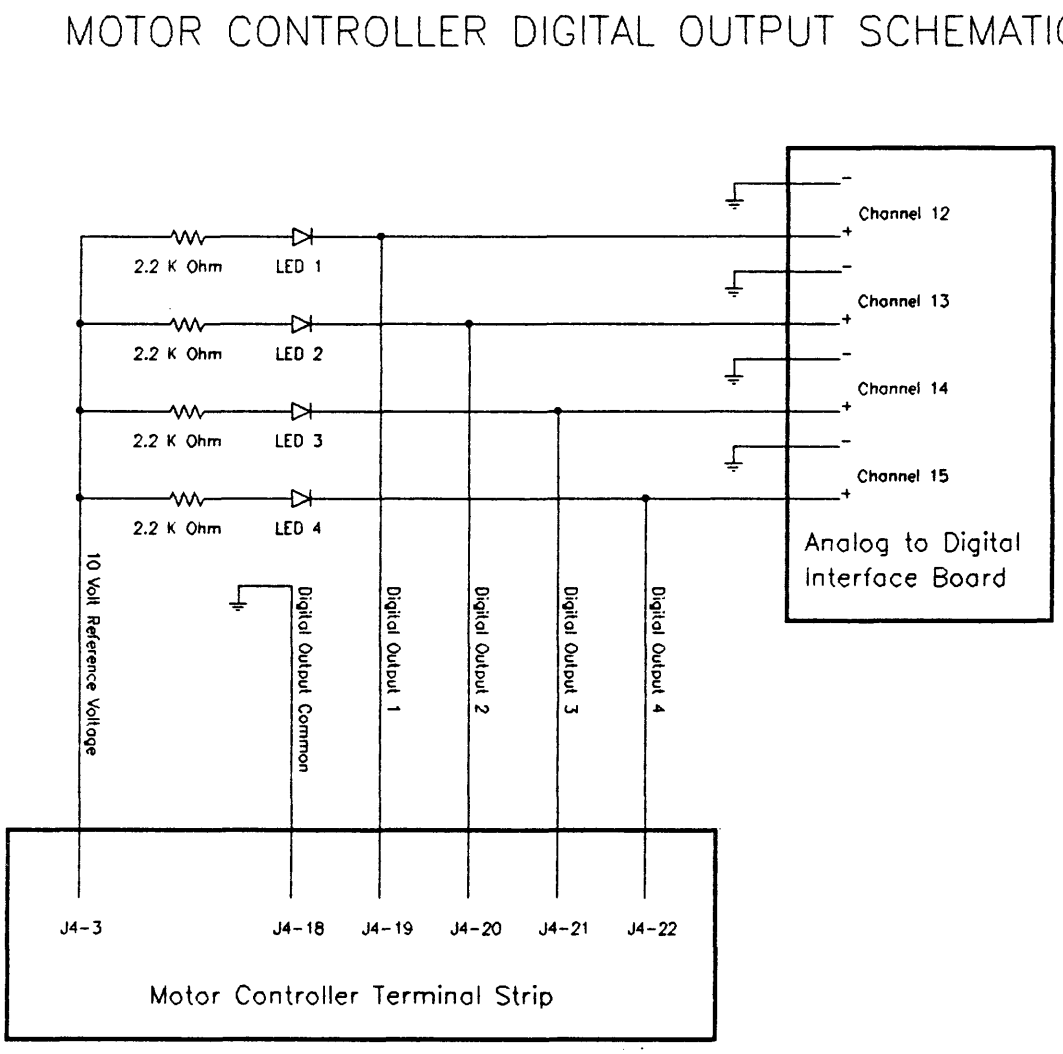

Figure C.3. Motor Controller Digital Output Schematic.

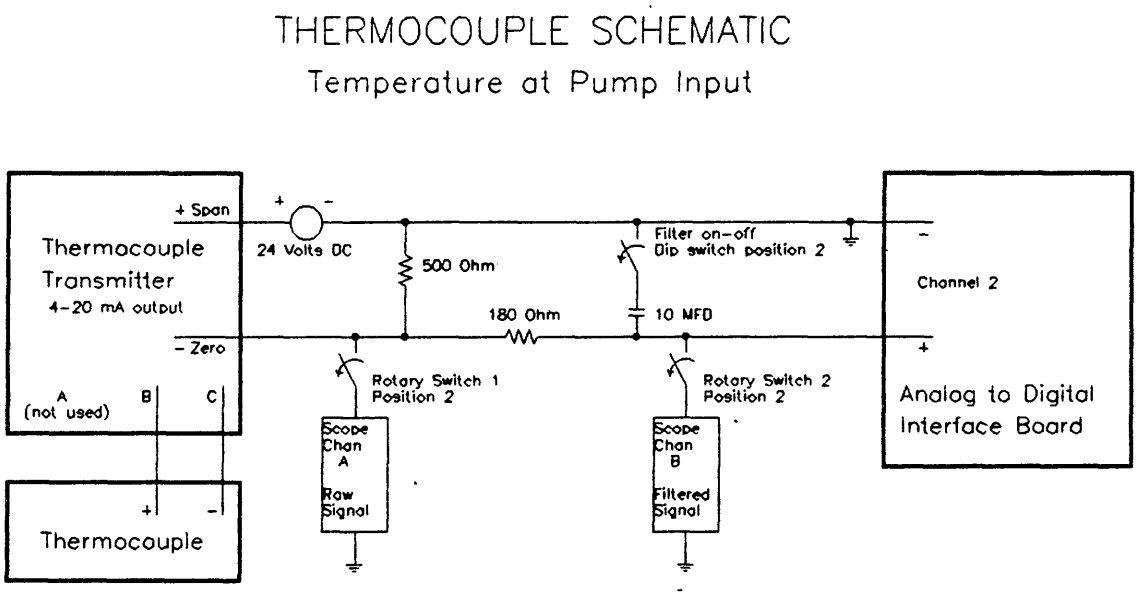

Figure C.4. Thermocouple Schematic - Temperature at Pump Input.

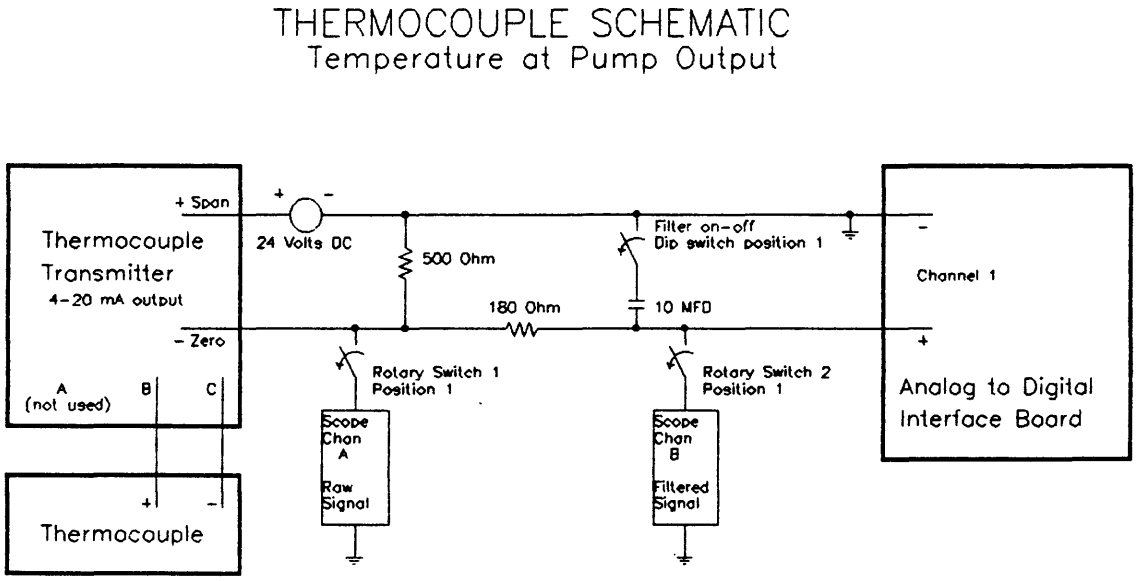

Figure C.5. Thermocouple Schematic - Temperature at Pump Output.

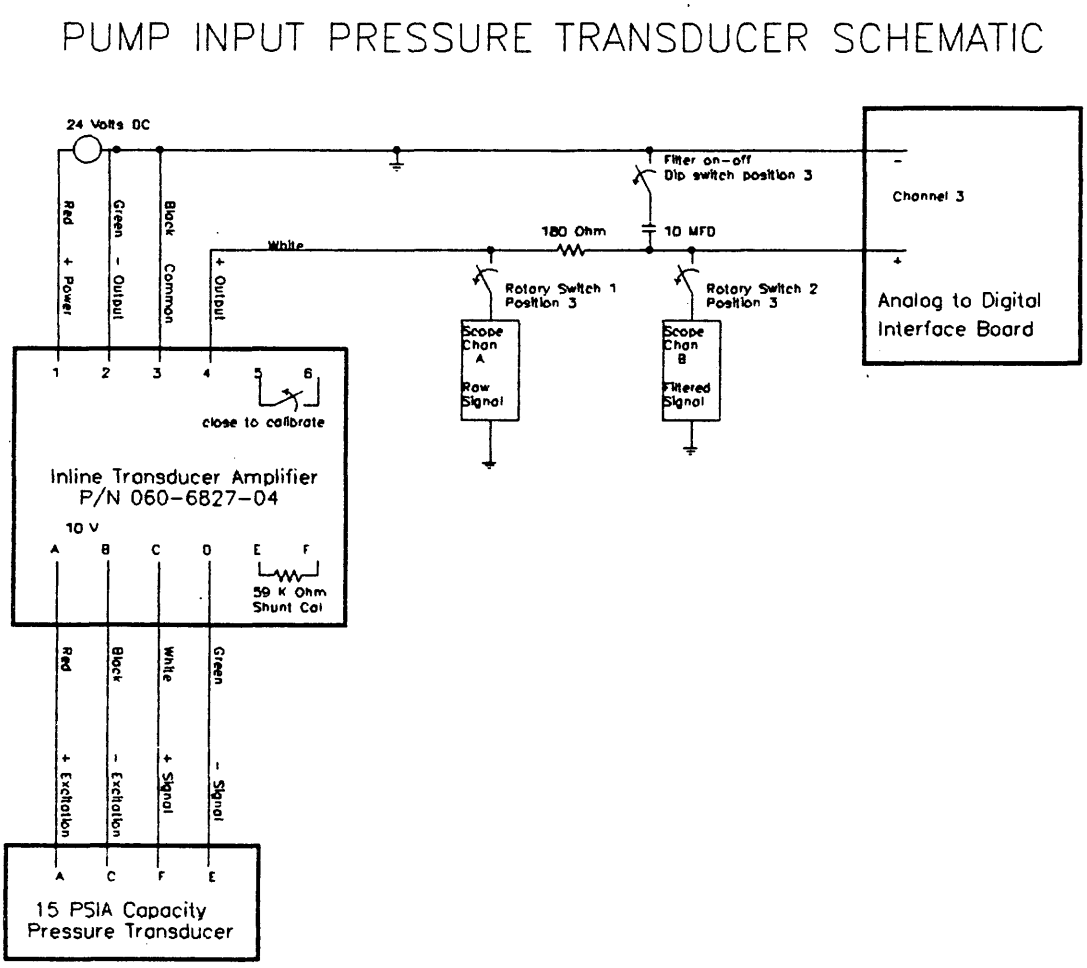

Figure C.6. Pump Input Pressure Transducer Schematic.

PUMP OUTPUT PRESSURE TRANSDUCER SCHEMATIC

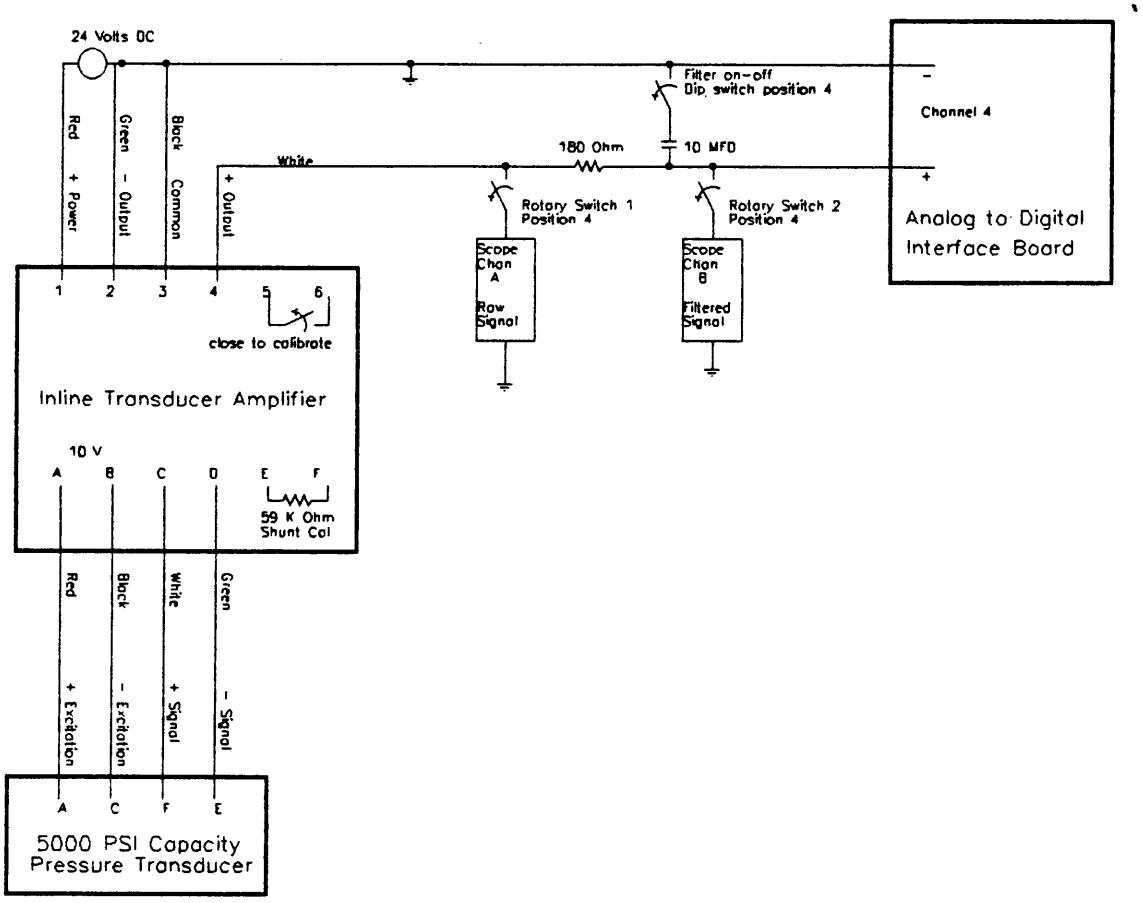

Figure C.7. Pump Output Pressure Transducer Schematic.

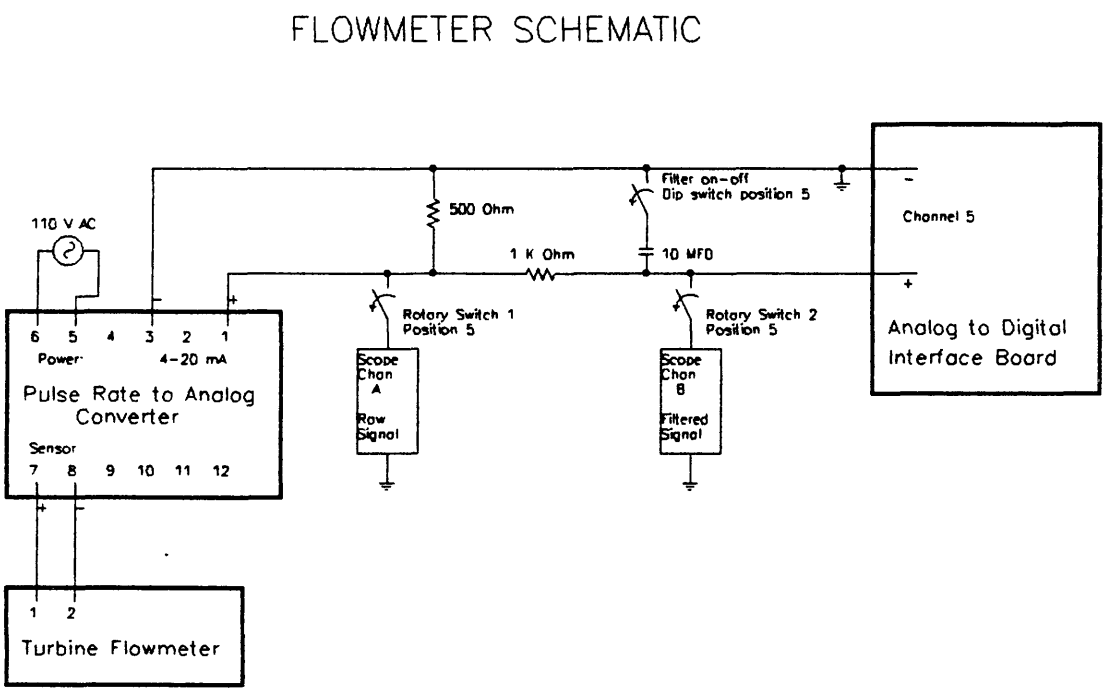

Figure C.8. Flowmeter Schematic.

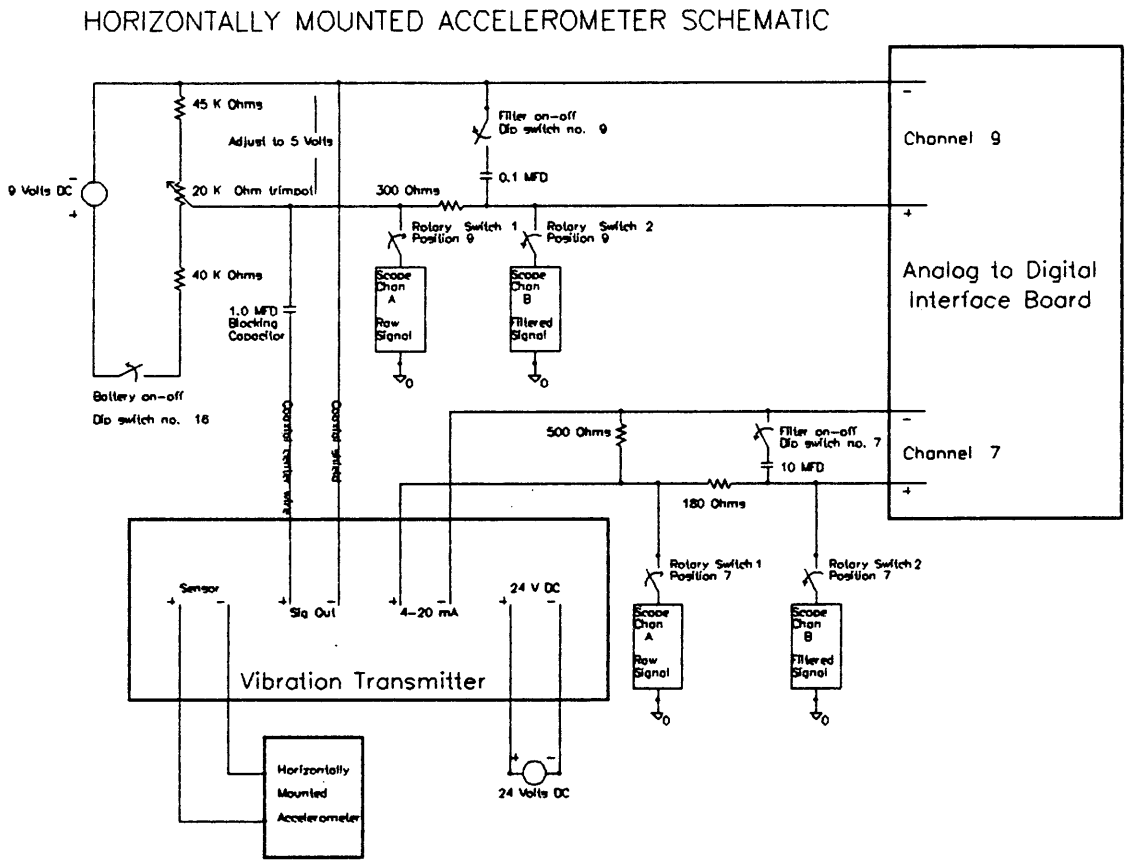

Figure C.9. Horizontally Mounted Accelerometer Schematic.

VERTICALLY MOUNTED ACCELEROMETER SCHEMATIC

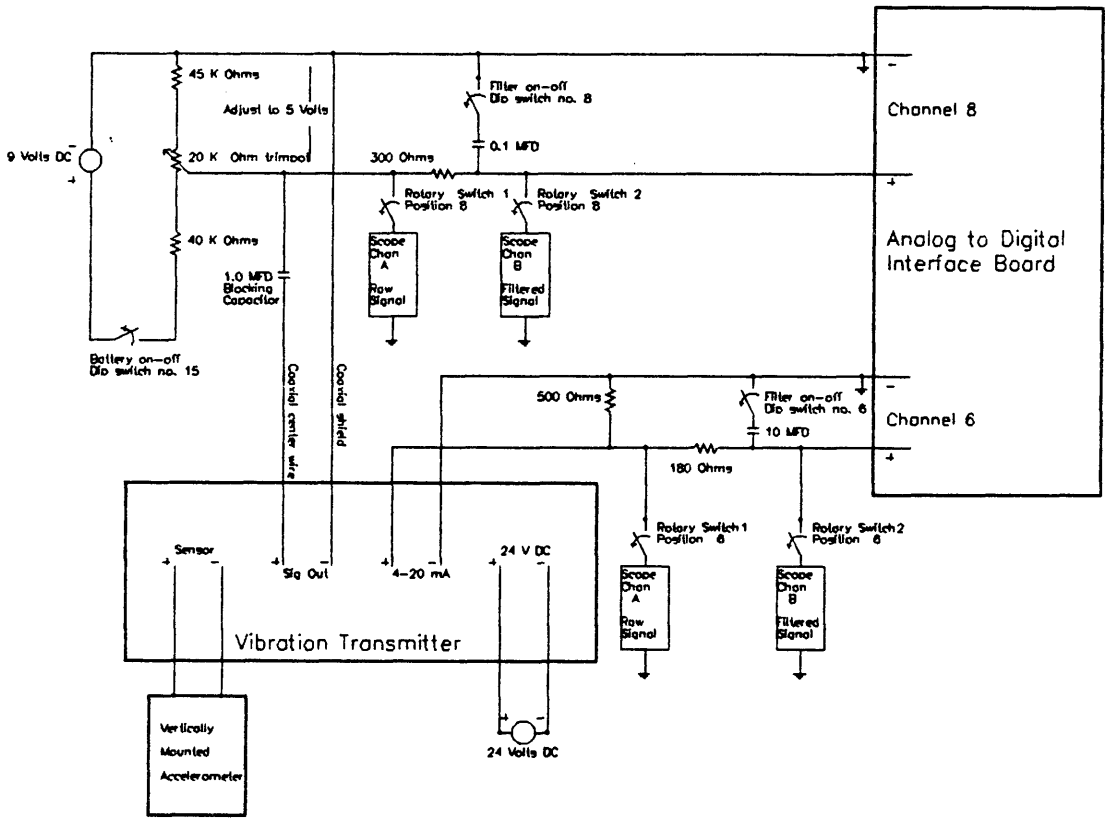

Figure C.10. Vertically Mounted Accelerometer Schematic.

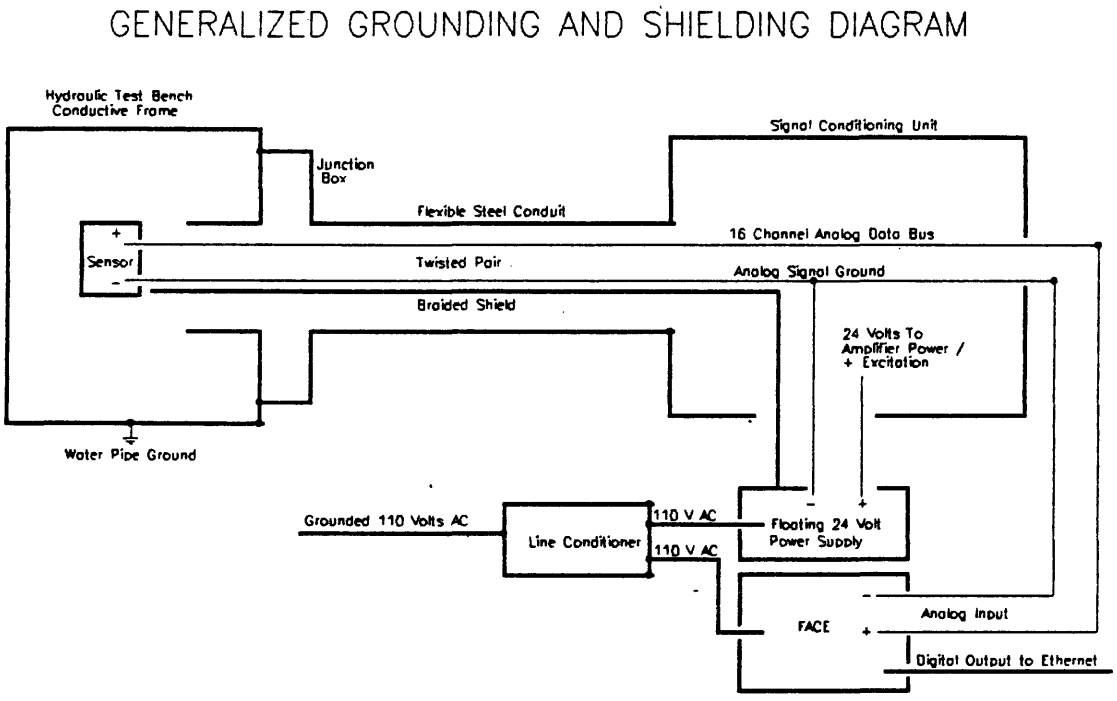

Figure C.11. Generalized Grounding and Shielding Diagram.

Appendix D.

RELATIVE EFFECTIVENESS OF SHIELDING MATERIALS: A FORTRAN 90 PROGRAM

This FORTRAN 90 program was developed in 1995 from published equations (Ott, 1976). The program estimates the relative electromagnetic shielding effectiveness of 12 different metals, given 1) the frequency (f, Hertz) of an electromagnetic noise source, 2) the distance (d, meters) from the noise source, and 3) the thickness (t, inches) of a plane sheet of shield material. The program is intended to aid designers of electronic equipment in selection of shield materials, and to help dispel some of the folklore surrounding the subject of electromagnetic shielding. The program takes into account 1) absorptive losses, 2) reflective losses, and 3) losses due to multiple reflections in thin shields. Electric and magnetic fields are considered separately if the shield is located in the near field, i.e., if $d < \lambda/(2\pi)$, where λ is the electromagnetic field wavelength.

Section D.1 contains the FORTRAN code, section D.2 contains samples of program output, section D.3 contains graphed results and discussions thereof, and section D.4 discusses cost considerations of shielding materials.

D.1 FORTRAN 90 Program SHIELD.F90

```
IMPLICIT NONE
REAL:: f,t,d,L,
    EAg,ECu,EAu,EAl,EBrass,ENi,EBronze,ESn,EST1045,EPb,EMonel,ESS430,&
    MAg,MCu,MAu,MAl,MBrass,MNi,MBronze,MSn,MST1045,MPb,MMonel,MSS430
OPEN(1,FILE='C:\SHIELD.OUT')
WRITE(5,'(" Enter the frequency of EM radiation in Hertz."/)')
READ (5,*)f
WRITE(5,'(" Enter the distance from the source of EM radiation in
meters."/)')
READ(5,*)d
WRITE(5, '(" Enter the thickness of a sheet of metal in inches." /)')
READ(5,*)t
WRITE(5,'(" FREQUENCY OF EM RADIATION IN HERTZ =      "F12.4)')f
WRITE(5,'(" DISTANCE FROM THE EM SOURCE IN METERS =   "F12.4)')d
WRITE(5,'(" THICKNESS OF METAL SHEET IN INCHES =      "F12.4)')t
WRITE(1,'(" FREQUENCY OF EM RADIATION IN HERTZ =      "F12.4)')f
WRITE(1,'(" DISTANCE FROM THE EM SOURCE IN METERS =   "F12.4)')d
WRITE(1,'(" THICKNESS OF METAL SHEET IN INCHES =      "F12.4)')t
! EQUATION SET 1:   ELECTRIC FIELD and FAR_FIELD ATTENUATION
! EAg represents the electric field attenuation for silver, ECu for
```

```
! copper, etc.  ST1045 indicates steel (SAE 1045) and SS430 indicates
!stainless steel Electric field attenuation = absorptive lose +
!reflective loss. .   Multiple reflection loss can be neglected for
! electric fields (3).
Eag          =(3.34*t*SQRT(f*1.05*   1.0))       +
              (168-10.0*LOG10 (   1.0*f/1.05 ))
Ecu          =(3.34*t*SQRT(f*1.00*   1.0))       +
              (168-10.0*LOG10 (   1.0*f/1.00 ))
Eau          =(3.34*t*SQRT(f*0.70*   1.0))       +
              (168-10.0*LOG10 (   1.0*f/0.70 ))
Eal          =(3.34*t*SQRT(f*0.61*   1.0))       +
              (168-10.0*LOG10 (   1.0*f/0.61 ))
Ebrass       =(3.34*t*SQRT(f*0.26*   1.0))       +
              (168-10.0*LOG10 (   1.0*f/0.26 ))
ENi          =(3.34*t*SQRT(f*0.20*   1.0))       +
              (168-10.0*LOG10 (   1.0*f/0.20 ))
Ebronze      =(3.34*t*SQRT(f*0.18*   1.0))       +
              (168-10.0*LOG10 (   1.0*f/0.18 ))
ESn          =(3.34*t*SQRT(f*0.15*   1.0))       +
              (168-10.0*LOG10 (   1.0*f/0.15 ))
EST1045      =(3.34*t*SQRT(f*.1*1000.0))         +
              (168-10.0*LOG10 (1000.0*f/.10 ))
EPb          =(3.34*t*SQRT(f*0.08*   1.0))       +
              (168-10.0*LOG10 (   1.0*f/0.08 ))
```

```
Emonel      =(3.34*t*SQRT(f*0.04*   1.0))       +
             (168-10.0*LOG10 (   1.0*f/0.04 ))
ESS430      =(3.34*t*SQRT(f*.02* 500.0))       +
             (168-10.0*LOG10 ( 500.0*f/.02 ))
! EQUATION SET 2:  MAGNETIC FIELD ATTENUATION
!Magnetic field attenuation = absorptive loss + reflective loss +
multiple reflection loss.
Mag         =(3.34*t*SQRT(f*1.05*   1.0))            +
             (14.6+10.0*LOG10(f*d**2*1.05/   1.0 ))   +
             (20.0*LOG10(1.0-EXP(-2.0*t/(2.6/SQRT(f*   1.0*1.05)))))
Mcu         =(3.34*t*SQRT(f*1.00*   1.0))            +
             (14.6+10.0*LOG10(f*d**2*1.00/   1.0 ))   +
             (20.0*LOG10(1.0-EXP(-2.0*t/(2.6/SQRT(f*   1.0*1.00)))))
 Mau        =(3.34*t*SQRT(f*0.70*   1.0))            +
             (14.6+10.0*LOG10(f*d**2*0.70/   1.0 ))   +
             (20.0*LOG10(1.0-EXP(-2.0*t/(2.6/SQRT(f*   1.0*0.70)))))
Mal         =(3.34*t*SQRT(f*0.61*   1.0))            +
             (14.6+10.0*LOG10(f*d**2*0.61/   1.0 ))   +
             (20.0*LOG10(1.0-EXP(-2.0*t/(2.6/SQRT(f*   1.0*0.61)))))
Mbrass      =(3.34*t*SQRT(f*0.26*   1.0))            +
             (14.6+10.0*LOG10(f*d**2*0.26/   1.0 ))   +
             (20.0*LOG10(1.0-EXP(-2.0*t/(2.6/SQRT(f*   1.0*0.26)))))
Mni         =(3.34*t*SQRT(f*0.20*   1.0))            +
             (14.6+10.0*LOG10(f*d**2*0.20/   1.0 ))   +
```

```
              (20.0*LOG10(1.0-EXP(-2.0*t/(2.6/SQRT(f*   1.0*0.20)))))
Mbronze      =(3.34*t*SQRT(f*0.18*   1.0))             +
              (14.6+10.0*LOG10(f*d**2*0.18/   1.0 ))   +
              (20.0*LOG10(1.0-EXP(-2.0*t/(2.6/SQRT(f*   1.0*0.18)))))
MSn          =(3.34*t*SQRT(f*0.15*   1.0))             +
              (14.6+10.0*LOG10(f*d**2*0.15/   1.0 ))   +
              (20.0*LOG10(1.0-EXP(-2.0*t/(2.6/SQRT(f*   1.0*0.15)))))
MST1045      =(3.34*t*SQRT(f*.1*1000.0))               +
              (14.6+10.0*LOG10(f*d**2*.10/1000.0))     +
              (20.0*LOG10(1.0-EXP(-2.0*t/(2.6/SQRT(f*1000.0*0.10)))))
MPb          =(3.34*t*SQRT(f*0.08*   1.0))             +
              (14.6+10.0*LOG10(f*d**2*0.08/   1.0 ))   +
              (20.0*LOG10(1.0-EXP(-2.0*t/(2.6/SQRT(f*   1.0*0.08)))))
Mmonel       =(3.34*t*SQRT(f*0.04*   1.0))             +
              (14.6+10.0*LOG10(f*d**2*0.04/   1.0 ))   +
              (20.0*LOG10(1.0-EXP(-2.0*t/(2.6/SQRT(f*   1.0*0.04)))))
MSS430       =(3.34*t*SQRT(f*.02* 500.0))              +
              (14.6+10.0*LOG10(f*d**2*0.02/500.0))     +
              (20.0*LOG10(1.0-EXP(-2.0*t/(2.6/SQRT(f* 500.0*0.02)))))
!This section computes the critical distance from the electromagnetic
!source to the near - field - far field transition.  The transition
!occurs at distance of  L=(electromagnetic wavelength )/(2*Pi).  If the
!shield is placed in the far field the total EM field attenuation is
!governed by EQUATION SET 1.  If the shield is placed in the near field,
```

```
!attenuation of electric and magnetic fields must be considered
!separately.  In this case, electric field attenuation is governed by
!EQUATION SET 1 and magnetic field attenuation is governed by EQUATION
!SET 2.
L=299780000/(6.2832*f)
IF( d >= L ) THEN
   WRITE(5,'(" RELATIVE FAR-FIELD ATTENUATION IN dB "/)')
   WRITE(1,'(" RELATIVE FAR-FIELD ATTENUATION IN dB "/)')
   WRITE(5,'(" Silver                " F12.4)')EAg
   WRITE(5,'(" Annealed Copper       " F12.4)')ECu
   WRITE(5,'(" Gold                  " F12.4)')EAu
   WRITE(5,'(" Aluminum              " F12.4)')EAl
   WRITE(5,'(" Brass                 " F12.4)')EBrass
   WRITE(5,'(" Nickel                " F12.4)')ENi
   WRITE(5,'(" Bronze                " F12.4)')EBronze
   WRITE(5,'(" Tin                   " F12.4)')ESn
   WRITE(5,'(" Steel SAE 1045        " F12.4)')EST1045
   WRITE(5,'(" Lead                  " F12.4)')EPb
   WRITE(5,'(" Monel                 " F12.4)')EMonel
   WRITE(5,'(" Stainless 430         " F12.4)')ESS430
   WRITE(1,'(" Silver                " F12.4)')EAg
   WRITE(1,'(" Annealed Copper       " F12.4)')ECu
   WRITE(1,'(" Gold                  " F12.4)')EAu
   WRITE(1,'(" Aluminum              " F12.4)')EAl
```

```
   WRITE(1,'(" Brass                " F12.4)')EBrass
   WRITE(1,'(" Nickel               " F12.4)')ENi
   WRITE(1,'(" Bronze               " F12.4)')EBronze
   WRITE(1,'(" Tin                  " F12.4)')ESn
   WRITE(1,'(" Steel SAE 1045       " F12.4)')EST1045
   WRITE(1,'(" Lead                 " F12.4)')EPb
   WRITE(1,'(" Monel                " F12.4)')EMonel
   WRITE(1,'(" Stainless 430        " F12.4)')ESS430
ELSE
   WRITE(5,'(" RELATIVE NEAR-FIELD ATTENUATION IN dB")')
   WRITE(5,'(" ELECTRIC AND MAGNETIC FIELDS MUST BE CONSIDERED
SEPARATELY ")')
   WRITE(5,'(" THE FIRST  COLUMN REPRESENTS ELECTRIC FIELD
ATTENUATION")')
   WRITE(5,'(" THE SECOND COLUMN REPRESENTS MAGNETIC FIELD
ATTENUATION"/)')
   WRITE(1,'(" RELATIVE NEAR-FIELD ATTENUATION IN dB")')
   WRITE(1,'(" ELECTRIC AND MAGNETIC FIELDS MUST BE CONSIDERED
SEPARATELY ")')
   WRITE(1,'(" THE FIRST  COLUMN REPRESENTS ELECTRIC FIELD
ATTENUATION")')
   WRITE(1,'(" THE SECOND COLUMN REPRESENTS MAGNETIC FIELD
ATTENUATION"/)')
   WRITE(5,'(" Silver         "2F12.4)')EAg,    MAX(MAg,    0.0)
```

```
WRITE(5,'(" Annealed Copper"2F12.4)')ECu,    MAX(MCu,    0.0)
WRITE(5,'(" Gold           "2F12.4)')EAu,    MAX(MAu,    0.0)
WRITE(5,'(" Aluminum       "2F12.4)')EAl,    MAX(MAl,    0.0)
WRITE(5,'(" Brass          "2F12.4)')EBrass, MAX(MBrass, 0.0)
WRITE(5,'(" Nickel         "2F12.4)')ENi,    MAX(MNi,    0.0)
WRITE(5,'(" Bronze         "2F12.4)')EBronze,MAX(Mbronze,0.0)
WRITE(5,'(" Tin            "2F12.4)')ESn,    MAX(MSn,    0.0)
WRITE(5,'(" Steel SAE 1045 "2F12.4)')EST1045,MAX(MST1045,0.0)
WRITE(5,'(" Lead           "2F12.4)')EPb,    MAX(MPb,    0.0)
WRITE(5,'(" Monel          "2F12.4)')EMonel, MAX(MMonel, 0.0)
WRITE(5,'(" Stainless 430  "2F12.4)')ESS430, MAX(MSS430, 0.0)
WRITE(1,'(" Silver         "2F12.4)')EAg,    MAX(MAg,    0.0)
WRITE(1,'(" Annealed Copper"2F12.4)')ECu,    MAX(MCu,    0.0)
WRITE(1,'(" Gold           "2F12.4)')EAu,    MAX(MAu,    0.0)
WRITE(1,'(" Aluminum       "2F12.4)')EAl,    MAX(MAl,    0.0)
WRITE(1,'(" Brass          "2F12.4)')EBrass, MAX(MBrass, 0.0)
WRITE(1,'(" Nickel         "2F12.4)')ENi,    MAX(MNi,    0.0)
WRITE(1,'(" Bronze         "2F12.4)')EBronze,MAX(MBronze,0.0)
WRITE(1,'(" Tin            "2F12.4)')ESn,    MAX(MSn,    0.0)
WRITE(1,'(" Steel SAE 1045 "2F12.4)')EST1045,MAX(MST1045,0.0)
WRITE(1,'(" Lead           "2F12.4)')EPb,    MAX(MPb,    0.0)
WRITE(1,'(" Monel          "2F12.4)')EMonel, MAX(MMonel ,0.0)
WRITE(1,'(" Stainless 430  "2F12.4)')ESS430, MAX(MSS430, 0.0)
```

```
END IF

STOP

END PROGRAM SHIELD
```

D.2. Sample Output.

SAMPLE OUTPUT # 1

FREQUENCY OF EM RADIATION IN HERTZ = 1000.00

DISTANCE FROM THE EM SOURCE IN METERS = 0.10

THICKNESS OF METAL SHEET IN INCHES = 0.03

RELATIVE NEAR-FIELD ATTENUATION IN dB

ELECTRIC AND MAGNETIC FIELDS MUST BE CONSIDERED SEPARATELY.

THE FIRST COLUMN REPRESENTS ELECTRIC FIELD ATTENUATION.

THE SECOND COLUMN REPRESENTS MAGNETIC FIELD ATTENUATION.

Silver	141.45	22.48
Annealed Copper	141.16	22.05
Gold	139.10	18.89
Aluminum	138.32	17.68
Brass	133.76	10.21
Nickel	132.42	7.92
Bronze	131.89	7.00
Tin	130.98	5.41
Steel SAE 1045	129.68	16.28
Lead	127.92	0.00
Monel	124.65	0.00
Stainless 430	104.04	0.00

SAMPLE OUTPUT # 2

FREQUENCY OF EM RADIATION IN HERTZ = 60.00

DISTANCE FROM THE EM SOURCE IN METERS = 1.00

THICKNESS OF METAL SHEET IN INCHES = 0.03

RELATIVE NEAR-FIELD ATTENUATION IN dB

ELECTRIC AND MAGNETIC FIELDS MUST BE CONSIDERED SEPARATELY.

THE FIRST COLUMN REPRESENTS ELECTRIC FIELD ATTENUATION.

THE SECOND COLUMN REPRESENTS MAGNETIC FIELD ATTENUATION.

Silver	151.22	17.86
Annealed Copper	150.99	17.43
Gold	149.31	14.33
Aluminum	148.67	13.14
Brass	144.76	5.72
Nickel	143.57	3.44
Bronze	143.10	2.53
Tin	142.28	0.95
Steel SAE 1045	117.97	0.00
Lead	139.46	0.00
Monel	136.39	0.00
Stainless 430	108.69	0.00

SAMPLE OUTPUT #3

FREQUENCY OF EM RADIATION IN HERTZ = 10000.00

DISTANCE FROM THE EM SOURCE IN METERS = 1.00

THICKNESS OF METAL SHEET IN INCHES = 0.03

RELATIVE NEAR-FIELD ATTENUATION IN dB

ELECTRIC AND MAGNETIC FIELDS MUST BE CONSIDERED SEPARATELY.

THE FIRST COLUMN REPRESENTS ELECTRIC FIELD ATTENUATION.

THE SECOND COLUMN REPRESENTS MAGNETIC FIELD ATTENUATION.

Silver	138.47	64.22
Annealed Copper	138.02	63.70
Gold	134.83	60.07
Aluminum	133.67	58.71
Brass	127.25	50.65
Nickel	125.49	48.26
Bronze	124.80	47.31
Tin	123.64	45.67
Steel SAE 1045	188.20	114.80
Lead	119.86	40.07
Monel	116.02	33.98
Stainless 430	115.70	42.30

SAMPLE OUTPUT # 4

FREQUENCY OF EM RADIATION IN HERTZ = 1000000.00

DISTANCE FROM THE EM SOURCE IN METERS = 1.00

THICKNESS OF METAL SHEET IN INCHES = 0.03

RELATIVE NEAR-FIELD ATTENUATION IN dB

ELECTRIC AND MAGNETIC FIELDS MUST BE CONSIDERED SEPARATELY.

THE FIRST COLUMN REPRESENTS ELECTRIC FIELD ATTENUATION.

THE SECOND COLUMN REPRESENTS MAGNETIC FIELD ATTENUATION.

Silver	210.88	177.48
Annealed Copper	208.20	174.80
Gold	190.28	156.88
Aluminum	184.11	150.71
Brass	153.24	119.84
Nickel	145.82	112.42
Bronze	143.06	109.66
Tin	138.56	105.16
Steel SAE 1045	1070.00	1036.60
Lead	125.37	91.95
Monel	114.06	80.57
Stainless 430	380.88	347.48

SAMPLE OUTPUT # 5

FREQUENCY OF EM RADIATION IN HERTZ = 100000.00

DISTANCE FROM THE EM SOURCE IN METERS = 10000.00

THICKNESS OF METAL SHEET IN INCHES = 0.03

RELATIVE FAR-FIELD ATTENUATION IN dB

Silver	150.68
Annealed Copper	149.68
Gold	142.96
Aluminum	140.60
Brass	128.30
Nickel	125.18
Bronze	123.99
Tin	122.03
Steel SAE 1045	394.86
Lead	115.99
Monel	110.35
Stainless 430	174.22

SAMPLE OUTPUT # 6

FREQUENCY OF EM RADIATION IN HERTZ = 1000000.00

DISTANCE FROM THE EM SOURCE IN METERS = 10000.00

THICKNESS OF METAL SHEET IN INCHES = 0.03

RELATIVE FAR-FIELD ATTENUATION IN dB

Silver	210.88
Annealed Copper	208.20
Gold	190.28
Aluminum	184.11
Brass	153.24
Nickel	145.82
Bronze	143.06
Tin	138.56
Steel SAE 1045	1070.00
Lead	125.37
Monel	114.06
Stainless 430	380.88

D.3. Interpretation of Program Output.

Figures D.1, D.2, and D.3 were derived from the output of this program. Figure D.1 shows the effect of frequency (f) on attenuation, Figure D.2 shows the effect of thickness (t) on attenuation, and Figure D.3 shows the effect of distance (d) on attenuation. Only copper, steel, and aluminum are considered, as shielding conduit made from these materials is locally available.

Figure D.1 illustrates a situation where a 0.03 inch thick sheet of shield material is placed one meter away from an electromagnetic noise source. This situation approximates the conditions at the test bench, as the thickness of available conduit is .03 inches, and the sensing circuitry is on the order of one meter from the noise source. For this case, the program suggests that 1) copper shield is marginally better than aluminum for all frequencies, and 2) steel shield is superior to both copper shield and aluminum shield at frequencies above 1500 Hz. Although the noise emanating from the motor controller is broad band, much of it is above 1500 Hz, so steel is a logical choice as a shielding material in this application.

Figure D.2 illustrates the effect of shield thickness for a 5000 Hz noise source at a distance of 1 meter. The figure shows that for shield thicknesses above 0.02 inches, steel provides better attenuation than either aluminum or copper.

Figure D.3 shows that, for a shield thickness of 0.03 and an EM frequency of 5000 Hz, the magnetic field attenuation is independent of distance, but the electric field attenuation improves with distance.

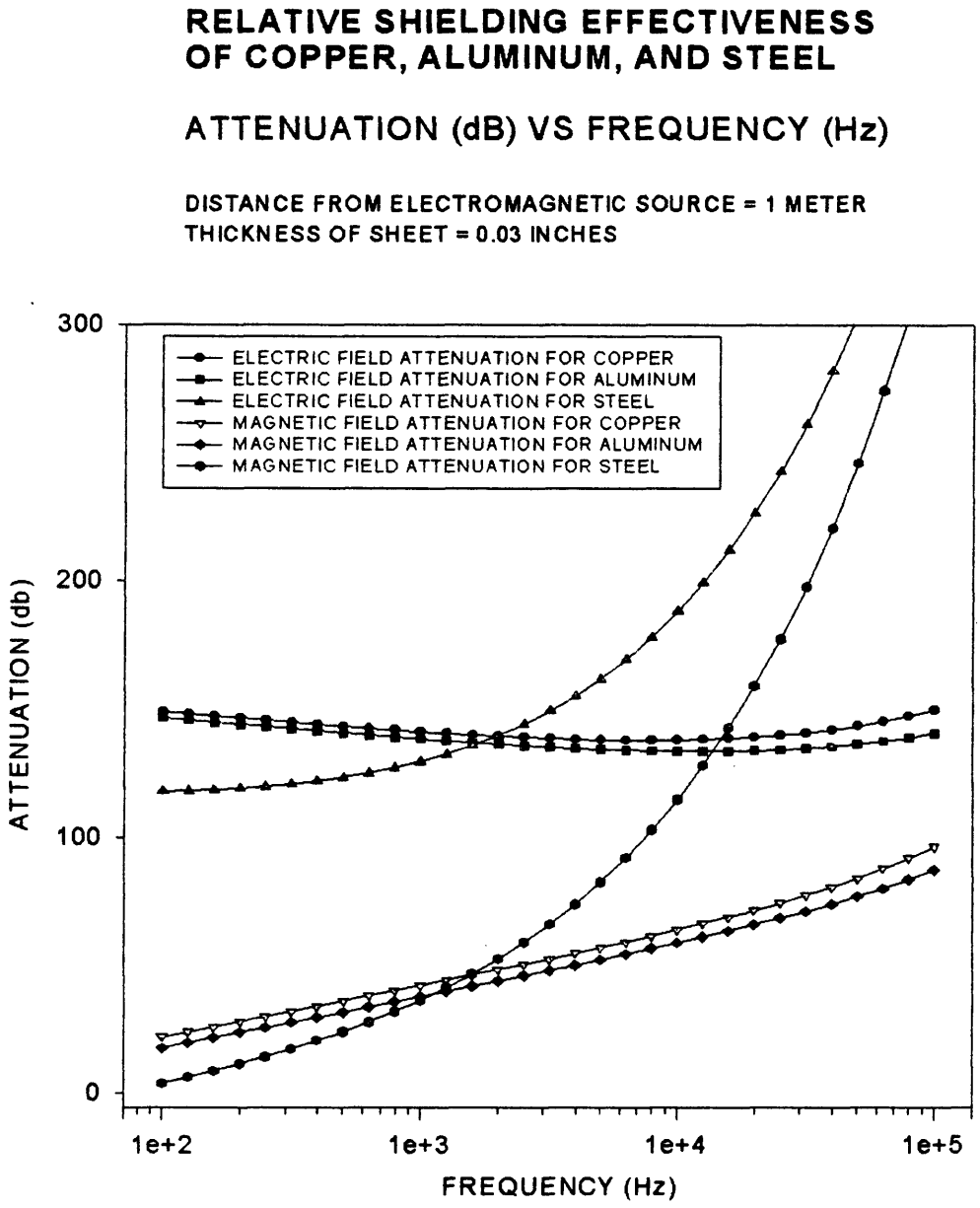

Figure D.1. Relative Shielding Effectiveness of Copper, Aluminum, and Steel - Attenuation vs. Frequency.

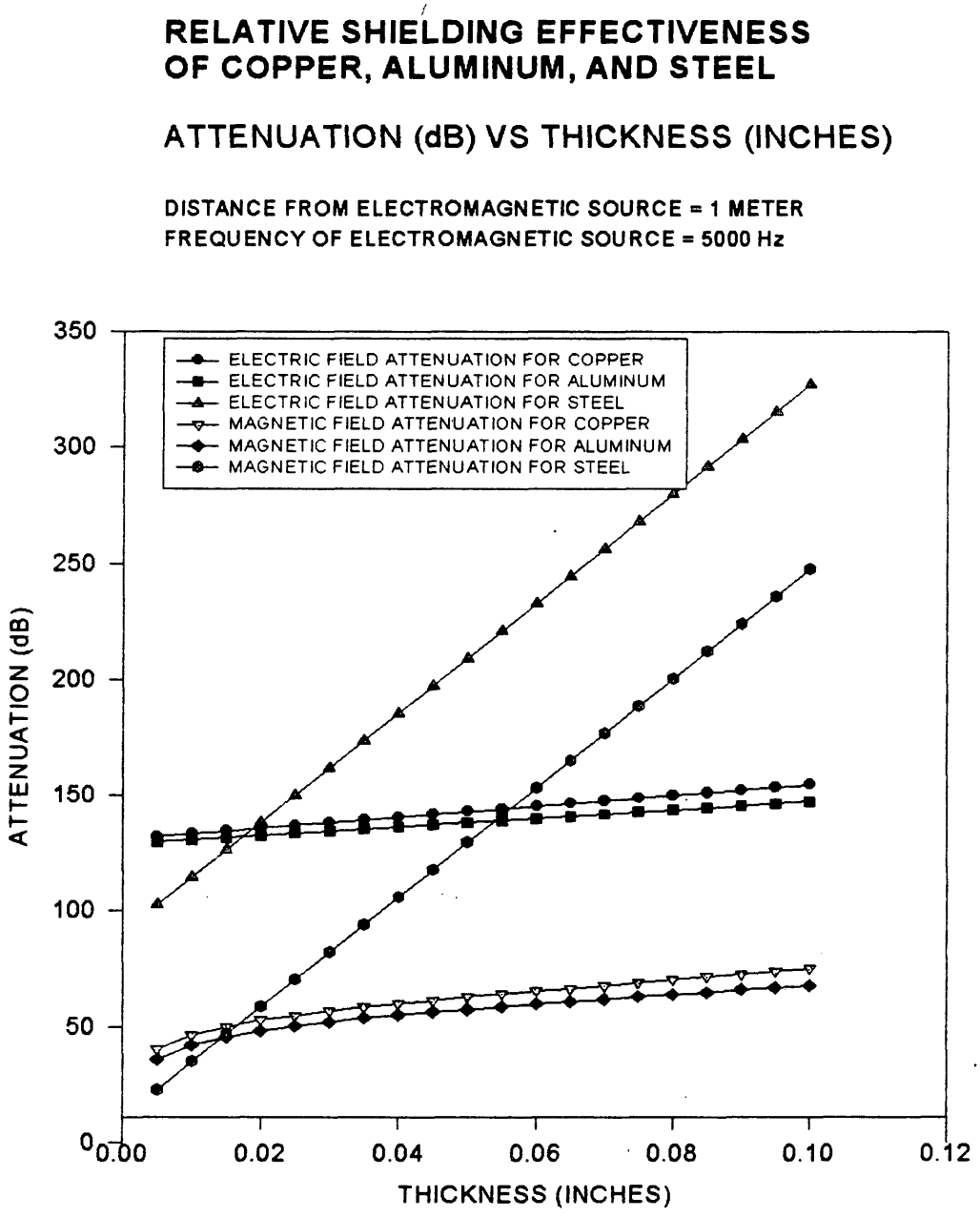

Figure D.2. Relative Shielding Effectiveness of Copper, Aluminum, and Steel - Attenuation vs. Thickness.

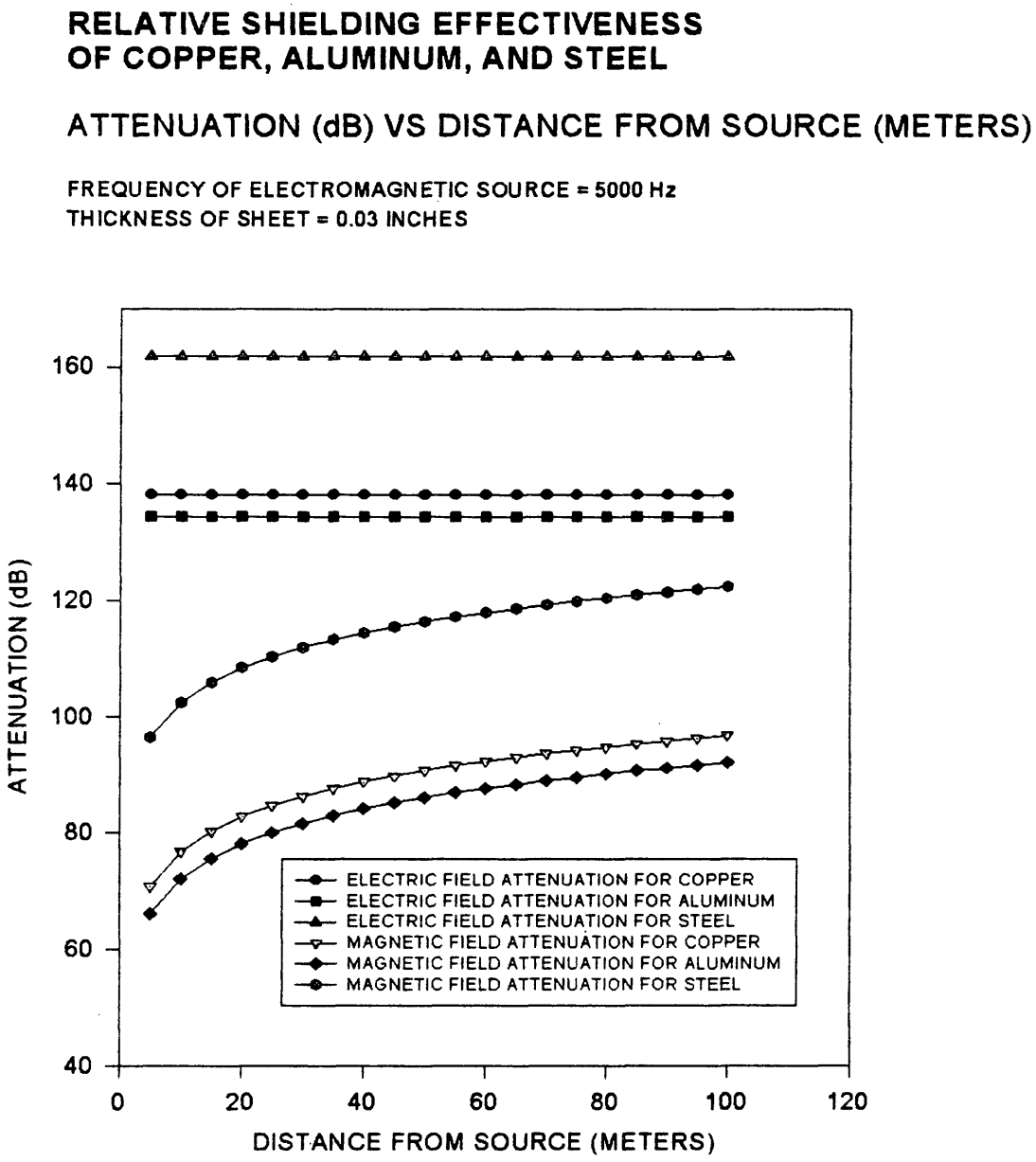

Figure D.3. Relative Shielding Effectiveness of Copper, Aluminum, and Steel - Attenuation vs. Distance from Source.

D.4. Cost Considerations.

The following analysis is constrained to aluminum, copper, and steel (not stainless steel), as these are the three most commonly used and locally available in the form of shielding conduit. Table D.1 is based on bulk commodity prices quoted in the Rocky Mountain News on December 21, 1995:

	PRICE PER WEIGHT (cents/lbm)	DENSITY (lbm/ft3)	PRICE PER VOLUME ($/ft3)
Aluminum	75.20	169	126.33
Copper	137.00	555	760.35
Steel	6.32	488	30.84

Table D.1. Bulk Commodity Price of Copper, Aluminum, and Steel.

The information in Table D.1 can be merged with program results to determine cost effectiveness in terms of dollars per decibels of attenuation for a given application. Table D.2 shows the cost effectiveness of copper, aluminum, and steel for a sheet thickness of 0.03 inches, 1 meter away from a 1 kHz source.

	DECIBELS OF ELECTRIC FIELD ATTENUATION PER DOLLAR	DECIBELS OF MAGNETIC FIELD ATTENUATION PER DOLLAR
Aluminum	0.1095	0.134
Copper	0.1857	0.0029
Steel	4.2049	0.527

Table D.2. Decibels of Attenuation per Dollar (for 0.03 Inch Sheets of Copper, Aluminum, and Steel at a Distance of 1 Meter from a 1 kHz Noise Source).

The above analysis is only a rough estimate which does not take into account manufacturing costs. In general, steel provides better attenuation per dollar than copper or aluminum. However, aluminum is lighter and easier to cut, and may be the preferred shield material where portability and ease of installation are required.

Appendix E.

PROCEDURES FOR OBTAINING OSCILLOSCOPE HARDCOPY OUTPUT

A Phillips model PM 3335 60 MHz Digital Storage Oscilloscope was used to generate the voltage traces in this report. Considerable experimentation, enough to warrant documentation here, was required to obtain paper prints of the oscilloscope traces. The paper traces were obtained with the method outlined below and then scanned as bitmaps for insertion into the word document.

E.1. Oscilloscope/Printer Serial Port Connections.

The 9 pin serial output on the back of the DSO must be routed to the 25 pin serial input on the back of the printer or computer according to Figure E-1:

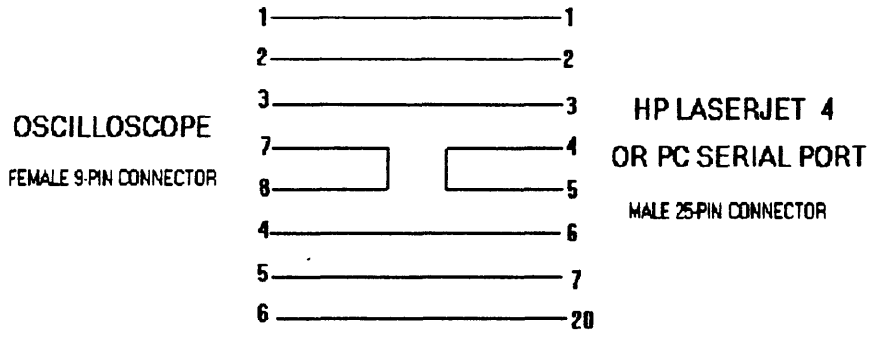

Figure E.1. Oscilloscope/Printer Serial Port Connections.

E.2. Printer Configuration.

If sending the digital oscilloscope trace directly to the HP Laserjet 4 printer, configure the printer as described below using the LCD display:

SERIAL MENU

RS232

PACING=DTR/DSR

BAUD RATE=4800

DTR POLARITY=HI

E.3. Oscilloscope Configuration.

Using the buttons below the CRT screen, configure the oscilloscope to the following parameters. The scope must be operating in DIGITAL MEMORY mode.

DIGITAL MEMORY

OPTIONS

RS232

BAUD 4800

DATA 8

PARITY NO

STOP 1

RETURN

PLOT

TYPE

HP2225

OUTPUT

RS232

RETURN RETURN RETURN

Now press the PLOT button on the upper right side of the scope. As data transfer occurs, the READY light on the printer will blink. Power may have to be cycled on both the scope and the plotter between plots. Once the paper copy is obtained it can be scanned and converted into a bitmap for incorporation into an electronic document.

E.4. PC Configuration for Direct Transfer of Digital Oscilloscope Data.

To send oscilloscope traces directly to a Windows-based PC for incorporation into a CORELDRAW electronic document, execute the following Windows commands:

PROGRAM MANAGER

MAIN

CONTROL PANEL

PORTS

COM2

SETTINGS

BAUD RATE 4800

DATA BITS 8

PARITY NONE

STOP BITS 1

FLOW CONTROL NONE

OK

CLOSE

ACCESSORIES

TERMINAL

SETTINGS

COMMUNICATION (set parameters)

SETTINGS

TEXT TRANSFERS

STANDARD FLOW CONTROL

OK

TRANSFERS

RECEIVE TEXT FILE

FILENAME.TXT

OK

Now hit PLOT key on oscilloscope. When transfer is complete, enter

STOP

TRANSFERS

SEND TEXT FILE as FILENAME.TXT

Rename to FILENAME.PLT

CORELDRAW

IMPORT FILENAME.PLT

EXPORT AS FILENAME.WMF

Although the procedure outlined above eliminates the need for paper scanning, it takes much more time than the scanning method. For this reason, all the oscilloscope traces shown in this report were obtained by scanning printer output.